12-2015

IN VITRO MULTI-SCALE PATIENT-SPECIFIC MODELING OF HEMODYNAMICS IN STAGE 1 NORWOOD PALLIATION FOR THE TREATMENT OF SINGLE VENTRICLE HEART DISEASE

TIANQI HANG
Clemson University, tianqi.hang39@gmail.com

IN VITRO MULTI-SCALE PATIENT-SPECIFIC MODELING OF HEMODYNAMICS IN STAGE 1 NORWOOD PALLIATION FOR THE TREATMENT OF SINGLE VENTRICLE HEART DISEASE

A Dissertation
Presented to
the Graduate School of
Clemson University

In Partial Fulfillment
of the Requirements for the Degree
Doctor of Philosophy
Mechanical Engineering

---

by
Tianqi Hang
December 2015

Accepted by:
Richard Figliola, PhD, Committee Chair
Tain-Yen Hsia, MD
Chenning Tong, PhD
Donald Beasley, PhD

ABSTRACT

Hypoplastic left heart syndrome (HLHS) is a congenital heart defect in which the left ventricle is severely underdeveloped. The Norwood procedure is the first stage procedure to make an unrestrictive systemic blood flow and at the same time balance it with the pulmonary flow. This is done by constructing a neo-aorta using the pulmonary artery root and the autologous aorta, and then installing a shunt to the pulmonary artery. Variations of the Norwood surgery include the modified Blalock-Taussig (mBT) shunt, which diverts blood from the innominate artery to the pulmonary artery (PA), and the Right Ventricle Shunt (RVS), which diverts blood from the right ventricle to the PA.

Recurrent neo-aortic coarctation (NAO) is a frequent complication of the Norwood procedure. It causes changes in circulation flow rate balances and hypertension in the aortic arch. Conventionally, the value of a coarctation index (CoI) is used in choosing interventions to treat NAO. Aortic arch morphology of Norwood patients is suspected to be a factor of hemodynamic response to NAO.

This study aims to develop and validate an *in vitro* model of the Norwood circulation and to use it to better understand the hemodynamic impact of progressive coarctation severity in the Norwood patients with mBT and RVS shunts. Five patient-specific cases were selected, each case having a different aortic morphology.

A multi-scale mock circulatory system (MCS) was developed to simulate patient-specific Norwood circulation. The MCS couples a lumped parameter network (LPN) model of the circulation with the 3D test section of the aorta and superior arteries. The

system includes branches for the pulmonary, upper body, lower body and single ventricle. The MCS was set to patient specific conditions based on the clinical measurements. Flow rate and pressure measurements were made around the circulation model. The native arch anatomy of each patient was morphed to simulate coarctation by controlling the amount of narrowing of the aortic isthmus, while keeping the original patient-specific aortic geometry intact. Separate NAO models were created to provide for a range of CoI. Aortic pressure measurements were made to study pressure drop and recovery effects. In a further study, the MCS was modified to simulate the Norwood circulation with RVS. The NAO models were used to study coarctation effects.

The MCS was validated against clinical measurements. The experimental measurements demonstrated that the time-based flow rate and pressure developed within the circulation recapitulated clinical measurements ($0.72 < R^2 < 0.95$). The results showed good fidelity in replicating the mean values of the Norwood circulation at the patient-specific level ($p > 0.10$).

The system demonstrated the coarctation effects in the Norwood circulation with mBT. For all patient cases, the single ventricle power (SVP), mean pressure difference, and Q_p/Q_s increased noticeably when CoI < 0.5 ($p<0.05$). An increased SVP correlated with abnormal aortic arch morphology (dilated or tubular).

Measurements from two of four cases studied showed that substituting the mBT with the RVS can relieve pulmonary overcirculation and improve the pulmonary to systemic flow balance (Q_p/Q_s). Using the RVS reduced SVP requirements by 74.5 mW

on average. A tubular arch morphology was associated with a higher SVP with the RVS than those patients with a dilated arch.

The study has shown that the hypothesis, “NAO may not need immediate surgical intervention at an early stage for some patients” was accepted. Aortic arch morphology does affect the hemodynamic response to NAO. Any morphological abnormality causes extra SVP. The RVS can relieve overcirculation and is associated with lower SVP level and SVP changes in some of the patients.

ACKNOWLEDGEMENTS

I would like to thank all the persons, groups and organizations that have assisted to make this dissertation possible, in particular:

The Leducq foundation and Department of Mechanical Engineering at Clemson University for supporting the research project and me financially.

I would like to acknowledge department travel and purchase staff Ms. Gwen Dockins, machine shop staffs Mr. Michael Justice, Mr. Stephen Bass, and Mr. Jamie Cole for their helps.

My dissertation committee Dr. Chenning Tong, Dr. Donald Beasley and Dr. Tain-Yen Hsia have provided many and constructive suggestions along the way. I would like to thank them for their suggestions.

I would like to acknowledge my colleagues in Leducq Transatlantic Network Modeling of Congenital Heart Alliance (MOCHA) group, especially Dr. Giovanni Biglino, Dr. Alessandro Giardini, Dr. Chiara Corsini and Dr. Catriona Baker, for the all the discussions, consultations and inspirations. Working with such a multi-disciplinary international team has helped me to spark creativity and new ideas.

I would like to acknowledge post-doctoral fellows Dr. Marija Vukicevic, Dr. Chad Smith and Dr. Timothy Conover for reading this dissertation, years of research collaboration and beer drinking together in Nicks. In particular, Dr. Timothy Conover, the Jedi master of experimentation and computer simulation, has been

working with me since day one, his inputs and helps are invaluable, and I cannot imagine how I could have completed the work without Tim's help.

Special thanks to my research advisor Dr. Richard Figliola, whom I respect profoundly. Dr. Richard Figliola is not only an exceptional scholar but also an inspiring educator. I thank him for being the advisor who inspires me to think harder rather than tell me what to do. I thank him for teaching me the most useful things: critical thinking and scientific mentality.

Lastly, I would like to thank my family. My parents have selflessly supported me all along. I thank them for the years of understanding, for being tolerant rather than dogmatic, and for motivating me to always aim higher. I am also thankful to my late grandfather, he would be very proud of me.

Three and half years of Clemson experience has been the highlight in my life. I have met great people and sparked diverse ideas and opinions through talking and drinking with them. I have appreciated and will continue to pursue the utter beauty of science and engineering. I have enjoyed three years of peaceful country life, living in the rural area has changed me much. I started to pay much more attention to the nature around me, I started to appreciate the beauty of sunset, to watch the leaves changing color and to listen to the rhythm of the rain.

To quote Shakespeare: I can no other answer make, but, thanks, and thanks.

TABLE OF CONTENTS

Table of Contents (Continued) Page

LIST OF TABLES

LIST OF FIGURES

List of Figures (Continued)

List of Figures (Continued)

Figure Page

List of Figures (Continued)

List of Figures (Continued)

Figure Page

NOMENCLATURE

Hypoplastic Left Heart Syndrome	HLHS
Pulmonary Vascular Resistance	PVR
Systemic Vascular Resistance	SVR
Right Ventricle Shunt	RVS
Waterson Shunt	WS
Bilateral Pulmonary Artery Banding	bPAB
Coarctation	COA
Coarctation Index	CoI
Recurring Neoaortic Coarctation	NAO
Cardiac Output	CO
Electrocardiogram	ECG
Chest Computed Tomography	CT
Magnetic Resonance Imaging	MRI
End to End Anastomosis	EEA
Subclavian Aorto-plasty	SFA
Mock Circulatory System	MCS
Lumped Parameter Network	LPN
Computational Fluid Dynamics	CFD
Left Subclavian Artery	LSA
Right Subclavian Artery	RSA
Left Pulmonary Artery	LPA

Pressure-Volume	PV
Ventricle Assist Device	VAD
Cardiovascular Magnetic Resonance	CMR
Time-Averaged Wall Shear Stress	TAWSS
Oscillatory Shear Index	OSI
End Diastolic Volume	EDV
Fluid Structure Interaction	FSI
Descending Aorta	DA
Blood Pressure	BP
Magnetic Resonance	MR
Lumped Parameter	LP
Resistance	R
Compliance	C
Pressure	P
Volumetric Flow Rate	Q
Ascending Aorta	Asc.Ao
Proximal	Prox
Pulmonary Shunt	Pul
Atrium	Atri
Brachiocephalic Artery	bc
Left Common Carotid Artery	LCC
Transverse Arch	TA
Proximal Transverse Arch	PTA

Distal Transverse Arch	DTA
Aortic Isthmus	AI
Neoaorta	NA
Single Ventricle Power	SVP
Oxygen Delivery	OD
Single Ventricle	SV
Neoaortic Coarctation	NAO
Polytetrafluoroethylene	PTFE
Mean Aortic Pressure	MAP
Single Atrial Pressure	SAP
Regurgitation Fraction	RF
Random error	s
Systemic error	b
Total Vascular Resistance	TVR
Impedance	Z
Total Vascular Compliance	TVC
Diameter ratio of transverse arch over descending aorta at diaphragm	TA/DD

CHAPTER ONE

INTRODUCTION: STAGE 1 PALLIATION FOR THE SINGLE VENTRICLE HEART DISEASE

Introduction

The human heart has four chambers. The upper chambers are called atria, while the lower chambers are called ventricles. Atria receive blood flowing into the heart, and then ventricles pump blood out of the heart. Specifically, the left ventricle pumps oxygenated blood to the aorta, the large artery that carries blood to the body, while the right ventricle pumps blood to the pulmonary artery, to exchange CO_2 for oxygen in the lungs.

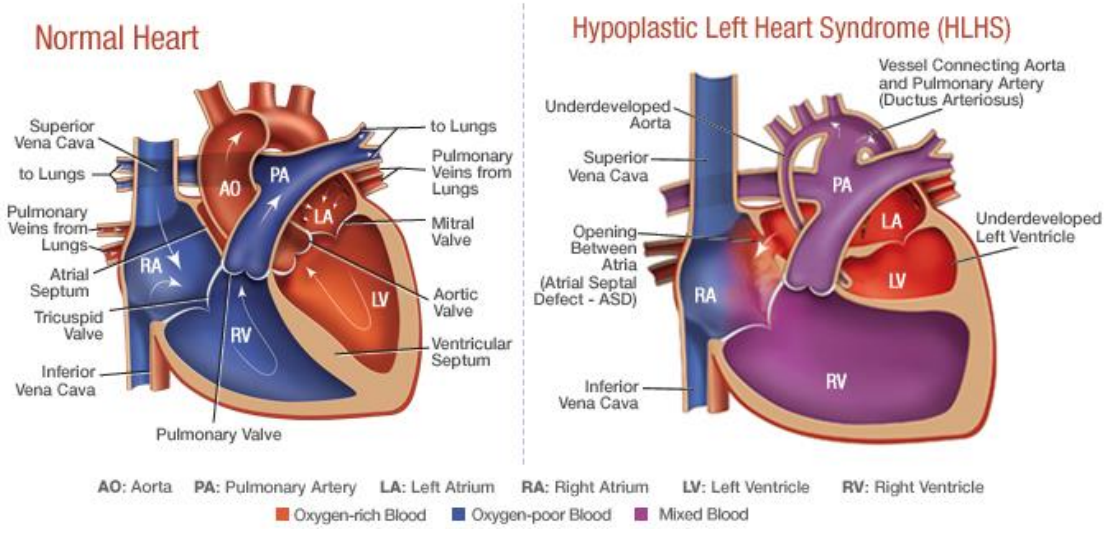

Figure 1.1 Normal Heart anatomy versus HLHS heart anatomy (The Children's Hospital of Philadelphia, n.d.) .

A child with a single ventricle defect is born with a heart with only one ventricle that is large enough or strong enough to pump effectively. Hypoplastic left heart syndrome (HLHS) is a rare congenital heart defect in which the left ventricle of the heart is severely underdeveloped, and generally shows severe endocardial

fibroelastosis (Norwood, 1981). In a child with HLHS, the mitral valve is usually too small or completely closed, the left ventricle is very small, and also the aortic valve is small or completely closed. Figure 1.1 illustrates the normal heart anatomy and the HLHS heart anatomy. HLHS can be diagnosed in utero and requires surgical treatment immediately after birth.

HLHS is fatal without treatment. However, even with the treatment, the mortality is still very high. A study of mortality rates of the Stage 1 Norwood procedure between 1996 through 2005 revealed an early mortality rate of 17.1% and a two year mortality rate of 40.1% for HLHS patients. (Atallah, 2008)

Different surgical strategies to treat HLHS have been developed in the last decades, however the philosophy of the strategies have been consistent, that is, to suppress the venous and oxygenated blood mixing, bypass the underdeveloped chamber, convert the two parallel circulations to series with only one functional ventricle. (Fontan, 1971)

While treating the neonatal patient, Norwood et al. analyzed the complications and causes of death, finding that pulmonary vascular resistance (PVR) is naturally high for neonates because of their immature lungs. Thus a three-staged surgical strategy has been developed to improve the survival rate. (Norwood, 1981)

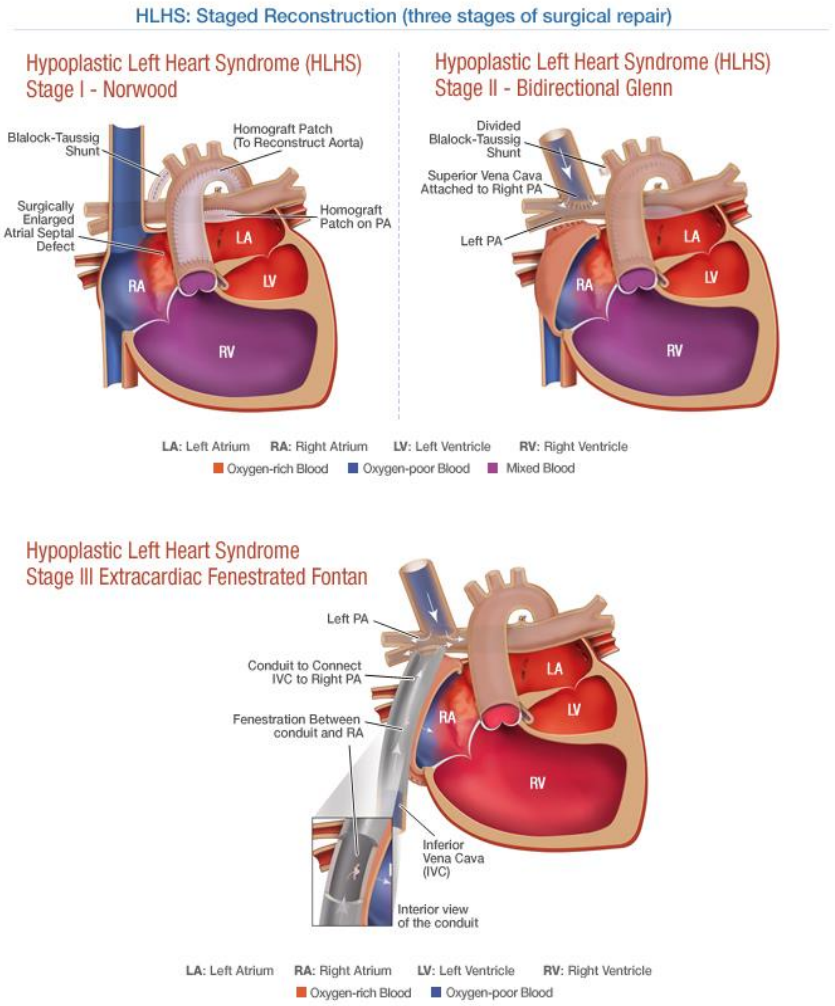

Figure 1.2. Staged repair for HLHS, left upper picture illustrates a Norwood Procedure with mBT shunt, the right upper figure illustrates a Bidirectional Glenn procedure with shunt removed, lower figures illustrates a Fontan procedure. (Philiadephia, n.d.)

The three stages of surgeries are typically performed in the first few years of patients' lives, depending on their growth rates. Figure 1.2 presents the post-operative heart anatomy of the three surgical stages respectively. The stage 1 surgery usually takes place within a few days of birth. The goal of stage 1 surgery is to make an unrestrictive systemic blood flow, and at the same time balance the pulmonary flow or, specifically, balance the Q_p/Q_s ratio. Referring to Figure 1.2, this can be achieved

by constructing a neo-aorta using the pulmonary artery root and the autologous aorta, and then installing a shunt to the pulmonary artery (Norwood procedure). Alternatively, banding the pulmonary artery and stenting the descending aorta may be considered, depending on the condition of the patient (Norwood, 1981). The volumetric load on the single ventricle is doubled, and oxygenated blood from the lungs mixes with the deoxygenated blood of the systemic venous return.

The stage 2 surgery is usually performed about six months after stage 1, when the lungs are sufficiently developed, reducing PVR. The goal of stage 2 is to reduce the mixing of oxygenated and deoxygenated blood by diverting only the venous return from the upper body to the lungs (Glenn, 1965). In the stage 2 surgery, referring to the upper right subfigure in Figure 2, the shunt is removed and the superior vena cava is attached to the pulmonary artery directly through the Glenn connection, so only deoxygenated blood from the lower body enters the atrium. Removing the shunt also restores the volumetric load on the single ventricle to a natural value.

The stage 3 surgery is usually performed at about 18 to 36 months after stage 2. By that time, the lower body portion of systemic blood flow has increased, and the lungs are mature enough that the PVR is low, requiring less pressure to drive pulmonary flow. The goal of stage 3 surgery is to stop the mixing of oxygenated and deoxygenated blood by diverting the lower body systemic venous return directly to the lungs. Referring to the lower subfigure of Figure 2, the inferior vena cava is surgically connected to the pulmonary artery, directing the deoxygenated blood to the lungs. Then, all deoxygenated blood flows passively through the lungs (Fontan, 1971).

In essence the circulation path has been restored to a normal serial path, but without the benefit of the right ventricle.

The stage 1 surgery

The purpose of the stage 1 surgery is to create an unrestrictive systemic blood flow and, at the same time, attempt to balance the pulmonary flow with the systemic flow, the Q_p/Q_s ratio.

Through the past decades, the most prevalent way to achieve these goals is the Norwood procedure. The main pulmonary (aorta?) artery is dissected from the pulmonary artery root. The root is used to reconstruct a neoaorta, and then a cardiopulmonary shunt is created to connect the aorta to the main pulmonary artery. The shunt diameter is designed to provide the correct pulmonary blood flow, balanced with the systemic flow. Figure 1.3 illustrates the procedure's outcome, creating parallel pulmonary and systemic circulations (Pennati, 2010). Systemic vascular resistance (SVR) and pulmonary vascular resistance (PVR) must be carefully manipulated to achieve a balanced circulation with adequate systemic oxygen delivery. Since both the systemic and pulmonary circulation are supplied by the single ventricle, the relative distribution of blood flow to the systemic and pulmonary circulations is determined by their relative resistances.

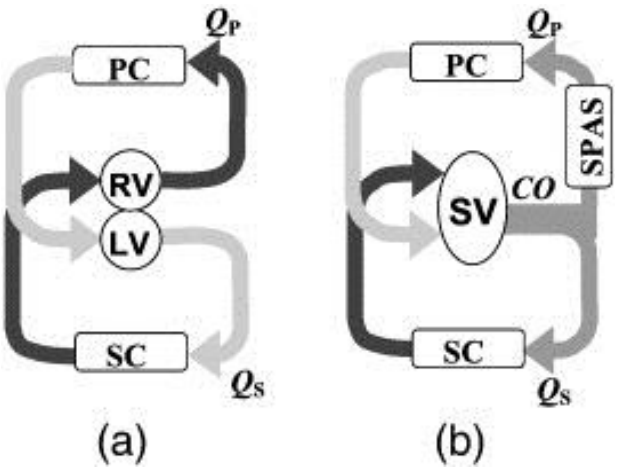

Figure 1.3. Comparison of (a) normal circulation and (b) stage 1 reconstructed parallel systemic and pulmonary circulation. RV= Right ventricle, LV = left ventricle, PC= pulmonary circulation, SC= systemic circulation, SPAS= systemic to pulmonary artery shunt. (Pennati, 2010)

There are several variations of the stage 1 surgery. Figure 1.4 illustrates the most prevalent configurations for the placement of the shunt in the stage 1 surgery. (Pennati, 2010) (Tomoyasu, 2009).

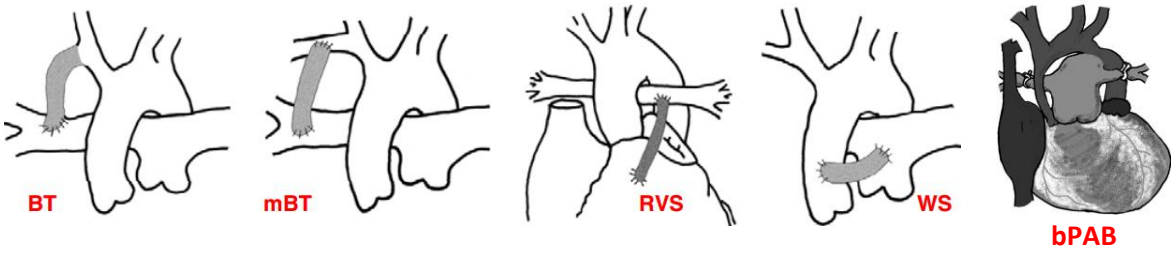

Figure 1.4. Variations in stage 1 procedure, BT denotes a BT shunt, mBT denotes an mBT shunt, RVS denotes a right ventricle shunt and WS denotes a Waterson shunt or central shunt, and bPAB denotes bilateral Pulmonary Artery Banding. (Pennati, 2010)

The BT shunt, initially reported in 1945 to treat tetralogy of Fallot, was named after its developers Blalock and Taussig. As shown in Figure 1.4 (left), the original procedure proposed was to cut one branch of the subclavian artery or carotid artery, and connect the cut end directly to the pulmonary artery, forming a shunt

(Blalock, 1945). However, the drawback of the BT shunt is that the cut artery completely interrupts some blood supply to the upper body. With the introduction of polytetrafluoroethylene (PTFE) as a biomaterial into practice, the modified BT shunt (mBT shunt) technique was developed. Illustrated in Figure 1.4 (second left), a non-valved shunt made of PTFE is sewn into place between either the subclavian or the carotid artery, and the corresponding side branch of the pulmonary artery (Moulton, 1985). The mBT shunt physiology is characterized by high pulse pressure and diastolic runoff. This reduces diastolic coronary circulation, and is implicated in blood "stealing" from the systemic arteries, especially the individual artery to which the shunt is attached.

A Waterson shunt (WS) (second right in Figure 1.4), or Central shunt, was reported in 1961 as an approach to treat tetralogy of Fallot (Waterson, 1961). The WS is composed of a conduit installed between the ascending aorta and the main pulmonary artery as shown in Figure 1.4 (second from right), thus resulting in a more balanced flow distribution between the two pulmonary arteries. It is also considered as an alternative for a neonate with a small subclavian artery.

A right ventricle shunt (RVS), also known as a Sano shunt, is constructed with a PTFE non-valved conduit between the right ventricle and the right pulmonary artery, as shown in Figure 1.4 (center). Compared with the mBT shunt, the RVS is usually larger in diameter. It provides a more pulsatile pulmonary blood flow and, at the same time, a less pulsatile systemic blood flow with less diastolic pressure runoff. It obviates the reduced diastolic blood flow in the coronary circulation associated with the mBT shunt. (Sano, 2003) The concept was first presented by Norwood et al.

Norwood et al described it as “placement of valved or non-valved conduit from the right ventricular outflow tract to the distal main pulmonary” (Norwood, 1981).

Bilateral Pulmonary Artery Banding (bPAB) is another option for Stage 1 Surgery. bPAB was first proposed by Muller et al in 1952 as a successful case report (Muller, 1952). The goal of bPAB is to reduce the pulmonary artery pressure and excess pulmonary blood flow. As illustrated in Figure 1.4 (right), the surgical technique to achieve this is to install a band around the one or both sides of the pulmonary artery to reduce blood flow into the lungs, preventing pulmonary over-circulation, thus regulating the balance of Q_p/Q_s. The limitation of this technique is that resistance of the banded location is very sensitive to the tightness of the band, so it is very difficult to achieve the optimal tightness, thus to achieve the desired balance of pressures and flows. It is only applicable where there remains a sufficient aorta to provide systemic circulation, or else the ductus arteriosus can be kept patent.

The advantages of the various stage 1 configurations are always debated among surgeons, especially the comparison of the most prevalent RVS and mBT shunts. Till today, it is very hard to say which option is better.

In the 2000s, for the first time, some nonrandomized studies reported some short-term advantages of RVS compared with mBT shunts (Ohye, 2007) (Mahle, 2003) (Mair, 2003) (Sano, 2003), which triggered the interest for more RVS research. Among these studies, the most representative one is Sano et al’s study. In Sano’s study, significant improvement in both long term and short-term RVS patient survival rates compared with mBT patient survival rates was observed. In particular, aortic

diastolic runoff into pulmonary circulation was eliminated with RVS. Hence the diastolic pressure was restored, systolic hypertension was relieved, and ventricular work was reduced. Also worth noting, Sano et al's study achieved very successful results with low weight patients (<2kg), and hemodynamic instabilities never occurred in the initial nineteen patients. Sano et al also pointed out that even one might argue that the drawback of RVS is that the non-valved shunt allows diastolic retrograde flow. Since stage 1 patients are very small and experiencing fast growing, it has been observed that the diastolic reverse flow decreased and trans-conduit pressure increased in the months after the procedure (Sano, 2003). In a larger clinical study, based on a sample of 275 mBT shunts and 274 RVS shunts from 15 clinical centers all across America, and using the transplant-free survival at 12 months as the criterion, patients with RVS shunts were healthier than patients with mBT shunts.

On the other hand, one can intuitively argue that RVS is more invasive because it requires an incision on the ventricle. Also, a clinical study was conducted to compare the interventions after Norwood Procedure using Sano vs. mBT shunt. Based on the sample size of 37 Sano shunt and 70 mBT shunt patients, it was found that significantly more interventions were required with the Sano shunt, whose complications included closure of the femoral or subclavian veins, cerebral embolic or bleeding events, and cardiopulmonary resuscitation (Fischbach, 2013).

Complicated physiological changes also make the Norwood surgery difficult. Neonate's PVR decreases rapidly during the first few months of life due to the development of lungs. This phenomenon results in decreased systemic flow rates and increased pulmonary flow rate. Eventually these changes can cause unbalanced Q_p/Q_s

in the Norwood circulation. Meanwhile, there is a large variety of native aortic arch morphologies and coarctations to be considered. The aortic arch morphology ranges from dilated to normal to tubular. Coarctation variation can range from localized coarctation to interrupted aortic arch. Additionally, shunt placement and surgical anastomosis design are also influential in the final surgical results.

In light of the aforementioned physiologies and pathologies, it has been realized that a multi-scale model of Norwood circulation should be developed to further the understanding of the Norwood circulation. The model should be tunable over a range of these global parameters, such as PVR and SVR. It should also be able to show the effect of geometrical changes, such as aortic coarctation and stenosis. Most importantly, it should be a responsive model where effects of physiological change on both local and global hemodynamics can be studied.

In the following paragraphs, a multi-scale patient-specific *in vitro* model of Norwood Circulation is presented to meet the aforementioned requirements. The model is a bench-top MCS which can be retuned within a workday. It is flexible to change so it can be adapted to research of different purposes. The model will be validated against clinical measurement to prove its reliability.

Aortic coarctation

Coarctation (COA) is derived from the Latin word ‘Coarctatio’, which means crowding or drawing together, fitting closely together, tightening. Coarctation of the aorta, or aortic coarctation, was first reported by Morgagni who described such an anomaly in an autopsy in 1760 (Morgagni, 1760). Paris was the first to describe the full pathological features around 1791 (Paris, 1791). However, the first surgical repair

of COA was not reported until 1945 by Crafoord and Nylin (Crafoord, 1945). Symptoms of the COA include exercise intolerance, headache, and shortness of breath, chest pain, nosebleeds, cold feet, and leg pain after exercise.

Aortic coarctation is defined as a narrowing of the aortic isthmus, which is between the left subclavian artery and the ductus arteriosus. It is different from an interrupted aorta, in which the aortic arch has a discontinued aortic wall, while aortic coarctation still has a continuous aortic wall (Lee, 2013). The morphology of COA can vary widely. The narrowing can be very localized and acute, or it can be very gradual and harmonious. This observation was first made by Bonnet when he distinguished coarctation into the "adult" type and the "infantile" type, which represent localized coarctation and long uniform segment respectively (Bonnet, 1903). Edwards et al later described the different types of COA in a more anatomical way. Edwards named the long segment of narrowing aortic arch as tubular hypoplasia, while the other morphology, a sharp localized stenosis, was defined as coarctation. Edwards also explained that it is because of a curtain-like enfolding of the aortic media into the lumen of aorta that forms a localized zone of stenosis. Tubular hypoplasia, on the other hand, has a normal aortic media (Edwards, 1965) (Edwards, 1948). Severity of the aortic coarctation is characterized by a non-dimensional parameter called Coarctation Index (CoI); it is defined by the diameter ratio of the narrowest part of coarctation to the descending aorta at the diaphragm.

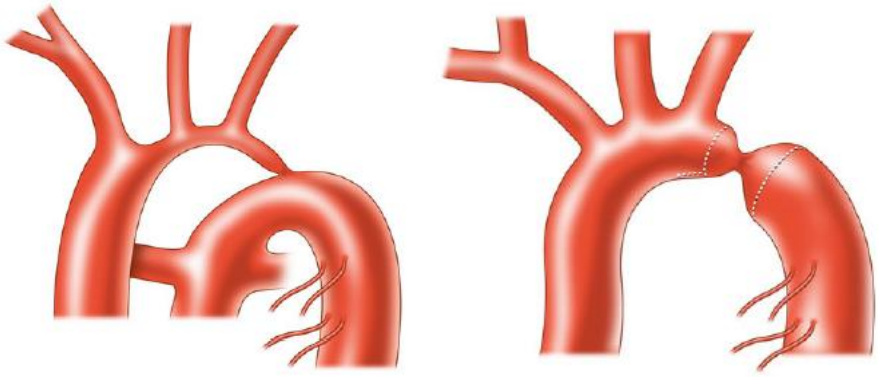

Figure 1.5 Morphologies variations of aortic coarctation, the left subfigure illustrates a very tubular aortic coarctation, the narrowing of aortic arch is uniform stretching from RSA to DA. The right subfigure illustrates a more localized morphology, aortic arch acutely narrows down just past LSA, and then morphs back to normal diameter (Da Cruz, 2013).

Each year 0.03% to 0.04% of live newborn infants suffer from COA (Hoffman, 2002). COA is represented in 7% of the anomalies in live new born infants with congenital heart defects and is more common in males than females (Samanek, 1999) (Campbell, 1961). COA is also very prevalent among patients with HLHS, occurring in more than 80% of newborns with HLHS. This can be attributed to the undeveloped ventricle not supplying sufficient blood to the aorta. The occurrence rate of COA between the staged surgeries, or in this case, the recurring neoaortic coarctation (NAO), is between 0-37%. NAO, as a frequent complication of Norwood Procedure, is one of the major reasons for high morbidity. Recall the key of Norwood Procedures is to achieve balanced pulmonary circulation and systemic circulation. NAO can cause reduced cardiac output (CO) and reduced descending aorta flow. It can also affect the upper body arteries flow and pulmonary shunt flow, upsetting the balance of systemic circulation to pulmonary circulation.

Whether the COA can be “cured” remains a controversial topic. Due to the excellent initial outcome of the repair at the early stage, some regard the result as good and permanent. However, others argue that it is clear that those patients go on to develop hypertension at early stage of life, which causes devastating consequences (Lee, 2013).

There are various types of techniques to diagnose and repair aortic coarctation and tubular hypoplasia, depending on the patient’s condition. Techniques used for COA diagnosis include: electrocardiogram (ECG), chest X-ray, echocardiography, chest computed tomography (CT or CAT) scan, Magnetic resonance imaging (MRI) of the chest, and cardiac catheterization. Among all these technique the most popular techniques are echocardiography and cardiac catheterization because these two examinations give physicians a direct measure of pressure gradient or pressure differential across the coarctation.

Figure 1.6. Pathology specimen demonstrating a section of aortic coarctation. (Edwards J. C., 1965)

There are also a spectrum of choices to treat aortic coarctation, which include end-to-end anastomosis (EEA), subclavian flap aorto-plasty (SFA), percutaneous balloon angioplasty and expandable endovascular stent.

In the HLHS patient, coarctation is normally corrected during stage 1 surgery. However, because the neoaorta was reconstructed during stage 1, there is still a very high chance, 11%-37%, of recurrent COA, NAO in this case (Go, 2014). For patients who underwent Norwood Procedure, the development of NAO can be lethal (Corsini, 2012).

It has long been recognized that COA can cause pressure drop in the lower body, increased pressure in the ascending aorta and decreased lower body flow. This is because the presence of COA or NAO is equivalent to increased LBSVR. Additionally, in Norwood Circulation, the presence of NAO can also disturb shunt flow and upper body flow. Severe NAO needs immediate surgical intervention. Mild and slight NAO often times does not have significant effect on the Norwood Circulation, and so surgical intervention is unnecessary. When to intervene surgically is a very difficult decision to make. Surgeons want to avoid unnecessary surgical intervention as neonate patients, at this point, just went through the Norwood Procedure and are usually very fragile. On the other hand, surgeons fear the risks that are caused by not correcting NAO surgically. Coarctation severity index (CoI) has been the rule of thumb when it comes to the decision of intervening a NAO surgically or not.

However, in a recent unpublished clinical study, clinicians in Great Ormond Street Hospital in London UK found that Norwood patients with different aortic arch morphologies tend to respond differently to narrowing coarctation (COA) (Giardini A.). For example, coarctation severity does not seem to directly predict Single Ventricular Power (SVP) change. Some patients with very low CoI (severe COA) in a

tubular aortic arch show little increase of ventricular power change and pressure gradient with additional narrowing. Conversely, ventricular power increase in patients with dilated arch tends to be more rapid than in those with tubular arch. This observation makes coarctation treatment planning even trickier.

This clinical hypothesis has not been validated due to the difficulty of monitoring the pressure gradient across NAO precisely with the development of NAO, and it is even more difficult to precisely examine the global hemodynamic response to NAO clinically. Hence, *in vitro* modeling may help to validate the hypothesis and understand the hemodynamics of these cases.

Background and methods of *in vitro* multi-scale patient-specific study

There are three basic realms in which hemodynamics can be studied: *in vivo*, *in vitro* and *in silico*. *In vivo* methods involves taking necessary vital measurements on a living human or animal subject, *in vitro* method means running tests on a fully characterized mechanical system with known parameters under a highly controllable laboratory environment, and *in silico* means numerical simulation and modeling on a computer. When testing clinical hypotheses, the best choice of obtaining meaningful measurements is *in vivo* study, for it is conducted under the native physiological environment (Camp, 2009). However the disadvantages of *in vivo* study are that it is dangerous to perform, expensive and unethical, and limited in number. These drawbacks call for the need to build a less expensive, compact, and easy to use *in vitro* system or *in silico* model, making a large number of experimental runs practical.

When designing a model either *in vitro* or *in silico*, there is the common problem of scale. Fluid mechanics in a test section naturally concerns fine spatial resolution, down to the Kolmogorov scale. It is completely impractical to model the entire living body at this level of detail, when only pressure and flow boundary conditions are required for the test section. However, in any medical study, the main question is how the test section, such as an anastomosis site or a shunt, or a device such as a check valve, will interact with the body. One solution is to use a system of time-varying ordinary differential equations to represent the pressures and flows of the several districts of the body as lumped parameters with no spatial resolution, thus providing a zero-dimensional or 0D model. Concurrently, a three-dimensional or 3D model of the surgical site is developed and the equations of motion, a set of partial differential equations, solved. The pressure and flow rate variables in the 0D model are then coupled with the inflow and outflow boundary conditions of the 3D model. This coupling of a 0D LPN to a 3D fluid test section is termed "multi-scale" or "multi-domain" (Migliavacca, 2005). The LPN addresses the systems-level pressures and flows throughout the circulation. The evolving fluid dynamics in the test section address the fine-scale local-level details of flow in the 3D domain to answer questions such as wall shear stress, stagnation zones, or specific pressure gradients. The exchange of information between models determines the time-based solutions. The resulting flows and pressures at the boundaries feed back into the LPN via the inlet and outlet boundaries. This feedback is the hallmark of the multi-scale strategy. A well-designed LPN will not only create the expected baseline conditions for the 3D section, but will also respond with the correct sensitivity to changes in flow through

the 3D section. Thus, a multi-scale hemodynamics model can predict how an experimental vasculature or flow device will perform in the dynamic environment of a patient's body.

The various elemental values, which are the "parameters" of the LPN, can be set to generic (or common) values for a patient of a given body area size, to produce predictive results, or they can be tuned to match as much specific clinical information as is available for a given patient. Setting these parameters is not necessarily easy. The values of parameters such as resistance, inertia and compliance of complex shaped vessels cannot be measured directly in the clinic, only estimated from available pressure and flow data. Likewise, the test section can be designed either with a generic three-dimensional shape of the surgical site, or it can be made patient-specific using MRI, CT, or other imaging data from the patient's own anatomy. The uniqueness of patient-specific physiologies affects surgical outcomes significantly. (Hornik, 2011).

Figure 1.7a shows an example schematic of a multi-scale model for the Norwood circulation, in the electrical circuit analogy style. The flow resistance and volumetric compliance elements of a LPN are conveniently represented using electrical resistance and capacitance symbols. The test section (aortic arch) geometry was taken from MRI of a pre-Glenn patient in London (Biglino, 2012). Figure 1.7b shows a schematic of the same model in the "plumbed" style within a mock circulatory system, using adjustable valves for flow resistance and compressible air chambers for compliance. This *in vitro* patient-specific mock circulatory system (MCS) illustrates a multi-scale scheme. It is based on practical representation of the

overall circulation as 0D lumped parameter networks (LPN) made up of plumbing parts, and patient-specific 3D models of the test section, which is the blood volume at the site of the anastomosis, shunt, or other intervention. Three-dimensional test sections, called phantoms, of varying shapes can be built by rapid prototyping technology from the prepared imaging files and inserted directly into the MCS test loop. The LPN can be retuned to match the desired conditions of the simulation.

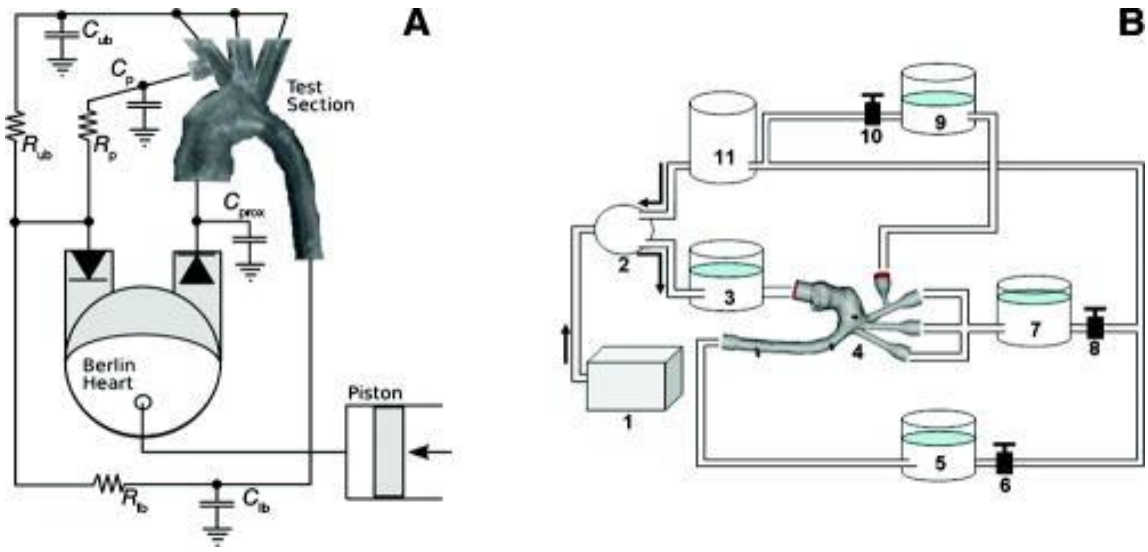

Figure 1.7. A: schematic of reduced lumped parameter network model used for the mock circulatory system and measurement points used throughout the system. A: Electrical schematic of the circuit, where C_{prox} = proximal compliance, C_{ub} = upper body compliance, R_{ub} = upper body resistance, C_p = pulmonary compliance, R_p = pulmonary resistance, C_{lb} = lower body compliance, and R_{lb} = lower body resistance. B: Plumbing schematic representation of the circuit, showing (1) the PC-controlled piston, (2) Berlin Heart, (3) C_{prox}, (4) test section, (5) C_{lb}, (6) R_{lb}, (7) C_{ub}, (8) R_{ub}, (9) C_p, (10) R_p, (11) atrial chamber (Biglino, 2012).

State of the art stage 1 palliation modeling

The previous modeling of stage 1 palliation is limited compared to stage 3 and stage 2 modeling due to the unique pathology in each case, and difficulties with the complex fluid dynamics in the shunt (Corsini, 2012). Biglino et al provides a detailed review of the engineering tools to study the first stage palliation of HLHS (Biglino,

2013). Also, Pennati et al provided a comprehensive literature review regarding the methodology of modeling systemic to pulmonary shunts in newborns with HLHS (Pennati, 2010).

In silico models were developed during the past decades to study the Norwood circulation. The first attempts to model Norwood circulation dates back to 1994 when Barnea et al described an analytical model to model the whole cardiovascular system. Barnea and colleagues developed two mathematical models at 1994 and 1998 to investigate the effect of distribution of flow between systemic circulation and pulmonary circulation on systemic oxygen delivery in neonates with HLHS. Barnea applied simple theoretical analysis, finding that the pulmonary to systemic flow ratio Q_p/Q_s is associated with systemic arterial oxygen availability (Barnea, 1994) (Barnea, 1998). Later on, 3D CFD models were developed by several groups. Migliavacca et al developed a 3D realistic CFD model to study the effect of shunt size on pressure drop and flow change across the shunt (Migliavacca, 2000). Song et al described a 3D simplified CFD model to study the effect of shunt size change on energy loss (Song, 2001). Waniewski et al. developed a 3D realistic model of the left subclavian artery (LSA), the left pulmonary artery (LPA), and the mBT shunt to study the effect of shunt size (3 and 4 mm) and shunt shape (straight and curved) on the wall shear rates (Waniewski, 2005). Malota et al developed a 3D realistic CFD model of the LSA, the LPA, and the mBT shunt to study the effect of an axial pump into the mBT shunt, and the effect of size on the pressure gradient and flow across the shunt (Małota, 2007).

These early studies were all limited by the fact that those models, although providing very detailed local or global hemodynamics, cannot be used to describe the

effect of changing body variables such as SVR on the local or global hemodynamics; they lacked the feedback to the remainder of the circulation. The first attempt to break this limit is made by Migliavacca and colleagues in 2001, they presented a 0D lumped parameter model to simulate the whole cardiovascular system in order to investigate how changes of shunt size, PVR, and SVR could change the flow and pressures throughout the BT shunt (Migliavacca, 2001). This multi scale modeling method overcomes the limitation of previous models by coupling the shunt hydraulic behavior to the response of the whole system. Pennati et al published a study using the same method of 0D LPN modeling to study the PVR and shunt size's effect on the pressure gradient across the shunt in the same year.

Laganà et al first coupled the 0D LPN of circulation and the 3D model of a shunt in order to compare the coronary and pulmonary flow in a central shunt with an mBT configuration with three shunt sizes (Laganà, 2005). They found that average shunt flow rate is relatively higher for the central shunt option. And also, as expected, shunt flow increase as the shunt size increase. After that, several studies have been published using the multi-scale method. Migliavcca et al., using a 0D-3D coupled multi-scale method, developed a model of the whole cardiovascular system to study the effect of shunt size and different surgical techniques on the right ventricle's Pressure-Volume (PV) loop (Migliavacca, 2005). Bove et al., using a method similar to Migliavacca's, developed a 3D-0D coupled multi-scale model and validated the computational results against clinical measurements, in order to investigate the how different surgical techniques would change the ventricular performance in addition to pulmonary and coronary perfusion (Bove, 2007). Hsia et al. developed a 3D-0D

coupled model of Norwood circulation with a 5-mm RV-PA shunt, a RV-PA shunt with 3- or 2-mm stenosis at the RV anastomosis, a stenotic RV-PA shunt plus a 3.0- or 3.5-mm mBT shunt, or a 3.5-mm mBT shunt, in order to discuss the different cases' effects on hemodynamics. It was found that proximal stenosis of the RV-PA shunt results in decreased pulmonary blood flow, total CO, and oxygen delivery. Addition of a 3.0- or 3.5-mm mBT shunt causes pulmonary overcirculation, lowers systemic oxygen delivery, and decreases coronary perfusion pressure. Diastolic runoff through the stenotic RV-PA shunt increases retrograde flow back into the single ventricle (Hsia, 2009). Corsini et al. used a 3D-0D coupled multi-scale model of the whole cardiovascular system to simulate the hybrid stage 1 circulation with stented ductus arteriosus and banded pulmonary arteries. The effects of changing degrees of pulmonary banding and different stent sizes on Q_p/Q_s flow ratio, CO, and oxygen delivery were assessed. It was found in this study that balanced systemic and pulmonary blood flow is strongly associated with the degree of pulmonary arterial banding but not with the size of the ductal stent (Corsini, 2011).

Physical experimental models have also been developed for the purpose of validating clinical hypothesis and CFD models. Models usually take the form of MCS and can be of different complexity according to different purposes of the test.

The first attempt of *in vitro* modeling stage 1 palliation dates back to 1998, a pulsatile flow model was developed by Tacy et al to evaluate pressure gradient across the modified Blalock-Taussig shunt. This paralleled systemic and pulmonary circulation flow model included a pulsatile flow generator, Gore-Text BT shunt, and multiple flow resistor and compactor. The purpose of this study was to compare the

actual pressure gradient measured *in vitro* against those predicted using Echo Doppler probe for various shunt sizes. This study showed that good agreement between Doppler predicted pressure gradient and measured pressure gradient only occurs when shunt diameter is >5mm. Otherwise, Doppler predicted pressure gradient underestimates the *in vitro* measured actual pressure gradient (Tacy, 1998). A later study conducted by DeGroff et al focused on the same topic using a similar method. DeGroff et al developed a pulsatile flow model similar to Tacy et al, and a numerical model to study the accuracy of Doppler predicted pressure gradient under different scenarios: inlet stenosis shunt, diffusive stenosis shunt, outlet stenosis shunt, and no stenosis shunt. This study used both numerical method and *in vitro* method to confirm that Doppler predicted pressure gradients underestimates actual pressure gradients at high pressure gradient region for all shunt configurations (DeGroff, 2000).

Pennati et al developed an *in vitro* flow model to study the flow and pressure relationships in mBT shunts. This model used Gore-Tex shunts and compliant tubes to account for the distensibility of vessels, and also realistic surgical anastomoses were realized in the flow model. This study showed that pulmonary artery pressure change could affect the pressure flow relationship; this effect is significant at distal site. However the total pressure drop is not affected by the changes of pulmonary pressure. Effect of surgical anastomoses sites was investigated in this study; surgical anastomoses could cause cross section reduction at the site of suture, and should be taken into account in the future (Pennati, 2001). Bakir et al looked into vascular resistance-flow relationship using an *in vitro* model. This flow model used a ventricular assist device (VAD) to generate pulsatile flow, and was tested over a

range of pulmonary vascular resistance (Bakir, 2006). Biglino et al developed a MCS with a patient-specific approach to investigating HLHS physiology. Patient specific neoaortic morphology was obtained using cardiovascular magnetic resonance (CMR), and was made using modern 3D printing technology. The pulsatile flow was powered by a VAD driven by a computer-controlled hydraulic pump, and multiple resistive and compliant flow elements were employed around a 3D printed patient-specific neoaortic anatomic model to model the circulation of Norwood patients (Biglino, 2012). The model was initially developed to study the circulation of a Norwood patient, in which the mBT shunt was a non-valved conduit branching off from the innominate artery. Later the model was modified so it can also be used to study the circulation of a Norwood patient with a Sano shunt by directing a portion of fluid from the VAD to the pulmonary branch (Biglino, 2013). Such a MCS uses a multi-scale method that combines the 3D neoaortic model and 0D vascular LPN model, so it can be used to study the local fluid mechanics and as well as global hemodynamics of Norwood patients.

State of the art aortic coarctation modeling

Though modeling of the COA is more recent compared to the modeling of Norwood circulation, many *in vitro* and *in silico* COA studies have been published during the last decade. LaDisa et al published a literature review of recent methods of evaluating COA both computationally and experimentally (Ladisa, 2010). Like modeling of stage 1 palliation, various methods have been applied to model COA ranging from 0D LPN, idealized *in vitro* models, 3D simplified and realistic CFD models, multi-scale 0D 3D coupled models, and currently reaching the patient-specific modeling level.

In an early attempt to model aortic COA, De Mey et al. set up an idealized *in vitro* model to validate the clinical hypothesis that, even after successful repair of coarctation, Doppler derived pressure differences is still high without significant arm-leg pressure differences. De Mey combined *in vivo* patient and control data, and an *in vitro* hydraulic model, finding that the reliability of Echo Doppler is doubtful when evaluating the post-operation coarctation patients (De Mey, 2001). Subsequently, a simplified 3D CFD model of aorta and pulmonary arteries was generated by Pekkan et al. to study the embryonic aortic arch at late gestation. An *in vitro* validation accompanied this computational study to validate the computational results that large-scale recirculating flow exists in the aortic arch proximal to the ductus arteriosus (DA) (Pekkan, 2008).

As pointed out by De Mey et al. at 2001 and several previous clinical studies (Seifert, 1999) (Barth, 1987) (Marx, 1986) (Sharma, 1992), the accuracy of Echo Doppler prediction has always been an interest of the researchers. Baumgartner et al developed an *in vitro* study concerning the effect of stenosis geometry on the Doppler-catheter gradient relation. Stenoses of various geometries were simultaneously studied with Doppler and catheter pullback. Doppler predicted pressure gradient was compared with catheter measured pressure gradient for each case. They found, in the case of the highest gradients across flow obstructions that occur in the vena contracta, that Doppler predicted gradients have good agreement with catheter measurements. However, these gradients are significantly greater than catheter gradients that are measured farther downstream, due to pressure recovery. In an important finding, the overestimation phenomenon is most likely to be

considered clinically significant with a stenosis shaped like a gradually tapering inlet and outlet with an outflow angle greater or equal to 20 degrees (Baumgartner, 1993).

Giardini et al described a steady flow model with simplified COA model of different length and diameter in order to compare the Doppler predicted pressure gradients and *in vitro* catheter measured results (Giardini, 2010). This study found out that Doppler overestimates actual pressure gradient at the high pressure gradient region. Figliola et al used a similar method to assess the accuracy of Doppler predicted pressure gradient in stage 1 circulation with varying COA (Figliola, 2010). Keshavarz-Motamed et al. developed an *in vitro* multi-scale modeling 0D 3D coupled model and a 0D LPN to evaluate the severity of aortic coarctation, suggesting two new parameters: COA Doppler velocity index and COA effective orifice area, instead of the current prevalent criteria, coarctation index. The model provided was validated by *in vitro* measurements and clinical measurements (Keshavarz-Motamed, 2012) (Keshavarz-Motamed, 2011). Concerning the COA's impact on the left ventricle work load, Keshavarz-Motamed et al also used their model to assess the PV loop of the left ventricle, investigating the extra ventricular work due to COA.

During recent years, the development of MRI and MRA made patient-specific studies of COA possible. Multiple studies used MRI or MRA technology to obtain patient-specific anatomy of the aorta, and then conduct *in vitro* or *in silico* studies. Kim et al. developed a multi-scale *in silico* model with 0D LPN coupling with 3D patient-specific model. This CFD model concerns several scenarios including a normal human thoracic aorta under rest and exercise conditions, and an aortic coarctation model under pre- and post-interventions. The results of this study

demonstrated pressure and flow at various sites of the aorta and also evaluated ventricle function by constructing a PV loop from the LPN. Velocity fields within the domain of aorta, and mean wall shear stress of the aortic wall are also assessed in this study (Kim, 2009). LaDisa et al. expanded the model developed by Kim et al. and conducted two *in silico* studies. One study looks into the alteration of wall shear stress in aortic coarctation patients after being treated by resection with end-to-end anastomosis. The models are 3D patient-specific CFD models, with anatomy of the aorta extracted from imaging and blood pressure data for both COA patients and control groups. CFD analysis incorporated SVR and SVC in order to generate realistic blood flow velocity, time-averaged wall shear stress (TAWSS), and oscillatory shear index (OSI) results. Comparing the results of patients group and control group revealed several statistically significant local differences regarding TAWSS and OSI. Also, unique locations for plaque formation were identified (LaDisa, 2011). Another computational study published by LaDisa et al. used four patient-specific 3D CFD models. This study concerns the understanding of COA hemodynamic indices under resting and non-resting conditions, such as cyclic strain, TAWSS and OSI. They found that systolic BP increased and mean and peak ΔBP increased for the moderate native COA patient, and cyclic strain increased proximal to the coarctation for native CoA patients, but reduced throughout the aorta after treatment (LaDisa, 2011).

Biglino et al developed an *in vitro* 0D-3D coupled pulsatile MCS to model the stage 1 palliation circulation with an mBT shunt and aortic coarctation of three different severities (Biglino, 2012). Peak pressures right before COA, right after COA,

and distal to OCA were observed for three cases, demonstrating different degrees of pressure recovery. Change of global flow distribution caused by different severity of COA was also investigated in this study. Subsequently, Biglino et al. used similar methods and constructed a MCS for the stage 1 circulation with a Sano shunt (Biglino, 2013). Two test sections were employed in this study, a normal aortic arch and an aorta with coarctation. Effect of COA was successfully demonstrated. Next they used the *in vitro* patient-specific MCS described before to validate an *in silico* model, and to help make design decisions such as choosing appropriate CFD mesh and flow regime, and highlighting the importance of *in vitro* data (Biglino, 2014). Itu et al. published a study illustrating the process of *in silico* multi-scale modeling of aortic coarctation using a 0D-3D coupled model starting from extracting patient specific aorta anatomy from MRI. They constructed the model, applied the boundary and initial conditions, and eventually compared the *in silico* results with the *in vivo* results, which showed satisfactory correlation (Itu, 2013). Corsini et al. recently developed a multi-scale model investigating the effect of mBT shunt size and CoI on coronary perfusion after Norwood Operation. They found that simultaneous presence of a large shunt and severe coarctation can have adverse effect on coronary perfusion, and hypothesize that this could be the reason for poor clinical outcomes.

Limitations and future advances

Though the past decades saw a great development in modeling of the Norwood circulation and COA as stated in Sections 1.5 and 1.6, there are still limitations associated with current modeling studies (Pennati, 2010, Biglino, 2013).

1. Despite the emergence of the patient-specific model, most of the models now being used to study Norwood Circulation continue to be generic models. This is due to caution in performing the necessary interventional measurements, as well as the high cost of associated measurements. Unless a patient presents a need for intervention and the necessary measurements, they are not taken.
2. Patient specific values such as PVR and SVR are rarely realized in the models.
3. Previous global scale models are not capable of demonstrating the patient-specific arterial morphological effects, such as the effect of aortic arch morphology.
4. Previous 3D local scale studies are conducted predominantly by prescribing or enforcing boundary conditions. In those methods, there is no interaction of the test section/domain with the rest of the circulation.
5. Few COA studies focus on the effect of COA on the global or systems-level hemodynamics, especially for HLHS patients.

Research Objectives and Study Purpose

The research motivations are:

- Simulate the surgery using *in vitro* methods, develop therapies, and evaluate effectiveness.
- Improve understanding of the indications requiring intervention for neoaortic coarctation.
- Provide clinicians supporting information in choosing among surgical options.

In support of these motivations, the study specific aims are.

1. Replicate the Norwood circulation using an *in vitro* multi-scale model.

The aim is to generate cardinal physiological pressure and flow signals of Norwood circulation. A multi-scale *in vitro* patient specific model is built coupling an LPN network of the Norwood circulation around a 3D patient-specific aortic model. The system is tuned to patient specific R C values, and clinical values. Physiological flow rate and pressures measurements are made in the upper body, lower body, pulmonary system and aorta.

2. Validate the system's function using five patient cases having different morphologies.

The aim is to validate the multi-scale model using clinical measurements of flow rate and pressure. Five patients with different physiologies and morphologies are used. Statistical methods are applied to compare agreement between experimental and clinical measurements.

3. Study the system-level effects of coarctation on the hemodynamics of each patient with mBT shunt and differing aortic morphology.

The aim is to study the system-level hemodynamics responses to NAO narrowing. The severity of coarctation is progressively increased within the descending aorta for each patient. System-level changes are measured and ventricular power calculated for each case.

4. Compare systems-level response of mBT patients with the alternative RVS (Sano) procedure, including effects of coarctation severity.

The aim is to compare the system-level hemodynamic responses and ventricular power changes occurring between the mBT and RVS procedures among the five patient cases.

CHAPTER TWO

IN VITRO MULTI-SCALE PATIENT-SPECIFIC STAGE 1 MOCK SYSTEM

Three studies were conducted in order to achieve the aforementioned objectives and aims. This chapter discusses the research methods that were utilized in these three studies.

Selection of Patients and Anatomical Models

Five patients were identified and selected from clinical information collected from four medical centers under appropriate Institutional Review Board approvals (University of Michigan (UM), Great Ormond Street Hospital (GOSH), and Medical University of South Carolina (MUSC)). Four out of five patients had been diagnosed with HLHS and underwent a Norwood Procedure with mBT shunt. One patient had been diagnosed with Hypoplastic Right Heart Syndrome (HRHS) and underwent a Norwood Procedure with mBT shunt. The five patients each presented a different aortic morphology ranging from hypoplastic tubular to strongly dilated. Clinical measurements of the patients included ascending aortic pressure and pulmonary wedge pressure measurements by cardiac catheterization, mBT shunt flow and ascending aortic flow velocity measurements via either echo Doppler velocimetry or magnetic resonance. Clinical measurements of volumetric flow rate (Q) and blood pressure (BP) measurements of each case were used to assess local resistance and compliance values. Physiological characterization and clinical measurements are given in Table 2.1 in which patients are designated as MUSC7, GOSH22, MUSC2, UM5, and UM10. MUSC7 is the one with HRHS.

For each patient, a test section or phantom was created based on segmenting magnetic resonance (MR) imaging data. Commercial software (Mimics; Materialise NV, Leuven, Belgium) was used to prepare the virtual images for additive manufacture as previously described. (Schievano, 2007) The aortic arch, descending aorta, major superior arteries and shunt-brachiocephalic artery anastomosis were maintained patient-specific accurate. The coronary arteries were not modeled. The inlet to the aortic valve root was extended to provide for a connection to a heart pump. The phantoms were printed by stereolithography using a transparent rigid resin (Watershed XC 11122; DSM Somos, Elgin, IL). This transition is illustrated in Figure 2.1.

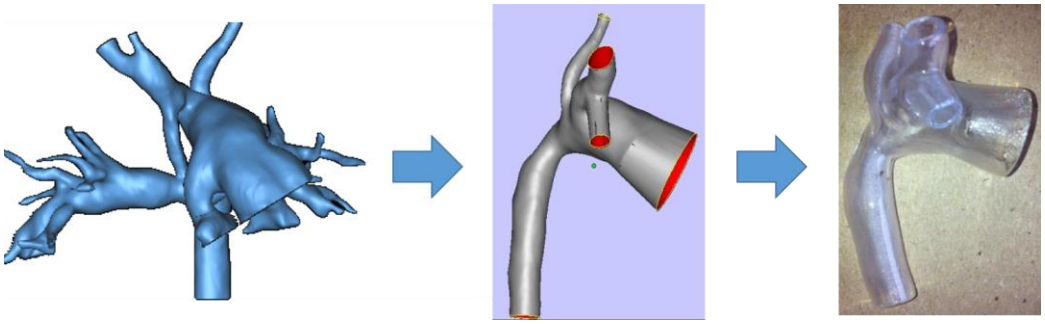

Figure 2.1 Aortic phantoms are constructed from 3D magnetic resonance image (left), prepared and manually modified using a commercial software in order to better fit the hoses (center), and then printed using 3D rapid manufacture.

The virtual models and resulting test sections are shown in Figure 2.2. Note that in Figure 9, noticeable extensions were built in from ascending aorta roots. The extensions are not physiological but were implemented for the purpose of better fitting the tubes.

Parameters	Patient Values				
	MUSC7	**GOSH22**	**MUSC2**	**UM5**	**UM10**
HR (bpm)	118	115	120	90	140
BSA (m^2)	0.26	0.27	0.3	0.28	0.34
Shunt Diameter (mm)	4.0	3.5	3.5	3.5	3.5
MAP (mm Hg)	51	50	56	54	73
SAP (mm Hg)	7	6	6	5.5	4
Q_p/Q_s	0.80	1.16	0.88	0.78	1.52
Q_{ub}/Q_{lb}	1.90	1.39	0.97	2.64	2.67
Native Coarctation severity	None	Slight	Slight	Moderate	Severe
Aortic arch morphology (TA/DD)	Very tubular (1.40)	Tubular (1.91)	Moderate (2.16)	Dilated (2.35)	Very Dilated (2.8)

Table 2.1 Physiological characterization and clinical summary of the 5 patients selected.

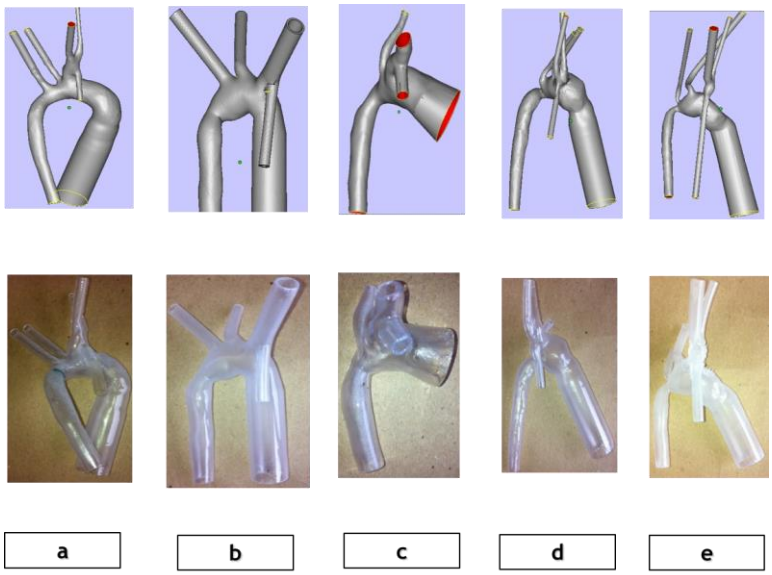

Figure 2.2 Aortic geometry of patients: (a) MUSC7, (b) GOSH22, (c) MUSC2, (d) UM5, and (e) UM10. The upper images are the blood volumes from MRI (with extensions added), and the lower photos show the actual test sections.

Mock Circulatory System Design

The mock circulatory system (MCS) of the Norwood circulation is a physical realization coupling an LPN of the circulation with an anatomically accurate, three-

dimensional (3D) test phantom of the neoaorta. A detailed multi-compartment LPN of the Norwood circulation was described by Hsia et al and applied here (Hsia, 2011). The LPN consists of three major circulation branches: upper body, lower body and pulmonary branch. This detailed model was reduced to a more practical level by using fewer elements through Thevenin impedance matching (Vukicevic, 2014) (Vukicevic, 2013), as depicted in Figure 2.3. Each branch is comprised of one distal resistance element and a compliance element (Westerhof, 2005). Inertance is realized by the mass of fluid. The system is tuned initially to a particular physiological state using generic reference values that are scaled using body surface area (BSA) for each impedance element, as previously described (Baretta, 2011), and then appropriate elemental values are adjusted based on available patient-specific clinical information. The MCS shows modifications from the previous study (Biglino, 2012): each superior artery is coupled with its own compliance element, each test phantom and system setup uses known clinical patient data. Flow rates and pressures measured throughout the circuit reflect these changes.

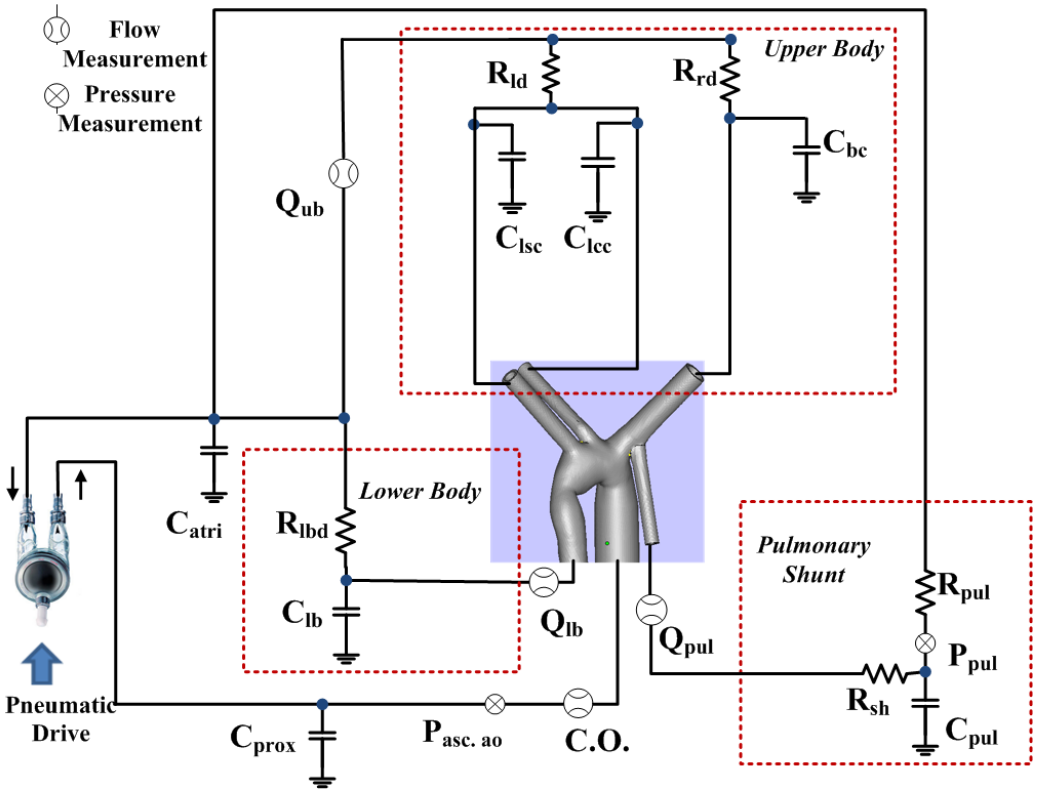

Figure 2.3 Reduced lumped parameter network model used for mock circulatory system with measurements points shown. R, resistance; C, compliance; P, pressure; Q, flow rate; C.O., cardio output; asc.ao, ascending aorta; prox, proximal; pul, pulmonary; sh, shunt; lb, lower body; atri, atrium; bc, brachiocephalic artery; lcc, left common carotid artery; lsc, left subclavian artery; l, left upper body vein; r, right upper body vein; d, distal resistance.

Figure 2.4 shows the physical MCS equivalent to the schematics in Figure 2.3. As seen, the lengths of tubing were minimized in order to reduce parasitic inertance, that is, the added inertance due to the experimental set-up connections as compared with the actual inertance in the infant patient.

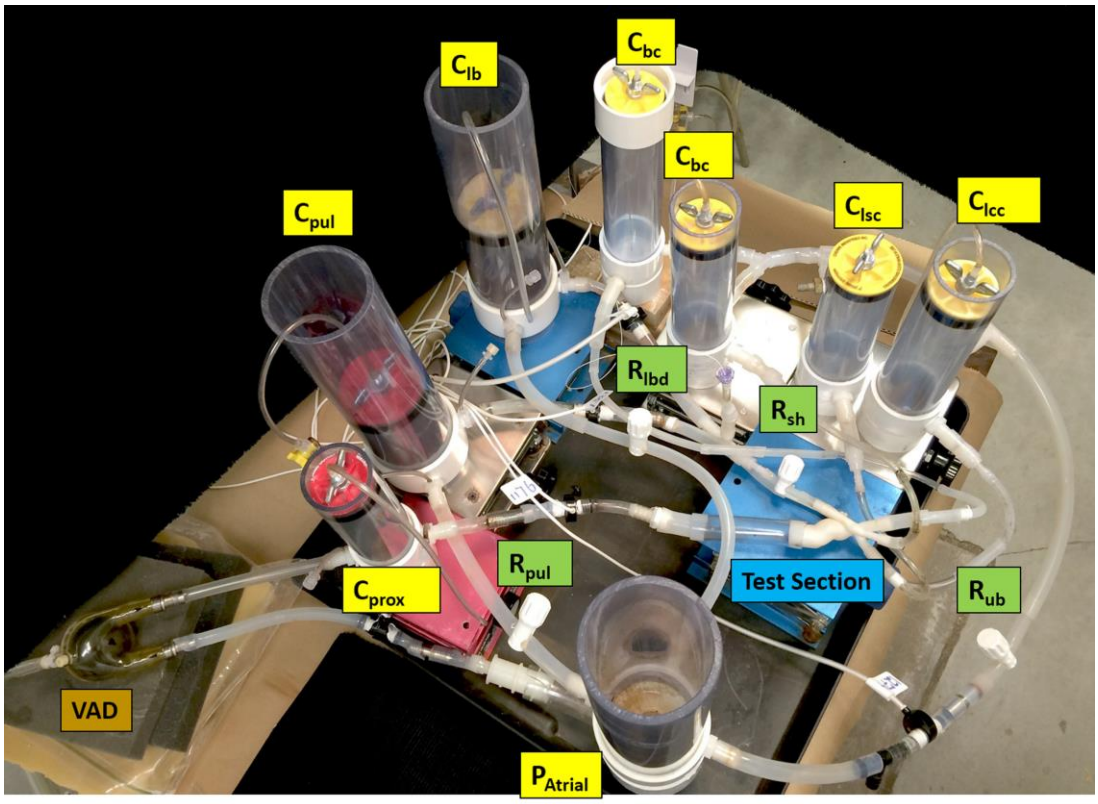

Figure 2.4. The bench top stage 1 Norwood palliation MCS shown is a physical realization of the model described in Figure 2.3.

Pulsatile flow pump: Ventricular Assis Device (VAD)

A ventricular-assist device (VAD) (Excor®, Berlin Heart 25 cc, Berlin, Germany) was used to develop the pulsatile aortic pressure and drive the cardiac output fulfilling the role of the single ventricle heart. This VAD consists of two sides: a blood filled side and an air filled side, separated by a flexible membrane. The VAD was driven pneumatically under computer control: high pressure is applied during systole and a small vacuum pressure is applied during diastole. High side compressed air is regulated to a desired pressure using a pneumatic needle valve. Vacuum pressure is regulated to a desired pressure using a piezo proportional pressure regulator (Type: PRE-U2, Hoerbiger, Schongau Germany). A 3 way valve (Model:

225B-111CAAA, MAC Valve, Dundee, MI, USA) was controlled by a computer and alternates between high air pressure and low air pressure. A computer generated 0-5V square wave was used to realize this alternating action in which high-level voltage (5V) to the 3-way valve allows high pressure to pass to the VAD, while low level voltage (0V) to the valve allowed low vacuum pressure to pass. The duration of high pressure to vacuum pressure within one heartbeat cycle determined the systolic ratio and the rate of each cycle determined the heart rate. The high pressure level and low pressure levels were adjusted to achieve the desired mean ascending aortic pressure while ensuring complete filling of the VAD. The VAD and its control system are shown in Figure 2.5. A sample of typical VAD air and liquid side pressure is shown in Figure 2.6.

Additionally, a proportional pressure regulator (Tecno-series, Hoerbiger, Germany) was tested to control high-side air pressure and could allow for automatic baroreceptor response (mean aortic pressure) or autoregulatory response (cardiac output) based on feedback from pressure transducers and flow rate probes. A proportional regulator sets its pressure regulation based on a supplied voltage signal, such as from the computer controller. This would introduce closed-loop control of the circuit. However, this feature was not used in the tests described later.

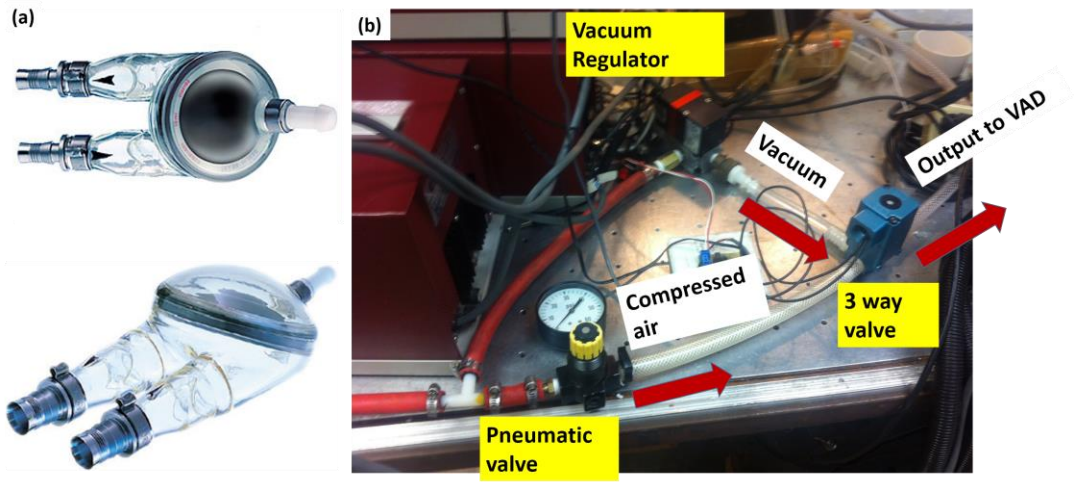

Figure 2.5. (a) Top view of the VAD (upper left) showing the air side and the isometric view of the VAD. (b) Driving system of the VAD.

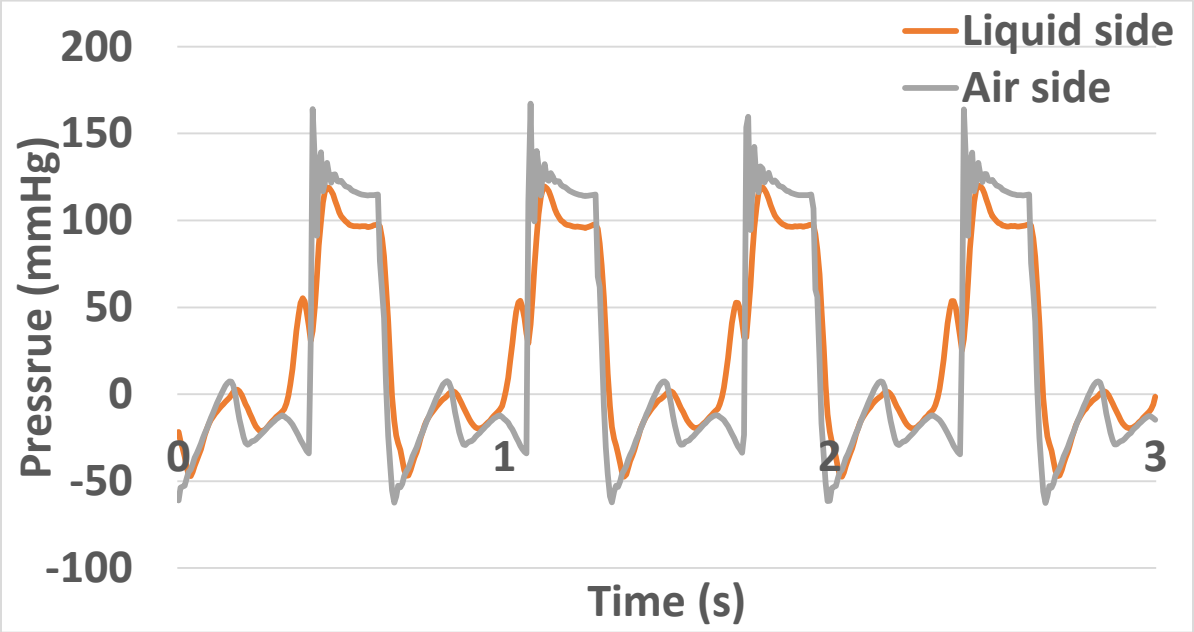

Figure 2.6. A sample of typical VAD air and liquid side pressure.

Resistive Elements

Each resistor (R) in the LPN network was realized using either a constant diameter tube or an adjustable needle pinch valve (Vukicevic, 2014). Figure 2.7 illustrates the usage of a reduced-diameter segment of tube and a pinch needle valve

in the system as resistive elements. Resistance value settings were confirmed under steady flow conditions based on pressure drop and flow rate. Resistance value control was confirmed using a steady flow condition based on $R = \frac{\Delta P^n}{Q}$, where n is 1 for laminar flows and n approaches ½ for turbulent flow through valves and stenosis. Given the low flow rates, nonlinearity was not a problem. The values for R_{shunt}, PVR UBSVR and LBSVR were calculated based on mean pressure and flow rate measurements as follows:

$$R_{shunt} = \frac{P_{Asc.Ao} - P_{pul}}{Q_{pul}} \quad (2.1)$$

$$PVR = \frac{P_{pul} - P_{atrium}}{Q_{pul}} \quad (2.2)$$

$$UBSVR = \frac{P_{Asc.Ao} - P_{atrium}}{Q_{ub}} \quad (2.3)$$

$$LBSVR = \frac{P_{Asc.Ao} - P_{atrium}}{Q_{lb}} \quad (2.4)$$

Resistances values used for each patient model are given in Table 2.2. The experimental resistance values are compared with their clinical references in Table 2.2, demonstrating the ability to closely match the patient-specific values.

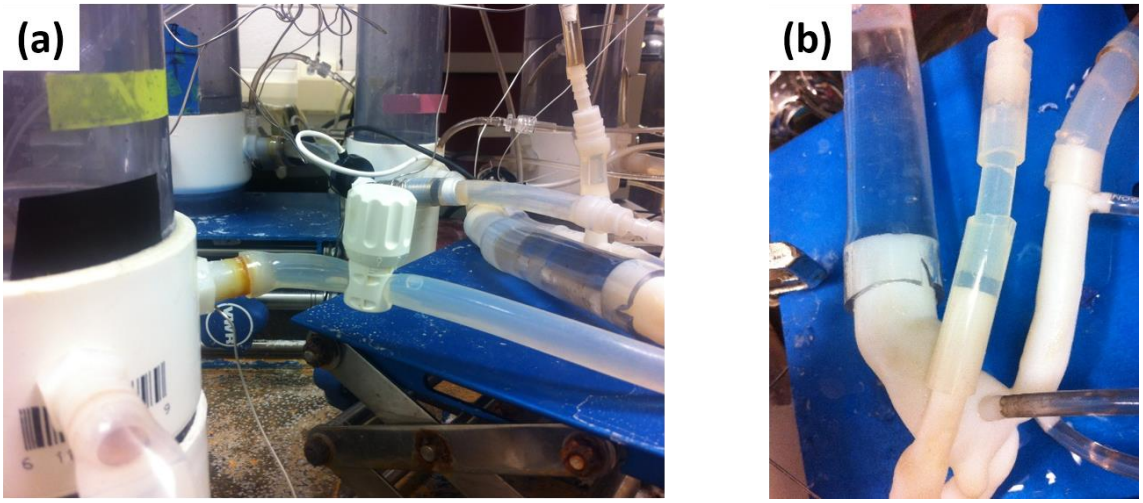

Figure 2.7 Use of (a) pinch needle valve and (b) hose in the system as resistive elements.

Compliant Elements

Air chambers were used as the compliance elements, where the compliance was provided by the compressibility of a predetermined volume of trapped air within a closed rigid cylinder (Vukicevic, 2014) (Vukicevic, 2013). The compliance value is calculated as $C = \frac{V}{P\ abs}$, in which V denotes the amount of air in the chamber, P_{abs} denotes the absolute pressure (working pressure) within the chamber. Such a rigid cylinder was made from a cylindrical acrylic tube, typically 50 to 75 mm in diameter, with one end closed off using a pipe cap and the other closed using a plumber's test plug (Oatey Corp, Cleveland, OH). The test plug could be moved to a position within the cylinder to achieve the desired air volume. Figure 2.8 illustrates an air chamber used in the system. Compliance values used for the tests are given in Table 2.2 for each patient model.

In order to compensate for the rigidity of the aortic phantom, a proximal aortic compliance air chamber was installed between the VAD and the phantom (Biglino, 2012). This technique enabled capturing the compliance of the aorta so as to enable a realistic ascending aortic pressure wave with realistic pulse pressure (i.e., the systolic to diastolic pressure).

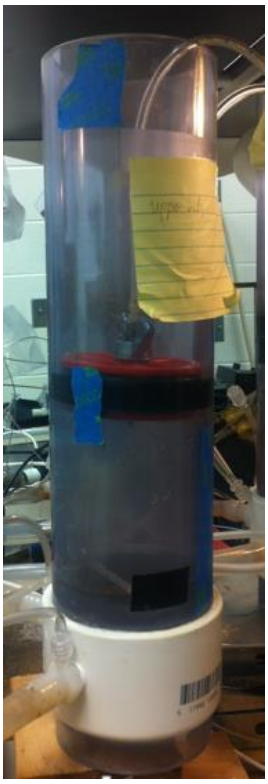

Figure 2.8: An air chamber in the system.

Atrial tank

Atrial pressure was set using a constant head tank. The atrial pressure was adjustable but maintained constant for each test case. The atrial head tank was made of a 100 mm diameter acrylic tank with a standpipe.

System Tuning and Setup

Preparation of the test bed for operation consists of tuning the LPN and setting the mean aortic and atrial pressures. The resistance elements of the LPN were adjusted to desired values under steady flow conditions by measuring pressure drop and flow rate across each corresponding branch of the system. The compliance elements were adjusted to the desired value by setting the correct liquid head pressure and air volume within each element. The atrium head tank was adjusted to attain the desired mean atrial pressure. The VAD air-side pressures were then adjusted to achieve the desired liquid-side mean aortic pressure. Lastly, the aortic compliance element was adjusted to achieve a desired pulse pressure.

Blood Analog Test Solution

Preliminary tests were conducted using a saline solution (30 cc per 4 L water) during setup and staging. A saline-glycerin blood analog was used (1060 kg/m^3, 3.3 x 10-6 m^2/s at 22^oC) during final tests.

Global Measurements

Measurement points for pressure and flow rate are indicated in Figure 2.3. Flow rates were measured with electromagnetic probes (P600 electromagnetic flow probes (P600 series, Carolina Medical Electronics, King, NC), each connected with its own flow meter control unit (Model FM501, Carolina Medical Electronics, King, NC). Calibration and zeroing of the flow measuring apparatus was conducted in zero flow condition per manufacturer's instructions. Ground wires were placed within the atrium head tank in order to stabilize the signals and reduce electrical noise.

Pressures were measured using either catheters or at wall taps connected to liquid-filled transducers (DTXplus, BD Medical Systems, Sandy, UT). Each pressure transducer was connected to a bridge amplifier (Model 2100, Measurements Group Inc., Raleigh, NC), which allowed for null adjustment and voltage amplification. The transducers have a stated sensitivity of 50 μV/mmHg. Calibration of each transducer and bridge system was confirmed by applying a known hydrostatic pressure to the sensor (literally, a known head of water provided by an elevated water-filled beaker) and using a two point pressure head calibration procedure.

All the date was acquired using a DAQ data acquisition system, which was comprised of a DAQ board and LabVIEW software (USB 6211, LabVIEW 8.6; National Instruments, Austin, TX), and measurements sampled at 160 Hz. A 0-5V square wave was generated from DAQ system to control the VAD 3-way valve, with the frequency and duty cycle of such square wave adjusted within LabVIEW. Figure 2.9 illustrates the architecture of the data acquisition system.

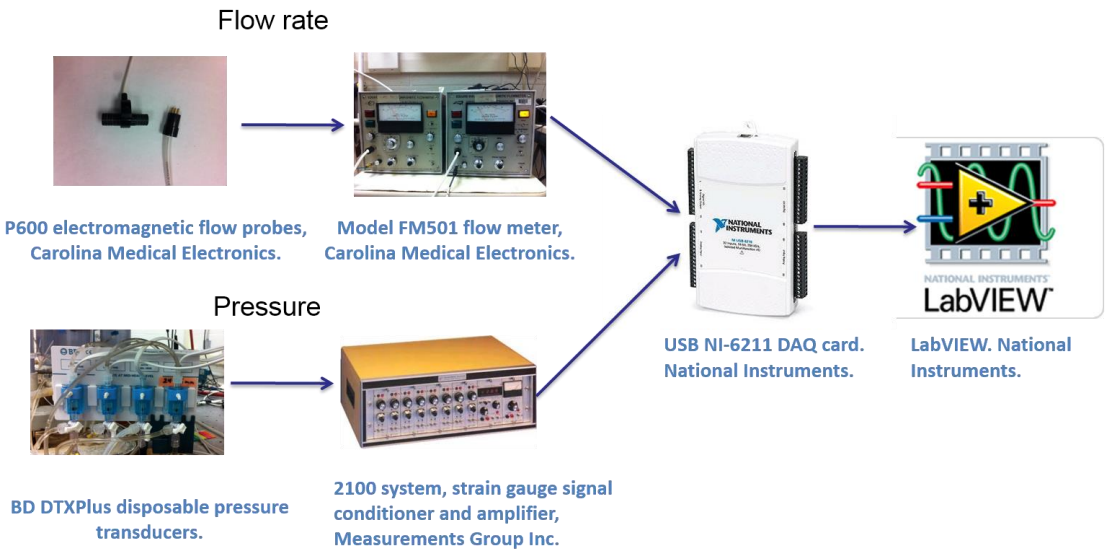

Figure 2.9: The architecture of the pressure measuring system, flow rate measuring system and data acquisition system.

For each patient case, compliance and resistance values were set under steady flow conditions and then mean aortic and atrial pressures, heart rate and systolic ratio were fixed to the clinical values (Table 2.2). The aortic proximal compliance was adjusted to minimize overshoot in the systolic pressure signal from the VAD. System-level measurements were recorded for each test case and statistical values determined over 25 contiguous cardiac cycles, a number deemed sufficient to achieve stationary mean values. Numerical trapezoidal integration was performed on all the flow and pressure data to calculate the mean flow rate using the equation shown above.

$$Q = \frac{1}{\Delta t}\sum_{i=1}^{n}\frac{(Q_i+Q_{i+1})\cdot(t_i+t_{i+1})}{2} \qquad (2.5)$$

Statistical Tests

Regression analysis was performed to quantify the agreement of clinical and experimental signals. For each time-based signal comparison, a scatter plot was made of the experimental data magnitudes versus the clinical data magnitudes at corresponding time points. Regression analysis ($y = x$) was then used to quantify the agreement and an R^2 value computed.

A paired *t* test was used to test for any statistically significant difference between the clinical and experimental mean values. For all experimental datasets, the time-based data over 25 contiguous heart cycles were used. A $p < 0.05$ was considered to indicate a statistically significant difference between the mean values calculated from the experimental and clinical datasets. A $p > 0.05$ indicated that there was no significant difference between the two mean values within the variation of the two datasets.

		MUSC7		GOSH22		MUSC2		UM5		UM10	
		Experimental	Clinical	Experimental	Clinical	Experimental	Clinical	Experimental	Clinical	Experimental	Clinical
Pulmonary	R_{puld} **(WU)**	8.9±0.4	9.46	5.3±0.3	6.00	13.1±0.5	10.17	9.5±0.4	9.15	8.3±0.3	9.50
	C_{pul} **(ml/mmHg)**	0.14±0.01	NA	0.22±0.01	NA	0.21±0.01	NA	0.23±0.01	NA	0.2±0.01	NA
	R_{sh} **(WU)**	51.9±0.8	51.35	38.7±0.5	39.00	70.7±1.3	77.97	60.3±1.0	57.75	61.0±0.7	58.50
Upper Body	R_{ld} **(WU)**	143.2±1.3	75.00	181.6±2.0	90.00	304.9±4.7	157.58	152.8±1.3	71.97	301.3±3.3	141.67
	R_{rd} **(WU)**	143.2±1.3		181.6±2.0		304.9±4.7		152.8±1.3		301.3±3.3	
	C_{lcc} **(ml/mmHg)**	0.90±0.01	NA	0.11±0.01	NA	0.11±0.01	NA	0.13±0.01	NA	0.12±0.01	NA
	C_{lsc} **(ml/mmHg)**	0.90±0.01	NA	0.11±0.01	NA	0.11±0.01	NA	0.13±0.01	NA	0.12±0.01	NA
	C_{bc} **(ml/mmHg)**	0.18±0.01	NA	0.22±0.01	NA	0.22±0.01	NA	0.26±0.01	NA	0.25±0.01	NA
Lower Body	R_{lbd}**(WU)**	138.8±8.8	140.63	123.6±7.0	125.00	157.2±9.4	152.94	181.1±13.6	190.00	364.7±37.3	377.78
	C_{lb}**(ml/mmHg)**	0.04±0.01	NA	0.04±0.01	NA	0.04±0.01	NA	0.05±0.003	NA	0.05±0.01	NA
Aorta Proximal	C_{prox}**(ml/mmHg)**	0.18±0.01	NA	0.23±0.02	NA	0.22±0.01	NA	0.25±0.01	NA	0.24±0.01	NA

Table 2.2: Elemental values used in the lumped parameter network and corresponding clinical reference. R, resistance; C, compliance; prox, proximal; pul, pulmonary; sh, shunt; lb, lower body; atri, atrium; bc, brachiocephalic artery; lcc, left common carotid artery; lsc, left subclavian artery; l, left upper body vein; r, right upper body vein; d, distal resistance. Set value ± uncertainty (95%). WU = Woods unit.

CHAPTER THREE

IN VITRO MULTI-SCALE PATIENT-SPECIFIC STAGE 1 PALLIATION MODEL VALIDATION RESULTS

Recall the ultimate goal of this study is to introduce an engineering tool which surgeons can use for understanding the general hemodynamics of HLHS patients, as well as patient-specific cases, also for clinical hypothesis and surgical technique testing, and validate the system against clinical measurements.

Results

For each patient case, the stroke volume, heart rate and systolic ratio and the atrial pressure were set to clinical values and the VAD pneumatic pressure adjusted to match the ascending aorta mean pressure. The pulse pressure was adjusted through the proximal aortic compliance element. At these settings, the pressures and volume flow rates were measured throughout the system and compared against the clinical pressure and flow rate tracings. The experimentally measured ensemble mean values with their standard error are reported in Table 3.1. It should be noted that clinical values reported in Table 3.1, due to its *in vivo* nature and limitation of instrumental resolution, have certain uncertainty. The uncertainty of the clinical mean pressure measurement is assigned as 1 mmHg, for clinical mean flow measurements, the uncertainty is 0.02 lpm; that is, a 1 mmHg difference in pressure and 0.02 lpm difference in flow are considered to be clinically insignificant.

The time-based experimental and clinical ascending aortic pressures are shown in Figure 3.1 for three cardiac cycles of four of the five cases; the GOSH22

clinical pressure signal was not available. Overall, the experimentally measured ascending pressures were able to reproduce the clinical signals well. Subtle differences are noted at peak systole. The MUSC2 and MUSC7 clinical signals both show a distinct dichrotic notch, which was difficult to reproduce from the polyurethane valves used in the VAD. Systolic contractility was also evaluated by comparing the rate of pressure change in systole between aortic pressure signals. Differences in dp/dt for MUSC7 and UM5 are less than 6.5% between clinical and experimental values, while for UM10 and MUSC2 the differences are about 12% and 32%. However, the values of the coefficient of determination (R^2) range from 0.77 to 0.9, successfully demonstrating the ability to reproduce the clinical signals in the system. Mean pulse pressures compare to within 9% except for MUSC2 at 16%. Mean experimental and clinical aortic pressures (Table 3.1) could be set to within 2 mmHg or within 3%. Differences between the measured and clinical mean aortic pressure are not statistically significant ($p > 0.10$).

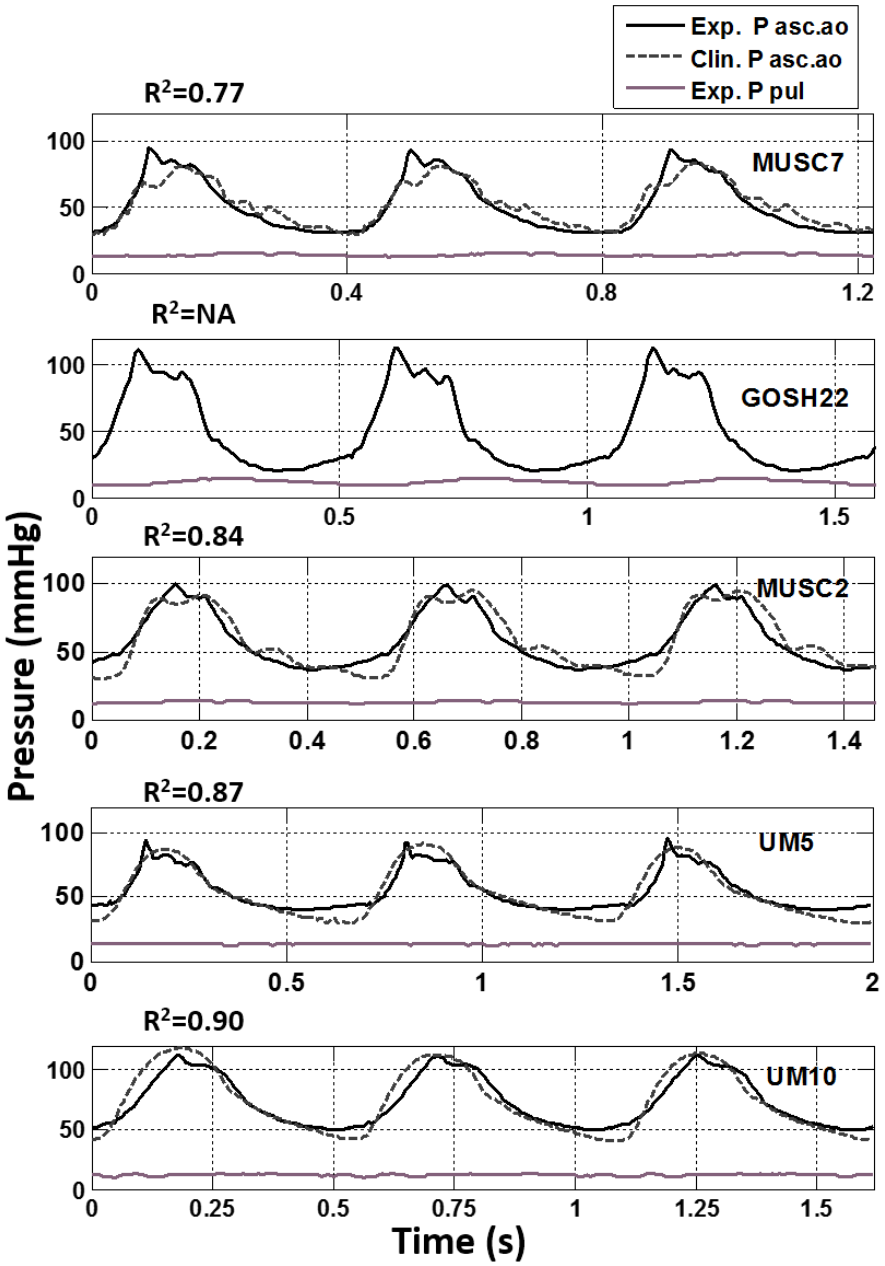

Figure 3.1. Clinical and experimental pressure signals for each of five patients. Pressure tracings includes pulmonary pressure (P_{pul}) and ascending aorta pressure ($P_{asc.ao}$).

With the system set up, the remaining experimental measurements demonstrate the consequence of the system tuning. The measured mean experimental values of cardiac output were within 0.02 lpm of the clinical measurements for each

of the five patients (Table 3.1). Differences between the measured and clinical cardiac outputs are not statistically significant ($p > 0.37$). The corresponding time-based ascending aortic flow rates, shown in Figure 3.2(a), follow the physiological characteristics of the clinical measurements well as R^2 values range from 0.88 to 0.95.

Time-based pulmonary shunt flow rates are compared in Figure 3.2(b). The pulmonary shunt signals match up well with R^2 values between 0.72 to 0.85 Shunt flow mean values agree to within 0.03 lpm or within 3%. At the systems level, the ratio of the pulmonary to system flow rates agree to within 11%. Differences between the measured and clinical pulmonary flow rates are not statistically significant ($p > 0.13$).

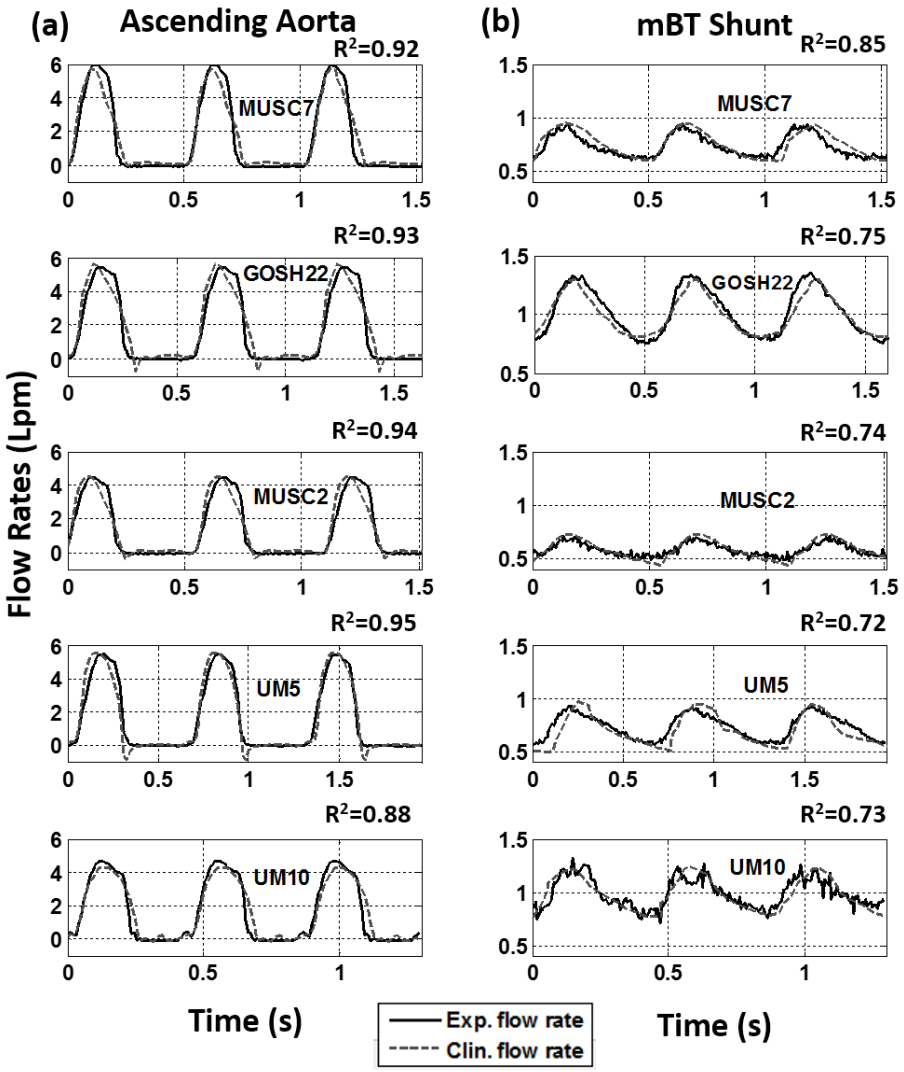

Figure 3.2: Clinical and experimental shunt flow rate and cardiac output for each of five cases.

Table 3.1 also shows mean upper body and lower body flow rates. The resulting difference between measured mean experimental values and clinical values of both upper body and lower body flow rates were within 0.02 lpm. Both upper body and lower body flow rates are in close agreement with clinical values, with no statistically significant difference between clinical and measured mean values ($p > 0.26$).

		MUSC7	GOSH22	MUSC2	UM5	UM10
Experimental Values	CO (l/min)	1.67±0.02	1.86±0.02	1.25±0.02	1.60±0.01	1.65±0.02
	Q_{pul} (l/min)	0.74±0.01	1.01±0.01	0.60±0.02	0.70±0.01	1.00±0.01
	Q_{ub} (l/min)	0.62±0.01	0.49±0.01	0.33±0.01	0.65±0.01	0.46±0.01
	Q_{lb} (l/min)	0.32±0.01	0.36±0.01	0.32±0.01	0.26±0.01	0.19±0.01
	$P_{Asc.\ Ao}$ (mmHg)	51.4±0.29	50.5±0.22	56.3±0.33	54.4±0.33	73.3±0.41
	P_{pul} (mmHg)	13.5±0.05	11.4±0.05	13.9±0.07	12.2±0.03	12.3±0.06
	dp/dt (mmHg/s)	642.5±0.16	1113.4±0.25	455.5±0.16	398.6±0.24	541.9±0.21
	Pulse pressure (mmHg)	53.4±0.10	74.4±0.21	54.6±0.14	50.3±0.28	63.7±0.14
	Q_p/Q_s	0.79±0.02	1.19±0.02	0.93±0.03	0.77±0.02	1.54±0.04
	Q_{ub}/Q_{lb}	1.94±0.04	1.36±0.03	1.03±0.03	2.50±0.05	2.42±0.06
Clinical Values	CO (l/min)	1.66	1.85	1.26	1.62	1.66
	Q_{pul} (l/min)	0.74	1.00	0.59	0.71	1.00
	Q_{ub} (l/min)	0.61	0.50	0.33	0.66	0.48
	Q_{lb} (l/min)	0.32	0.36	0.34	0.25	0.18
	$P_{Asc.\ Ao}$ (mmHg)	51	50	56	54	73
	P_{pul} (mmHg)	14	12	12	12	13.5
	dp/dt (mmHg/s)	630	NA	820	424	618
	Pulse pressure (mmHg)	50.5	NA	56.3	59.5	70.2
	Q_p/Q_s	0.80	1.16	0.88	0.78	1.52
	Q_{ub}/Q_{lb}	1.90	1.39	0.97	2.64	2.67

Table 3.1: Experimental and clinical mean pressures and flow rates (ensemble mean ± standard error).

Overall, looking at the pulmonary to systemic ratio (Q_p/Q_s), as shown in Table 3.1, the experimental results are in close agreement with clinical values and fall within their respective standard errors.

Another variable demonstrated in Table 3.1 is the mean pulmonary pressure. The resulting difference between measured experimental values and clinical values are within 1 mmHg with exception of MUSC2 and UM10. The differences in these two cases are 1.9 mmHg and 1.2 mm Hg, respectively. Differences between the measured and clinical pulmonary flow rates are not statistically significant ($p > 0.33$).

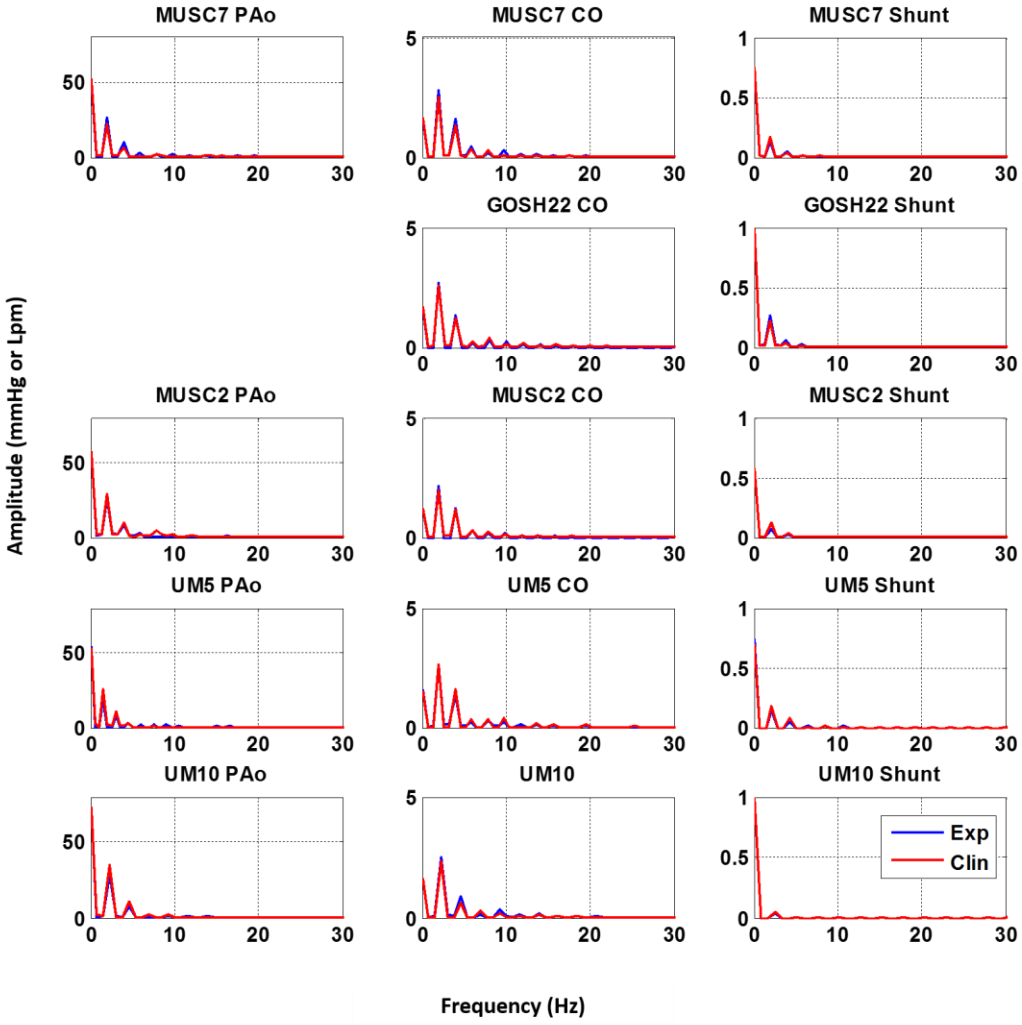

Figure 3.3: Frequency spectrum analysis of clinical and experimental measurements.

Frequency content comparisons between the experimental and clinical measurements were done using Fourier analysis. The discrete Fourier Transform (DFT) of the time series signals were computed using a Fast Fourier Transform (FFT) algorithm. The resulting frequency spectra are shown in Figure 3.3. Overall, the comparisons reveal that the experimental and clinical spectra are very similar, particularly for f < 10 Hz, with mean error < 5%. Above f >10 Hz the two datasets show differences indicating that the experimental system does not have the bandwidth

to recreate the higher frequency phenomena found in the clinical signals. These higher frequency details could be physiological in nature. For example, the dicrotic notch tends to show up near 20 Hz in clinical signals (Oppenheim, 1995) and the dicrotic notch is not well modeled with the VAD used in these tests. Some higher frequency content could be signal noise from the clinical measurement environment. Good agreements were seen at f=0 Hz (1.4% error on average) corroborating the results of the paired t-tests that the mean values were well matched. The signals were well matched near f= heart rate or about 2 Hz (3.7% error on average), indicating that the heart rate and pulsatility of signals were well recapitulated.

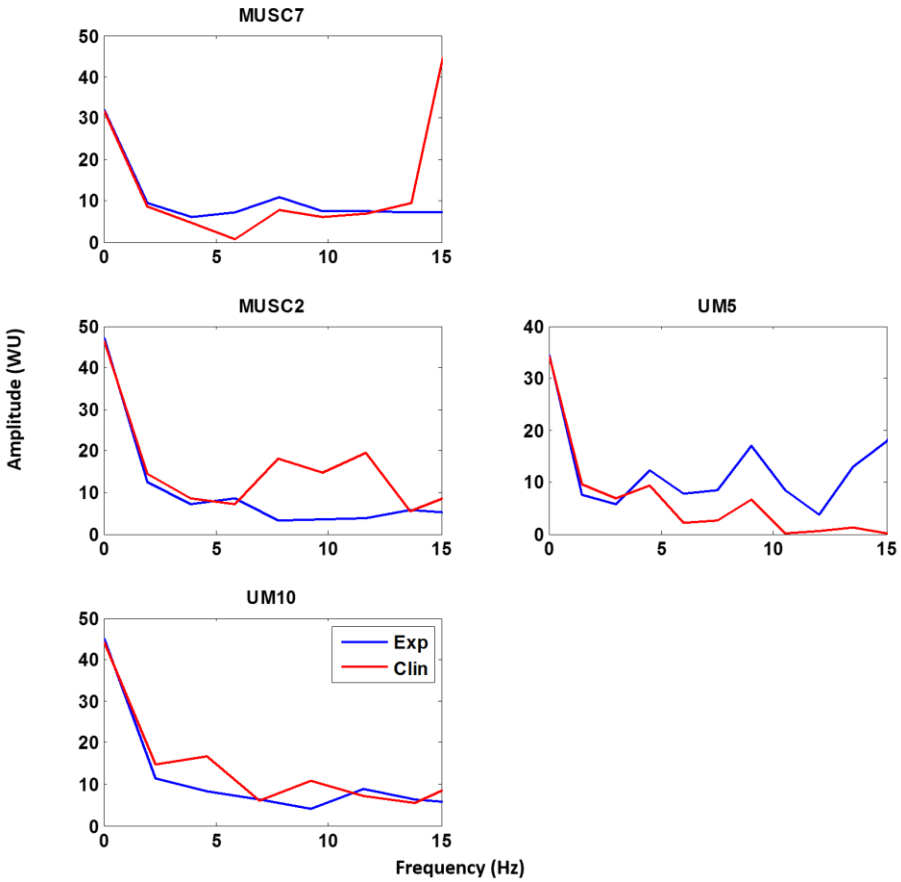

Figure 3.4: Impedance spectrum for four cases (GOSH22 lacks clinical measurements).

Impedance calculations were conducted from the pressure and flow spectra. Total vascular impedance (TVZ) is used to characterize afterload of the single ventricle. TVZ is analogous to electrical impedance and a function of system resistance and capacitance. To measure impedance, the following equation was used:

$$Z(\omega) = \frac{P(\omega)}{Q(\omega)}$$

Seven harmonics were calculated in this plot. The impedance at the zero harmonic Z (f=0 Hz) is equal to the total vascular resistance (TVR). Good agreements can be observed between experimental and clinical measured zero harmonic Z (1.4% error on average). This confirms that the total resistance as set within the system is very close to the patient's TVR, as intended. The impedance at the first harmonic Z1 is a function of the total vascular compliance (TVC). Overall, it can be seen that differences in impedance of compliances are more significant (17% error). This is due to the fact that compliance values in the system are based on parameter estimations, rather than clinical measurements. The estimation process introduces errors. Overall, the impedance spectra results further confirmed that the system setup recapitulated the intended patient –specific Norwood circulation faithfully.

Discussion

In this chapter, an MCS that is based on a lumped parameter network model coupled with an anatomically accurate, patient-specific aorta test section (3D models) was presented. The model was tested using 5 different patient-specific anatomies and tuned to their different physiologies. This multi-scale method allows for circuit

tuning to achieve patient specific settings while at the same time, allowing for detailed measurements within realistic test sections using accurate time-dependent boundary conditions. Based on the excellent validation of experimental measurements with clinical measurements, this multiscale in vitro model allows for realistic, time-dependent boundary conditions at the inflow and outflow boundaries of a three-dimensional (3D) model of a portion of the circulation, and more importantly, the boundary conditions are constantly and appropriately allowed to react by using a lumped parameter (0D) network.

This section has focused on the validation of the MCS as a test bench for patient-specific modeling. The VAD input condition fixed the known mean aortic and atrial pressures. The hemodynamic systems-level response, determined in terms of upper and lower body pressures and flow rates, and the aortic and shunt flow rates in five patients, were replicated with reasonable fidelity both in terms of mean values and time-based behavior. The advantages of this system are its compact nature, its ease of tuning, and its inclusion of relevant circulation branches to achieve realistic systems-level information. The test phantoms can be produced quickly, from imaging to realization within days. Patient-specific tuning does require more clinical pressure and flow rate information than may be typically available with a given patient, particularly in neonates. In such cases some elements of the LPN model may need to be extracted from available clinical data representative of these patients.

The in vitro model was operated in an open-loop mode whereby the mean aortic pressure and mean atrial pressures were manually fixed and held constant to known patient values. Alternatively, the system as configured could be used to

maintain a constant cardiac output. The auto-regulation of the heart (i.e. baroreceptor, HR variability) happens in the matter of seconds to minutes. It is not the objective to study the transient hemodynamics and physiology. In this sense, an open loop model should be considered sufficient. Such a model allows for studying the effects of parametric variation of one or more changes within the circulation. For example, this model can be used to study the effects of aortic coarctation on a patient. Such a system will be valuable for recreating the clinical setting so as to evaluate clinical situations that cannot usually be measured or attempted in patients, such as novel surgical procedures, or simulating interventional measurements, such as catheterization.

When coupled with a rigid anatomically accurate phantom, a proximal aortic compliance was needed between the VAD and aortic phantom to achieve a physiologically realistic ascending aortic pressure waveform and to prevent large amplitude aortic pressure ringing. Vukicevic et al. developed a thin walled, compliant phantom of a total cavopulmonary connection, and found that measured system pressures and flow rates were not significantly different from those measured using a rigid phantom paired with a proximal compliance. Representative values were used for the vascular compliance elements in this study. While aortic compliance could be extracted from appropriate MRI information, this was not attempted here.

The system was modified based on a previously described system (Biglino, 2011). In Biglino et al.'s study, tuning of the circuit was confirmed by qualitatively observation of Q and P, quantitative analysis was not made possible due to the lack of full set of data from the patients. Additionally, Biglino's group was not able to

produce physiological patient-specific waveform utilizing their system. One important observation Biglino et al. made in their study is that VAD's inflow and outflow valve were opened concurrently, causing concurrent presence of flow at both end. This phenomenon can be the reason why their waveforms measured were not physiologically accurate. Figure 3.5 shows simultaneous measurements of flow rate at inlet and outlet of the VAD in Biglino et al.'s study and this study. In this study, inertance of the system and VAD function were carefully manipulated, and the concurrent presence of inflow and outflow was eliminated. This is seen in Figure 3.3 whereby the inflow and outflow signals from the current setup are clearly delineated and do not overlap, indicating complete tricuspid and aortic valve closures during systole and diastole, respectively.

As mentioned in section 1.5, there are some other *in vitro* studies concerning the modeling the Stage 1 Norwood Circulation. Few previous models (Biglino, 2011, Bakir, 2006) demonstrate validation against any clinical measurements and no previous model validates against a wide range of patient-specific morphologies and physiologies, as was done here.

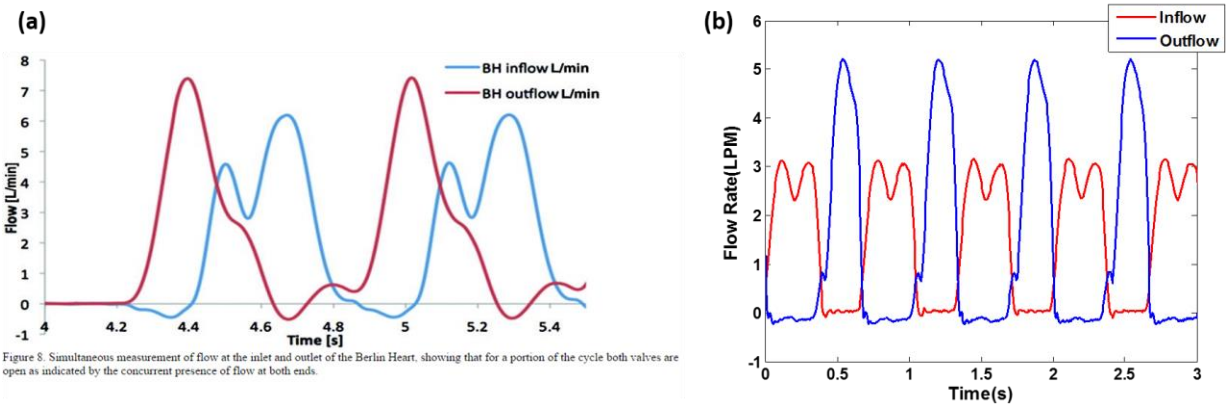

Figure 3.5: Simultaneous measurement of inflow and outflow of VAD (Berlin Heart) (a) Biglino et al. measurement. (b) A sample measurement in this study.

Secondly, most of the models (Pennati, 2001; DeGroff, 2000; Tacy, 1998) described in previous studies are limited and cannot be used to study the effect of changing parameters on both the local and global hemodynamics. For example, Pennati et al. described a model in 2001 that contains only the mBT shunt and pulmonary shunt as 3D flow domain (Pennati, 2001). The input condition to the 3D mBT shunt and PA, rather than being provided by the brachiocephalic trunk, is prescribed by a roller pump. This model can be informative only when one concerns the pulmonary circulation. However, this model is not capable of reproducing the effect of changing SVR on the pulmonary circulation. On the contrary, the model described in this dissertation is a 0D-3D coupled multiscale MCS, which contains pulmonary, lower body and upper body circulations. With the current model, changes in SVR would result in changes of Q and P in brachiocephalic trunk, and hence physiological input conditions can be achieved to the downstream mBT and PA domain. This feature is very advantageous to understanding this complex and delicate Norwood circulation.

One *in silico* study published by Corsini et al is the only few studies that share some characteristics with this study. Corsini's group developed a multi-scale 0D-3D coupled model to study the effect of coarctation on coronary perfusion after Norwood Procedure. They adopted the same method as in this study, they use a patient-specific 3D aortic flow domain coupled with 0D LPN tuned with patient-specific RCL values. They validated their system against clinical measurements and showed satisfactory results. Their results are shown in the Table 3.2 below. (Corsini, 2014)

		Clinical Data	
Variable	Model	Mean ± SD	Range
Input			
BSA (m^2)	0.33	0.30 ± 0.04	0.26–0.34
SVR (WU m^2)	21.4	20.1 ± 9.3	13.3–35
PVR (WU m^2)	3.63	2.75 ± 0.81	1.35–3.4
Results			
CO (mL/s)	30.3	27.4 ± 4.1	21–31
Q_{DAo} (mL/s)	6.7	4.7 ± 1.2	3–6
Q_P (mL/s)	16.5	14.1 ± 4.2	9.7–20
P_{Ao} (mm Hg)	62	56 ± 9	51–72
PPA (mm Hg)	15	13 ± 2	11–16
EDV (mL)	32	31 ± 3	29–35
ESV (mL)	17	14 ± 3	10–18

Table 3.2. Comparison Between the Baseline Model (3.5-mm Modified Blalock-Taussig Shunt<comma> No Aortic Coarctation) and Clinical Values From 5 Patients With Same Characteristics Recruited Within the MOCHA Group (Unpublished Data) BSA = body surface area; CO = cardiac output; EDV = end-diastolic volume; ESV = end-systolic volume; P_{Ao} = aortic pressure; PVR = pulmonary vascular resistance; Q_{DAo} = descending aortic flow; QP = pulmonary flow; SVR = systemic vascular resistance. (Corsini, 2014)

CHAPTER FOUR

IN VITRO MULTI-SCALE PATIENT-SPECIFIC STUDY OF COARCTATION IN STAGE 1 NORWOOD PATIENTS WITH MBT SHUNT RESULTS

In the previous chapter, an *in vitro* multi-scale patient-specific model was developed and validated to model the hemodynamics of a Norwood patient with an mBT shunt. Because of the proven reliability of this *in vitro* multi-scale patient-specific MCS, it was used to conduct a study of progressive coarctation in Norwood patients.

The goal of this chapter is to further the understanding of the indications requiring intervention for neoaortic coarctation (NAO). The study attempts to better understand the interaction of NAO severity, ventricular power change, and aortic arch morphology. The findings could improve patient management by providing supporting information to improve coarctation treatment, such as deciding when invasive intervention to treat NAO is necessary and avoid unnecessary procedures.

Methods

In order to maintain the native aortic geometry of each patient while simulating the geometry associated with increasing coarctation severity, the aortic models for each patient were morphed in virtual space to create the narrowing as described below. Separate test phantoms for each amount of coarctation severity were printed and tested. Tests within the MCS serve to determine the effect of coarctation severity on systems-level hemodynamics. In these tests, autoregulation control of cardiac

output was simulated by maintaining the cardiac output of each patient constant as coarctation severity increased.

Selection of patients

Four patients are used in this part of the study: GOSH22, MUSC2, UM5, and UM10. Patients' parameters are given in section 2.1.

Creation of coarctation

Severity of coarctation is defined by the diameter at the narrowest site of coarctation divided by the diameter of the descending aorta at the diaphragm, and the resultant ratio is termed the CoI. The native CoI of GOSH22, UM5 and MUSC2 are very close to 1, which indicates mild to no NAO in these four cases, so a progressive NAO can be added from CoI=1.0 to CoI=0.3. In UM10 the native CoI was 0.7.

The subtle challenge of increasing NAO in the test section was to control the amount of narrowing, while keeping the original patient-specific geometry intact. This was made possible using the "Inside Hollow" function of the software package 3-matic (Materialise, Leuven, Belgium). This feature allowed narrowing of the intended diameter of the vessel while maintaining the original geometric shape. The "Morphing" feature was used to blend the narrowed part to the native upstream and downstream sections. Illustration of created NAO is shown in Figure 4.1.

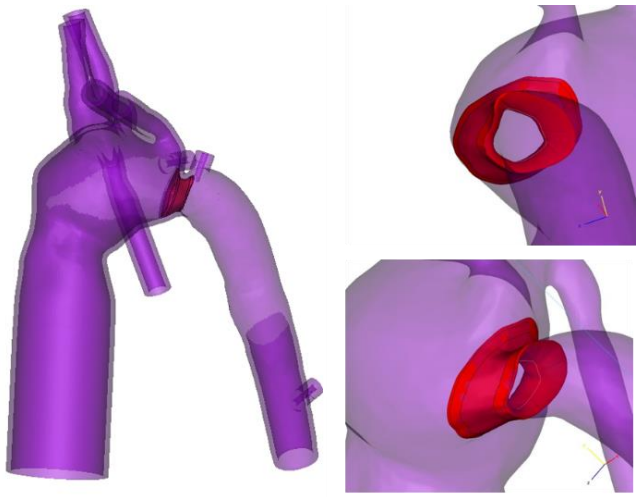

Figure 4.1. Coarctation (highlighted) added to the original UM5 test section geometry using 3-matic.

In vitro realization of homeostasis: Test Control

A coarctation affects the resistance of the descending aorta, altering the SVR of the circulation. The human body reacts to changes in the circulation by attempting to maintain perfusion. This physiological response was realized *in vitro* by controlling Cardiac Output (CO). In experimental tests, after changing the coarctation, the mean aortic pressure of the VAD was adjusted to restore the CO to the patient-specific baseline value. Mean aortic pressure and the distribution of flows among the upper body, lower body, and lungs were allowed to change in response to COA.

Pressure measurements

One advantage of an *in vitro* test bench over a numerical model is the ability to mimic certain clinical measurements. Here it was possible to mimic an interventional catheter measurement and to compare that measurement to a standard engineering wall pressure measurement.

In order to measure pressure across a coarctation, two methods were used.

- In method 1, wall pressure taps were built into the aortic arch and in the descending aorta. Using the diameter of the descending aorta at diaphragm as dimension D, wall taps were placed at (1) 2.5D upstream of the COA (noted as PRE), (2) 1D downstream of COA (noted as 1D), and (3) 10D downstream the COA (noted as POS).
- In method 2, a 2.13 mm diameter catheter (6.4 French) was used to measure the pressure at the aforementioned sites: PRE, 1D, and POS in the test sections. Pressure gradient was measured in each case using the pullback technique (Baim SD, 1991). The sites of measurements are shown in Figure 4.2.

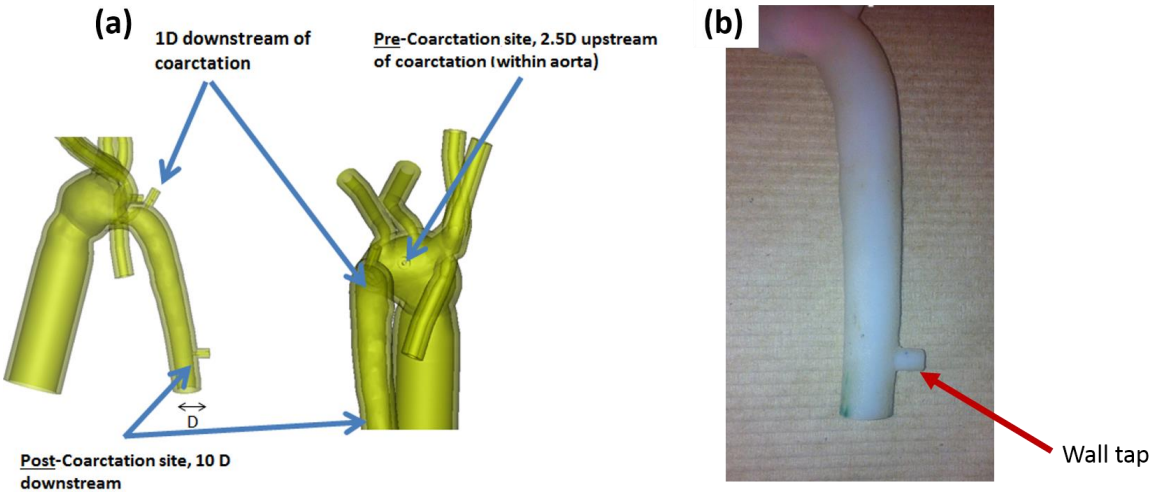

Figure 4.2. (a) Locations of pressure taps added to a patient-specific aortic test-section with coarctation. For catheter measurements, the catheter tip was placed on the blood vessel axis at the same locations. (b) 3D printed wall tap on descending aorta.

In the catheter pullback technique, the presence of the catheter can partially obstruct the COA throat. This blockage causes a rise in ascending aortic pressure and an overestimation of the pressure gradient. This is a classical issue. In this study the

pressure measurements via wall taps (with the COA unobstructed) were used for direct comparison to catheter measurements, to quantify the gradient overestimation. However in some of the smallest CoI cases in this study, catheter measurements were not possible because the catheter diameter exceeded the coarctation ID.

Single ventricular power

Single ventricular power (SVP) is the measure of work delivered by the single-ventricle heart to the vascular load. Addition of COA is effectively similar to adding extra SVR. The heart, under this circumstance, needs to maintain the same CO and oxygen delivery (OD), but aortic pressure is increased, which increases load on the ventricle.

A VAD is used to provide the function of the single ventricle (SV) in the mock circulation. The VAD used in this study is a Berlin Heart, driven by compressed air (Vukicevic, 2013), as shown in Figure 2.2 and Figure 2.5. The SVP is hydraulic power supplied by the VAD to the mock system. In Figure 4.3, Q_{in} and P_{in} denote the inflow volumetric flow rate and pressure into the VAD, and Q_{out} and P_{out} denote the outflow volumetric flow rate and pressure from the VAD. The VAD boosts flow from P_{in} to P_{out}. The flow rate delivered varies according to the driving air pressure and heart rate, and the mock vascular load.

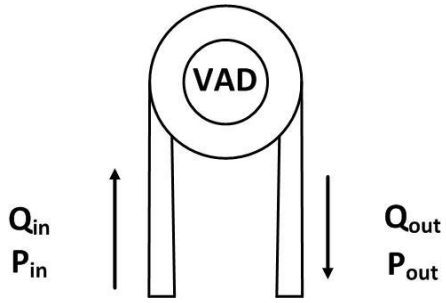

Figure 4.3. A Ventricular Assist Device (VAD). Qin and Qout denote volumetric flow rate of inflow and outflow. Pin and Pout denote the pressures of inflow and outflow.

The SVP, which is the time-averaged hydraulic power of the VAD, can be calculated based on measurements as below.

$$Power = \frac{1}{T_{cycle}}\left(\int Q_{out}(t)\cdot P_{out}(t)\,dt - \int Q_{in}(t)\cdot P_{in}(t)dt\right) = \frac{1}{T_{cycle}}\int Q_{out}(t)\cdot P_{out}(t)\,dt - Q_{in}(t)\cdot P_{in}(t) \quad (4.1)$$

The outlet flow is pulsatile in both pressure and flow rate, so it was measured with high temporal resolution, 160 samples/second, and the outlet term of the time integral was calculated directly from the data. The inlet flow was at constant pressure (atrial pressure in the mock system), so the inlet term of the integral can be calculated simply as the product of mean pressure and flow. From the continuity principle, mean Q_{in} is equal to mean Q_{out}.

Global measurements

Global measurements were conducted using the same method documented in section 2. Measurements were conducted in the same sites shown in Figure 2.2, plus the additional sites described in this section.

Results

In this study, hemodynamics changes in response to CoI change were studied. Pressure differentials (pressure differences between two locations) were calculated using two methods. In method 1, the pressure difference between the PRE and 1D locations was calculated, while in method 2, the pressure difference between the PRE

and POS positions was calculated. This procedure was repeated for both wall pressure tap measurements and catheterization measurements for each case and each patient. Likewise, the peak to peak gradient taken from the time-based wall tap and catheter pressure measurements between PRE and 1D was calculated, as was the peak to peak pressure gradient between PRE and POS, from wall tap data and again from catheterization data.

Mean flow rate was also calculated from the measurement. Time averaged mean flow rates over 25 cycles were calculated at ascending aorta, mBT shunt, upper body, and lower body. The pulmonary to systemic ratio Q_p/Q_s was also calculated for each of the cases.

GOSH22

GOSH22 has a slight tubular aortic arch. Figure 4.4 shows the hemodynamic response of GOSH22 to CoI variation. Mean and systolic pressure gradients were measured as described above. In subfigure (a), when CoI >0.5, there is hardly any change of mean pressure differential (≤ 5 mmHg for tap measurement; ≤ 10 mmHg for catheter measurements). However, when CoI < 0.5, mean pressure differential become very sensitive to CoI change. In subfigure (b), for CoI =1 to 0.6, peak to peak pressure gradient changed from 0 to about 15 mmHg for both catheter and wall tap measurements. However from CoI to 0.6 to 0.4, tap-measured peak to peak gradient increased by about 30 mmHg. From catheter measurements, peak to peak gradient increased by about 30 mmHg in response to a CoI decrease from 0.5 to 0.4. In GOSH22, there is very little difference between PRE-1D measurement and PRE-POS

measurements for both tap measurements and catheter measurements. In subfigure (c), SVP of GOSH22 showed a different pattern; the response is linear with about 20 mW increase. Flow rates are shown in subfigure (d). Ascending aorta flow rate, or CO, was held constant. A decrease in lower body flow rate by 0.07 lpm was observed. Shunt flow and upper body flow increased as expected, and Q_p/Q_s ratio was increased.

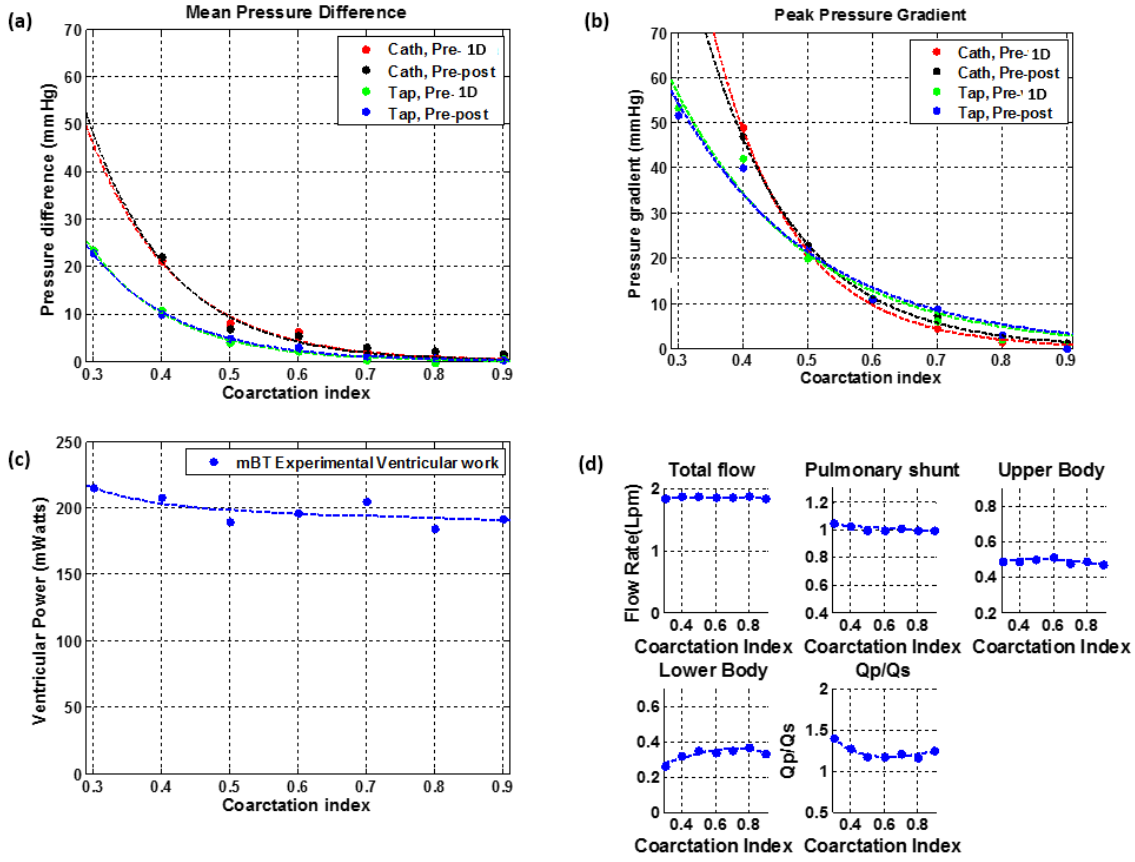

Figure 4.4. Measured hemodynamics of GOSH22 case in response to CoI variation: (a) mean pressure differential (b) peak to peak pressure gradient, (c) Single Ventricle Power, (d) flow rates.

MUSC2

The hemodynamic response of MUSC2 to CoI variation is reported in Figure 4.5. The native neoaortic arch morphology of the MUSC2 was considered "moderate",

neither tubular nor dilated. Patterns observed in GOSH22 also occurred in this patient. Overall trends for pressure differential and peak to peak pressure gradients had low sensitivity to CoI variation when CoI> 0.4, becoming they are very sensitive to CoI change for CoI<0.4. The SVP had hardly any change until CoI =0.43, then from CoI =0.43 ~ 0.23, SVP increased about 40 mW. Flow rates are shown in subfigure (d). Ascending aorta flow rate, or CO, was held constant. Decrease in lower body flow rate was observed. Shunt flow and upper body flow increased as expected, and Q_p/Q_s ratio was increased.

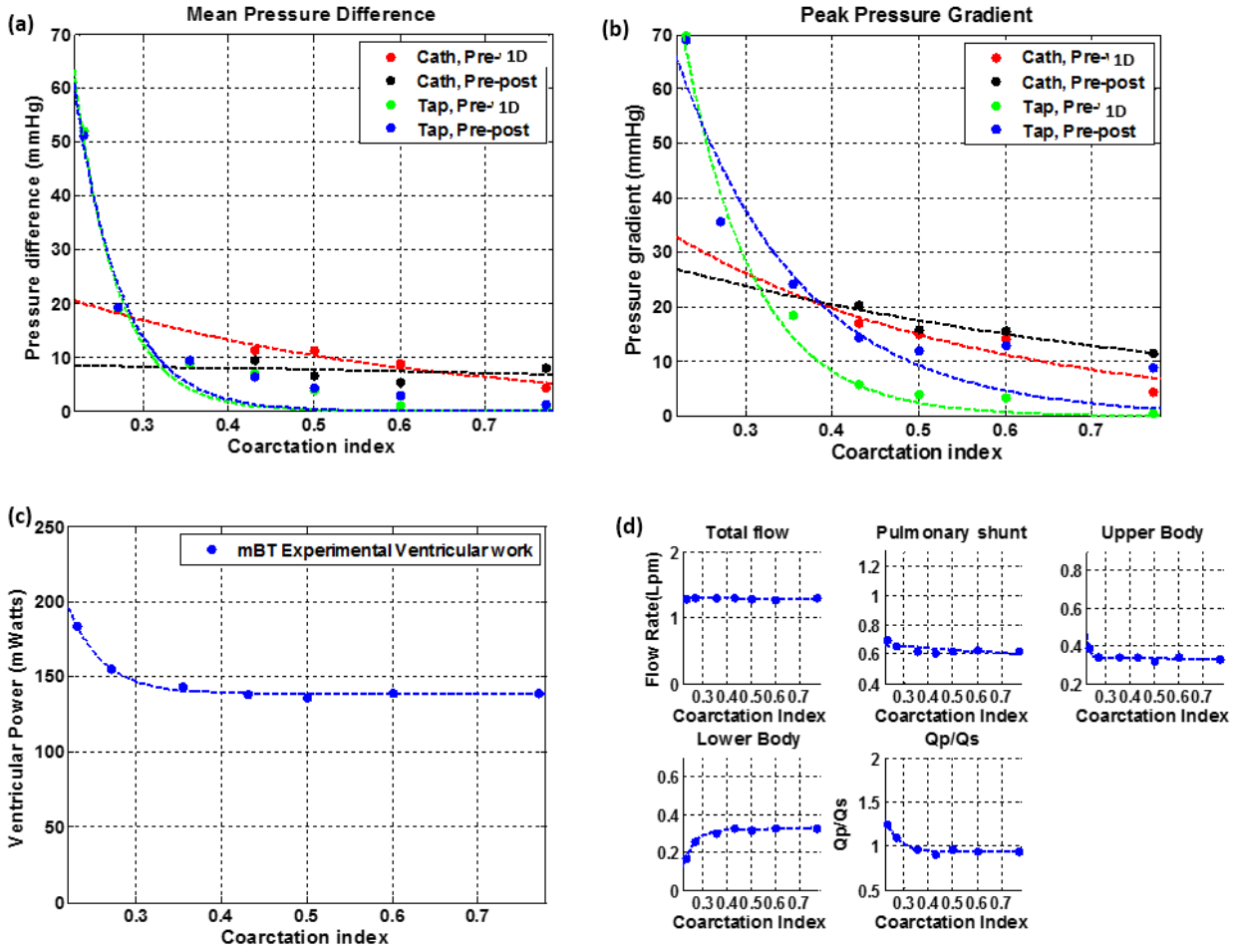

Figure 4.5. Measured hemodynamics of MUSC2 case in response to CoI variation: (a) mean pressure differential (b) peak to peak pressure gradient, (c) Single Ventricle Power, (d) flow rates.

UM5

The hemodynamics response of UM5 to CoI variation is shown in Figure 4.6. UM5 is the case with dilated aortic arch. Visually inspecting subfigure (a) and subfigure (b), one can tell that this set of pressure differential and peak to peak pressure gradient tracing behave differently from the previous two cases. The hemodynamics response to CoI variation is almost linear. This pattern also occurs in SVP response and system level flow rate change. Note that the overall increase of SVP is comparatively linear relative to the previous two cases. Ascending aorta flow rate, or CO, was held constant. Decrease in lower body flow rate by 0.06 lpm was observed with a linear response to CoI change. Shunt flow and upper body flow increased as expected, and Q_p/Q_s ratio was increased.

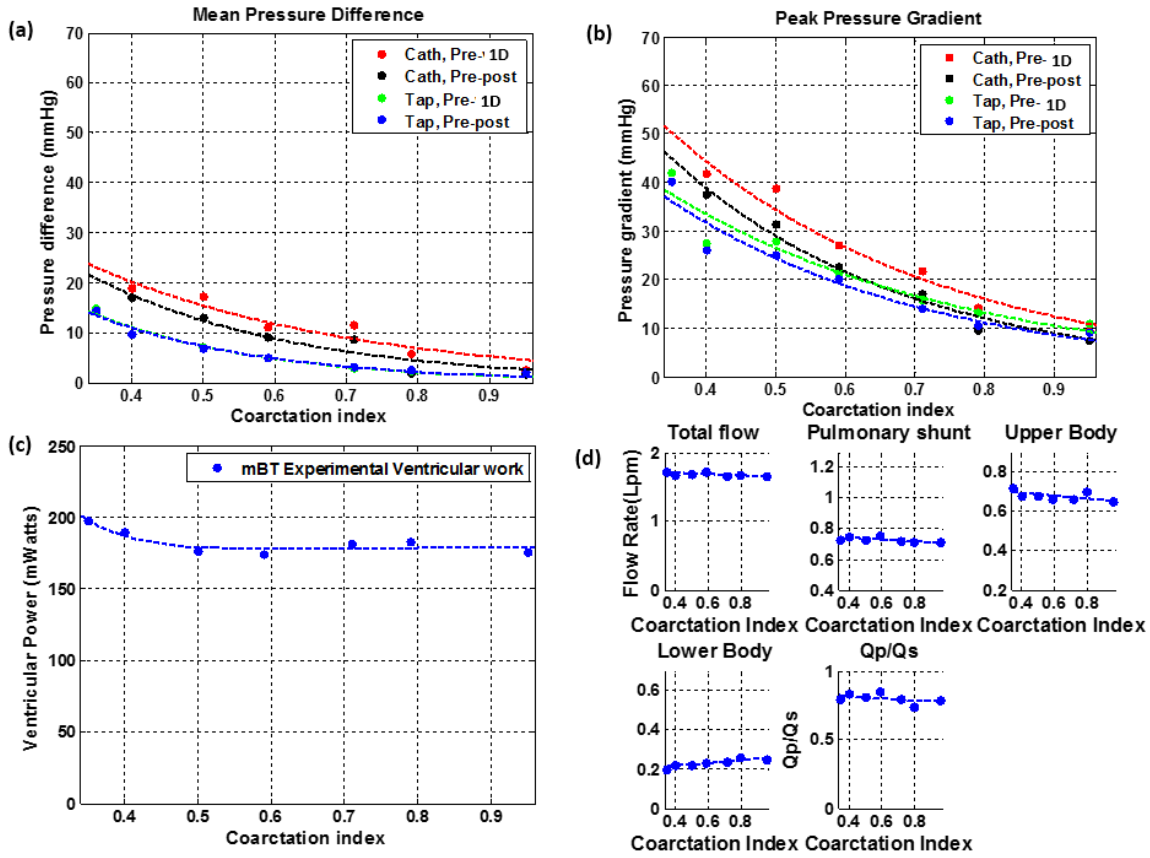

Figure 4.6. Measured hemodynamics of UM5 case in response to CoI variation: (a) mean pressure differential (b) peak to peak pressure gradient, (c) Single Ventricle Power, (d) flow rates.

UM10

Figure 4.7 shows the hemodynamic response of the UM10 case to CoI variation. UM10 has a dilated neoaortic arch. Due to the native NAO of the patient, CoI variation could only be realized from 0.72 to 0.28. Also, due to the narrow descending aorta, catheter measurements were not possible for most of the CoI range. Hence only wall tap measurements are reported in this case.

Overall, the pressure differential and peak to peak pressure gradients demonstrated a comparatively linear response to CoI variation. The baseline of SVP is higher than the other four cases, because of the high MAP and CO of the patient

(73mmHg, 1.86 lpm). Flow rate responses are reported in subfigure (d): CO was held constant, the mBT shunt flow and upper body flow increased overall, lower body decreased, and Q_p/Q_s increased.

The changes in flow rates are summarized in Table 4.1.

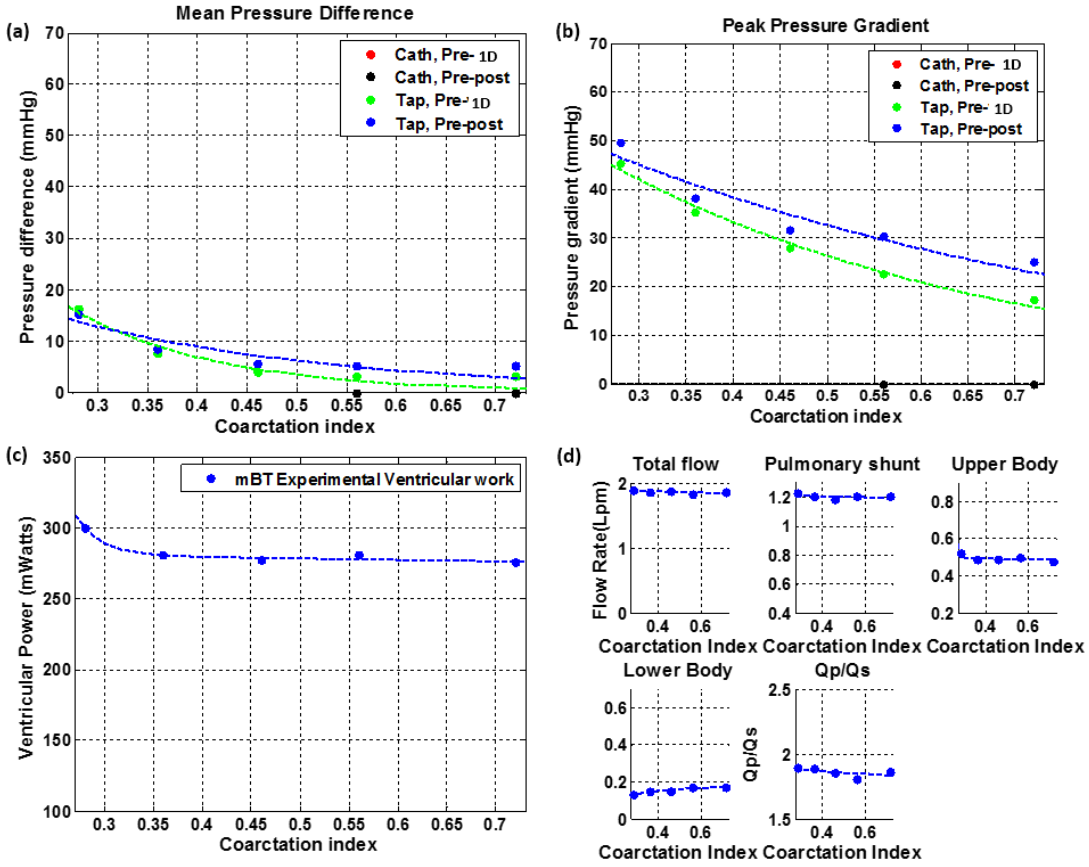

Figure 4.7. Measured hemodynamics of UM10 case in response to CoI variation: (a) mean pressure differential (b) peak to peak pressure gradient, (c) Single Ventricle Power, (d) flow rates.

	GOSH22	MUSC2	UM5	UM10
Dilation/Tubular	Tubular	Normal	Dilated	Very dilated
CoI	0.90~0.30	0.77~0.23	0.95~0.35	0.72~0.28
CO ± STD	1.86±0.01	1.29±0.01	1.67±0.02	1.87±0.02
Change in Q_{ub} (Lpm)	+0.02	+0.06	+0.03	+0.04
Change Q_{pul} (Lpm)	+0.05	+0.08	+0.05	+0.02
Change Q_{lb} (Lpm)	-0.07	-0.15	-0.05	-0.04
Change in SVP (mW)	+23.01	+44.81	+21.76	+24.63
Change in mean Aorta Pressure (mmHg)	+5	+15	+3	+5

Table 4.1. Flow change and ventricular power change over the range of Coarctation Index.

Discussion

The study allows some insight into the system-level response to COA in the Norwood circulation with mBT shunt. Some general trends can be observed from the results. With constant cardiac output (CO) maintained, decreases of lower body flow rate were observed as expected, due to the increases of total LBSVR induced by narrowed aorta. Shunt and upper body flow rates for all four cases also increased, as expected, due to the increase of pressure differences across both branches.

According to continuity:

$$CO = Q_{pul} + Q_{lb} + Q_{ub} \qquad (4.2)$$

Since CO was held constant, the amount of decrease in lower body should be equal to the amount of the increase in upper body and mBT shunt combined. That is:

$$-\Delta Q_{lb} = \Delta Q_{pul} + \Delta Q_{ub} \qquad (4.3)$$

Conservation of mass was confirmed to within ±0.03 lpm, well within the measurement error.

Referring to Table 4.1, changes in pulmonary shunt flow exceeded changes in upper body in all cases but UM10. This implies the pulmonary branch is more sensitive to coarctation effects than upper body for these cases. This phenomenon is expected from a mathematical perspective. For each of the patients, UBSVR is higher than PVR + R_{shunt}. This implies the body flow rate is more sensitive to pressure changes than pulmonary flow rate.

The exception case was UM10 in which the upper body flow rate changed about as much as did the pulmonary blood flow. The actual flow change in this case was very small (0.04 lpm), and so well within the statistical significance of measurement uncertainty.

Does CoI cause changes in the cardio-shunt flow phase difference? In order to answer this question, GOSH22 cardio-shunt flow phase differences are compared in Figure 4.8 for CoI=0.9 and CoI=0.3.

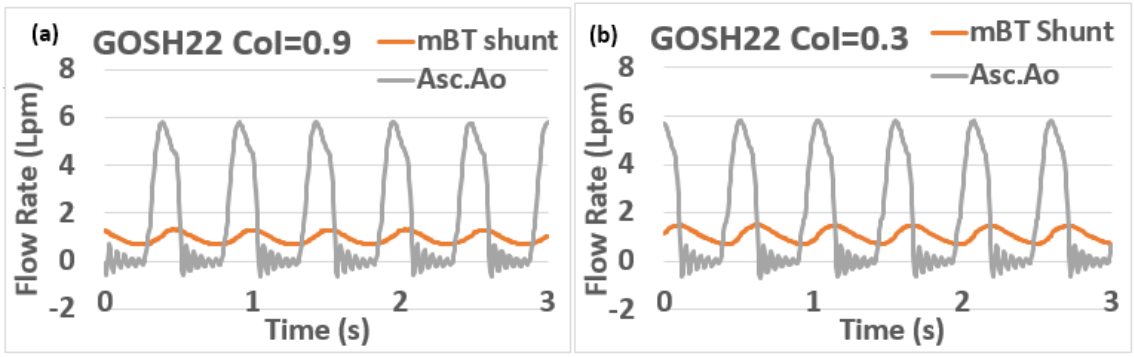

Figure 4.8. GOSH22 ascending aortic flow rate and shunt flow rate (a) CoI=0.9 (b) CoI=0.3.

In Figure 4.8, as CoI decreases, there is no discernable difference in cardio-shunt phase lag between the CoI =0.9 (mild) and CoI=0.3 (severe) scenarios. The same observations were reached after examining the other three patient-specific cases.

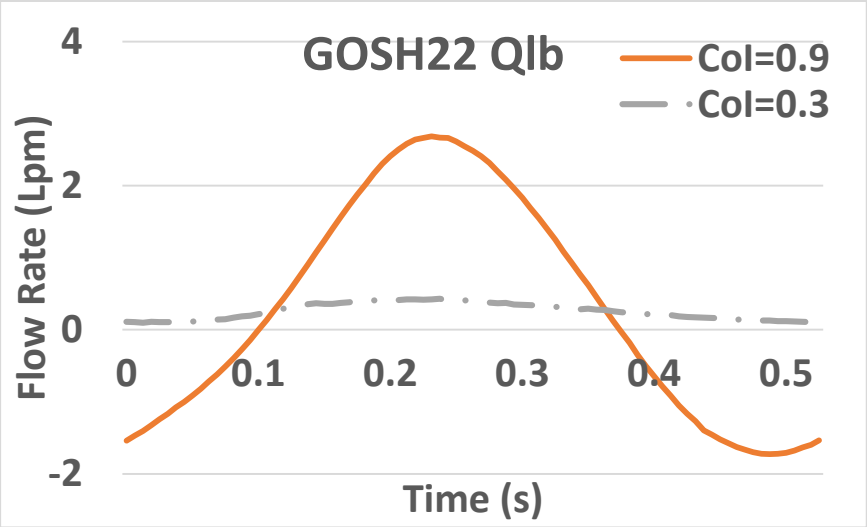

Figure 4.9. Ensemble lower body flow rate tracing for GOSH22.

Lastly, the ensemble Qlb flow rate curve in Figure 4.9 for CoI=0.9 and CoI=0.3 were compared. As COA was progressively added, the average Qlb decreased from 0.33 Lpm to 0.26 Lpm and pulsatility became muted. When CoI =0.9, the lower body flow rate had noticeable reverse flow, with reverse to forward flow ratio of 0.8. This is due to the compliance of descending aorta. Some of the reverse flow went to upper body branches and some of the reverse flow went to the pulmonary branch, the ratio of which is depended on the UBSVR to PVR+R_{shunt} ratio. In the case of COI=0.3, it was found that reverse flow was eliminated, lower body flow rate was completely forward flow, likely due to the added local increase in

resistance in the descending aorta. The same conclusions were reached after examining the other three patient-specific cases.

The measured ventricular power (SVP) over CoI for each patient is plotted in Figure 4.10(a). The increase in ventricular power due to increasing coarctation severity relative to the baseline coarctation was minimal for all cases between CoI = 1.0 to 0.5. This would indicate that coarctation severity is too modest to affect the single ventricle power. However, when coarctation severity progressively increased (CoI < 0.5), a noticeable increase in SVP was observed. This extra power load on the delicate single ventricle may indicate the need for intervention to relieve the coarctation.

From the SVP curves of Figure 4.10a, MUSC2 (Normal arch dilation) has the lowest SVP required, while the more tubular one (GOSH22) and the more dilated ones (UM5 and UM10) have higher SVP requirements. An abnormal arch morphology can act as a form of extra resistance to the system, as noted here. For the four cases studied, aortic arch morphology affects single ventricle power requirements ($p < 0.05$) and this is sensitive to CoI.

This effect of CoI on single ventricle power can be highlighted by studying the rate of change in SVP with coarctation severity. Define this change as the sensitivity:

$$S_{svp} = \frac{d\,\mathrm{SVP}}{d\,CoI} \qquad (4.4)$$

The sensitivity was calculated using a central differencing scheme except at the end-points where forward or backwards differecing was used. For central differencing, S was calculated between three successive points by:

$$S_i = \frac{f(x_{i+1}) - f(x_{i-1})}{2\Delta x} \qquad (4.5)$$

Forward differencing was applied between two successive points as:

$$S_{i=1} = \frac{f(x_{i+1}) - f(x_i)}{\Delta x} \qquad (4.6)$$

And backwards differencing was applied as:

$$S_{i=n} = \frac{f(x_i) - f(x_{i-1})}{\Delta x} \qquad (4.7)$$

Figure 4.10 (b) plots S_{svp} vs. CoI of all four cases. Sensitivity is near zero for all cases as CoI > 0.5. The sudden increase in sensitivity is clear for CoI < 0.5 and particularly as CoI is decreased further (more severe). This illustrates the nonlinear response of SVP change to CoI, and shows that the single ventricle power requirements significantly increase only when coarctation reaches severe stages, such as below CoI < 0.5.

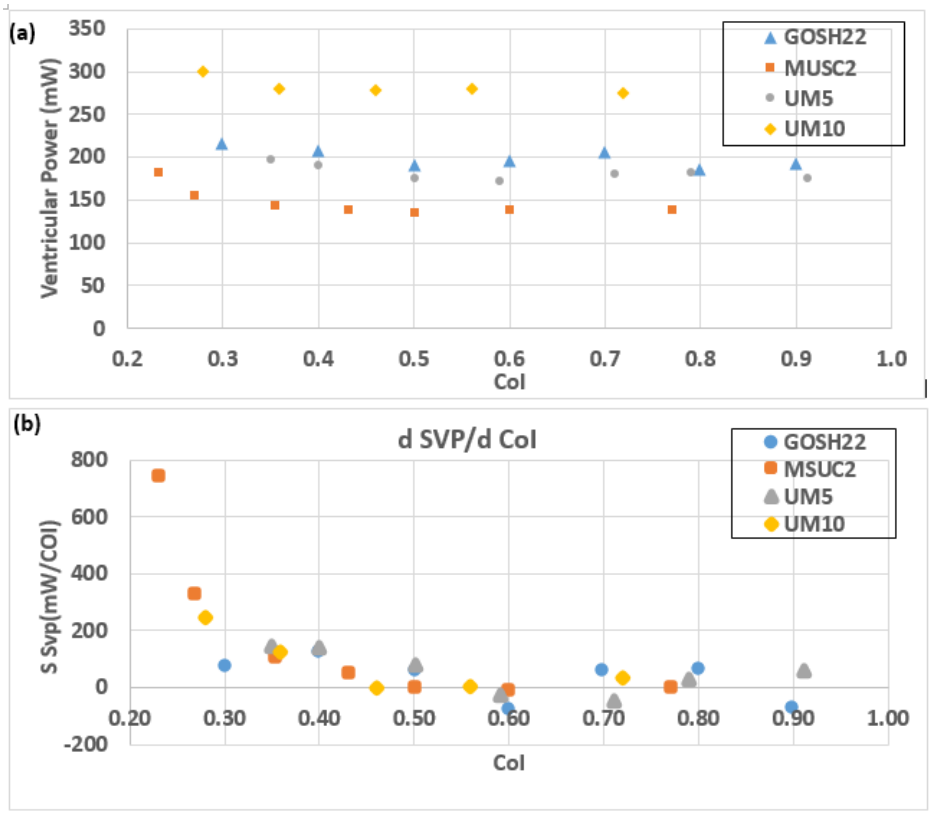

Figure 4.10. Scatter plot of (a) SVP vs. CoI and (b) S_{svp} against CoI for all four cases.

In order to quantify when statistically significant occurs, piecewise regression was conducted using SVP data. Piecewise regression partitions CoI into several separated intervals and fits a separate linear regression model to each interval of CoI. Piecewise analysis result in Figure 4.16 shows that breakpoint in the case GOSH22 is CoI=0.4, for MUSC2 are CoI=0.46 and 0.28, for UM5 is CoI= 0.49, and for UM10 is CoI=0.37. Overall, the results suggests that breakpoint for four five cases occurs when CoI<0.5. This is when statistically significant changes occur.

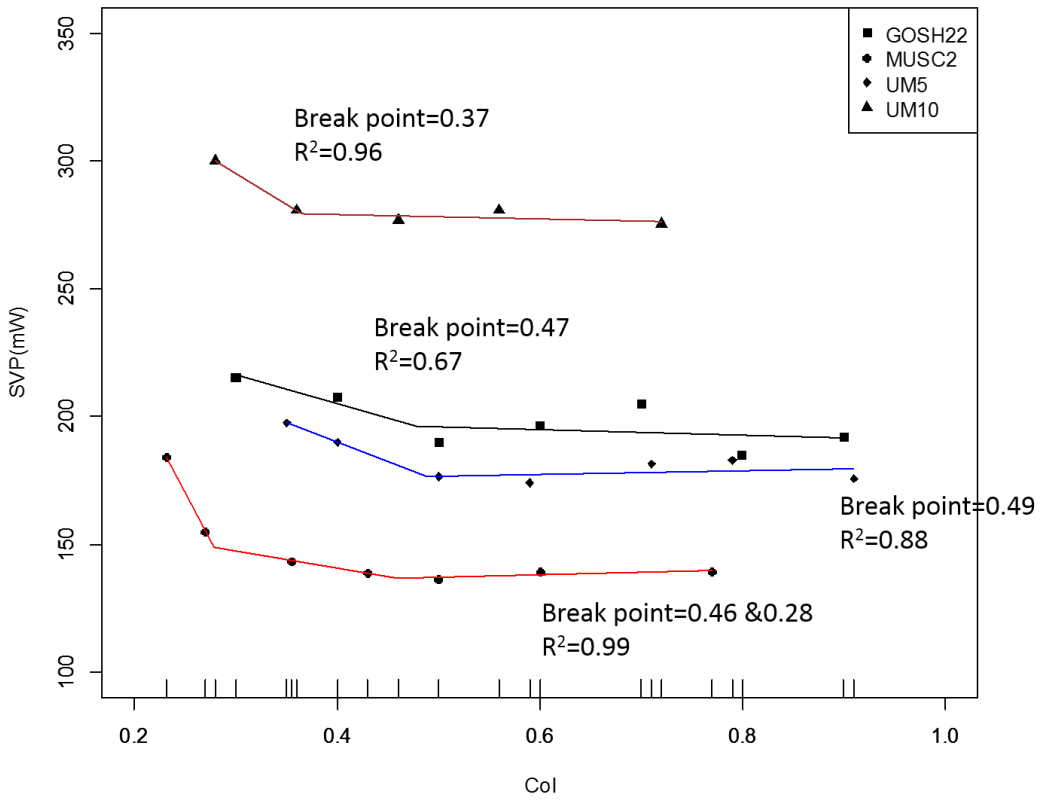

Figure 4.11. Piecewise regression results for five cases' SVP data, with estimated breakpoints and R^2 indicating the goodness of fit.

Figure 4.12 (a) illustrates Pre- to Post- mean pressure difference as measured by pressure tap. It can be seen from Figure 4.12 (a) that mean pressure differences are very similar for all for cases from CoI=0.35 to 1. When CoI dropped below 0.35, GOSH22 is 7 mmHg higher than UM10 and MUSC2. Again, define a sensitivity as

$$S_{pm} = \frac{d \text{ mean difference}}{d\ CoI} \qquad (4.8)$$

As illustrated in Figure 4.12 (b), the behavior is similar to that of SVP. From CoI = 1.0 to 0.5, S_{svp} data points scatter about 0, indicating no significant mean pressure difference change. When the CoI dropped below 0.4, the mean pressure difference

became increasingly sensitive to the CoI. Overall, the sensitivity responses are very similar for each patient; this could be an important clinical indication that CoI =0.5 is a threshold below which the mean pressure difference becomes significant for progressing coarctation.

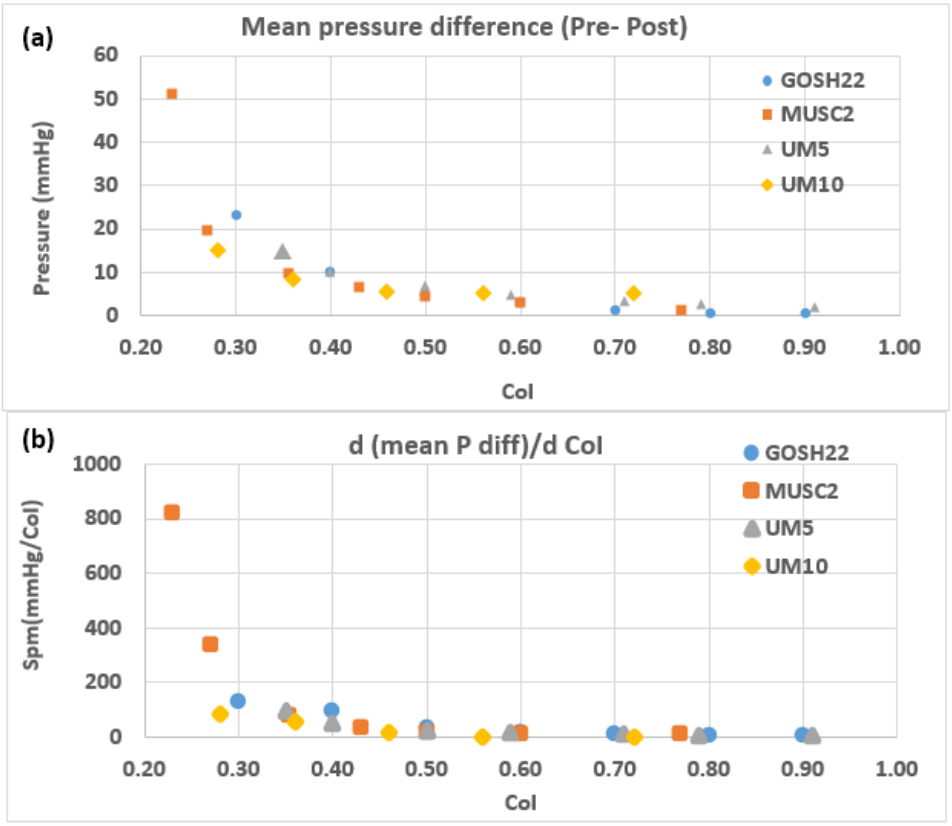

Figure 4.12. Scatter plot of (a) mean pressure difference vs. CoI and (b) S_{pm} against CoI for all four cases.

The aortic arch morphology differs for each patient. It can be concluded from the analyses of SVP and mean pressure difference alone, that aortic arch morphology should not be expected to reveal obvious differences in hemodynamics responses.

In addition to SVP and mean pressure difference, there are two other parameters that are of clinical interest. They are Qp/Qs and peak to peak pressure gradient. Figure 4.13 (a) illustrates peak to peak pressure gradient changes with CoI for all four patients. Overall, the pressure gradients increase gradually as CoI is decreased. When CoI falls below 0.5, the relative change in the pressure gradient increases. This can be better seen quantitatively through the peak to peak pressure gradient sensitivity, defined as

$$S_{pg} = \frac{d\,\Delta peak\ to\ peak\ gradient}{d\ CoI} \tag{4.9}$$

and plotted in Figure 4.13 (b). There is a noticeable change in the sensitivity for CoI < 0.5. All four cases demonstrate similar behavior, with no discernable difference among the four patients studied.

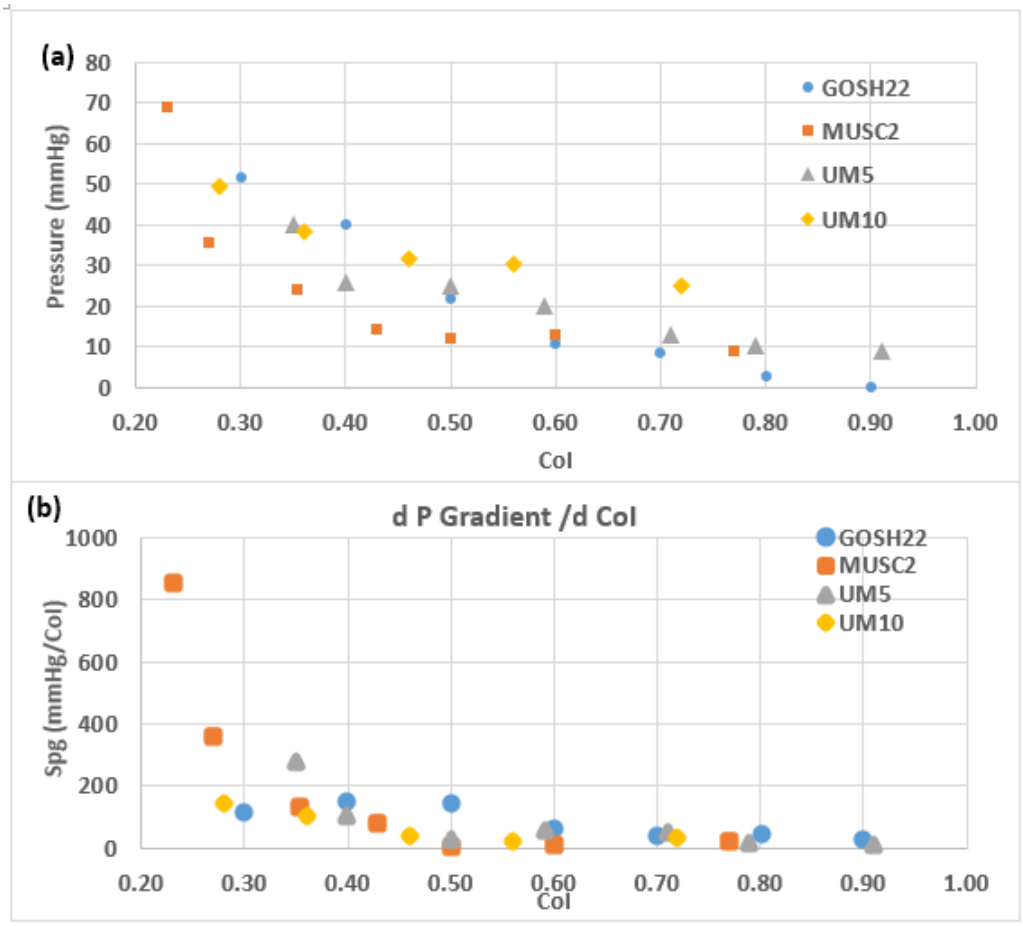

Figure 4.13. Scatter plot of (a) peak to peak pressure gradient vs. CoI and (b) S_{pg} against CoI for all four cases.

The peak to peak pressure gradient data indicates that it is less sensitive to changes in CoI than SVP or mean pressure gradient. Peak-to-peak gradient data are used clinically. The differences may be answered by examining the pressure waveform at “Pre” and “Post” wall tap site, as shown in Figure 4.14.

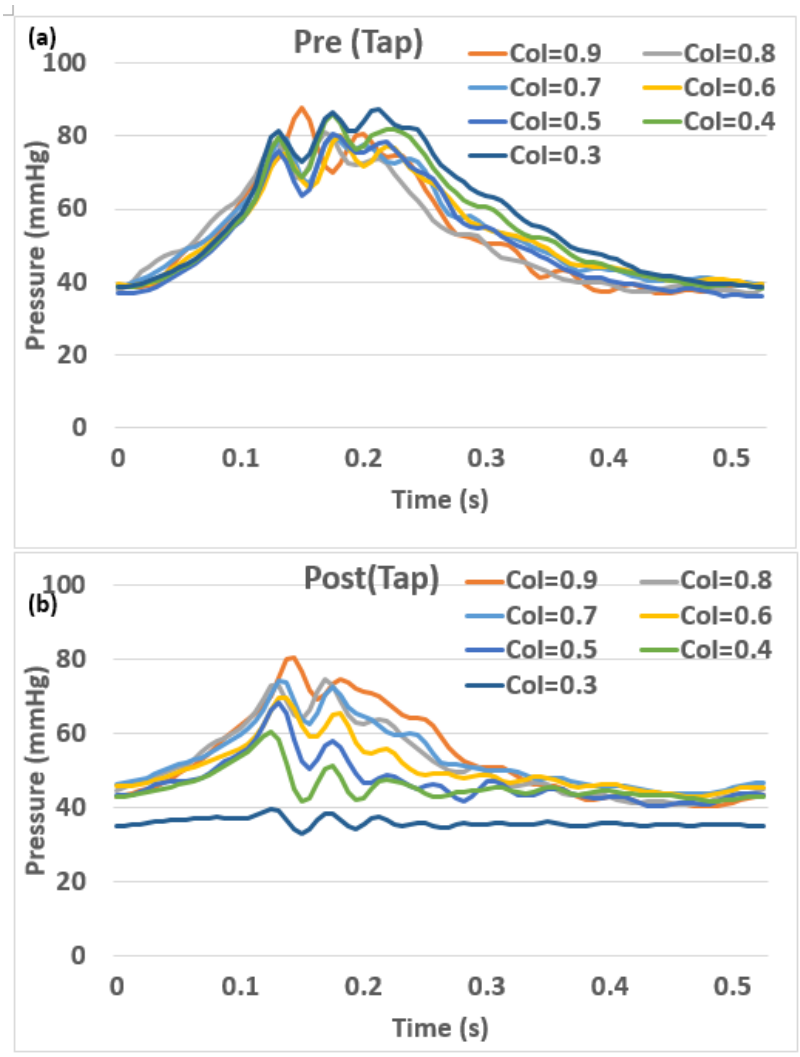

Figure 4.14. Ensemble pressure tracings at (a) Pre measure site (b) Post measure site.

From Figure 4.14, it can be seen that there are two effects coming into play here, one is the change in mean, this effect impacts peak to peak gradient like a baseline shifting. The other effect is the damping of P_{post} amplitude, directly increasing the gradient. This is due to the Coarctation resistance R_{coa} and downstream compliance C_{lb} work together as a RC filter, and as R_{coa} increases, the filtering effect becomes stronger. The damping effect begins immediately, even for small values of R_{coa}, whereas the mean value is reduced only as R_{coa} becomes

significant relative to R_{lb}. These two effects work together so the peak to peak gradient response is more linear than SVP and mean pressure responses.

Q_p/Q_s data can be examined in Figure 4.17 (a). There is a discernable difference in the achieved ratio for each patient. This would be a consequence of their individual physiology (PVR and SVR), as well as morphology. Define

$$S_{ratio} = \frac{d\ \mathrm{Qp/Qs}}{d\ CoI} \tag{4.10}$$

as the sensitivity of Q_p/Q_s to CoI. This is plotted in Figure 4.17 (b). Between 0.6 < CoI <1 the change in Q_p/Q_s with CoI is minimal. Below CoI < 0.5, Q_p/Q_s becomes more sensitive to CoI change. This can be quantitatively confirmed by the sensitivity plot in Figure 4.17(b). The rate of change in flow distribution Q_p/Q_s to CoI increases noticeably below CoI < 0.5. This indicates that CoI <0.5 may indicate a state where clinical intervention should be considered. The Q_p/Q_s versus CoI measurements for all four cases demonstrate a similar behavior in that the Q_p/Q_s balance of the native condition becomes affected only at severe CoI.

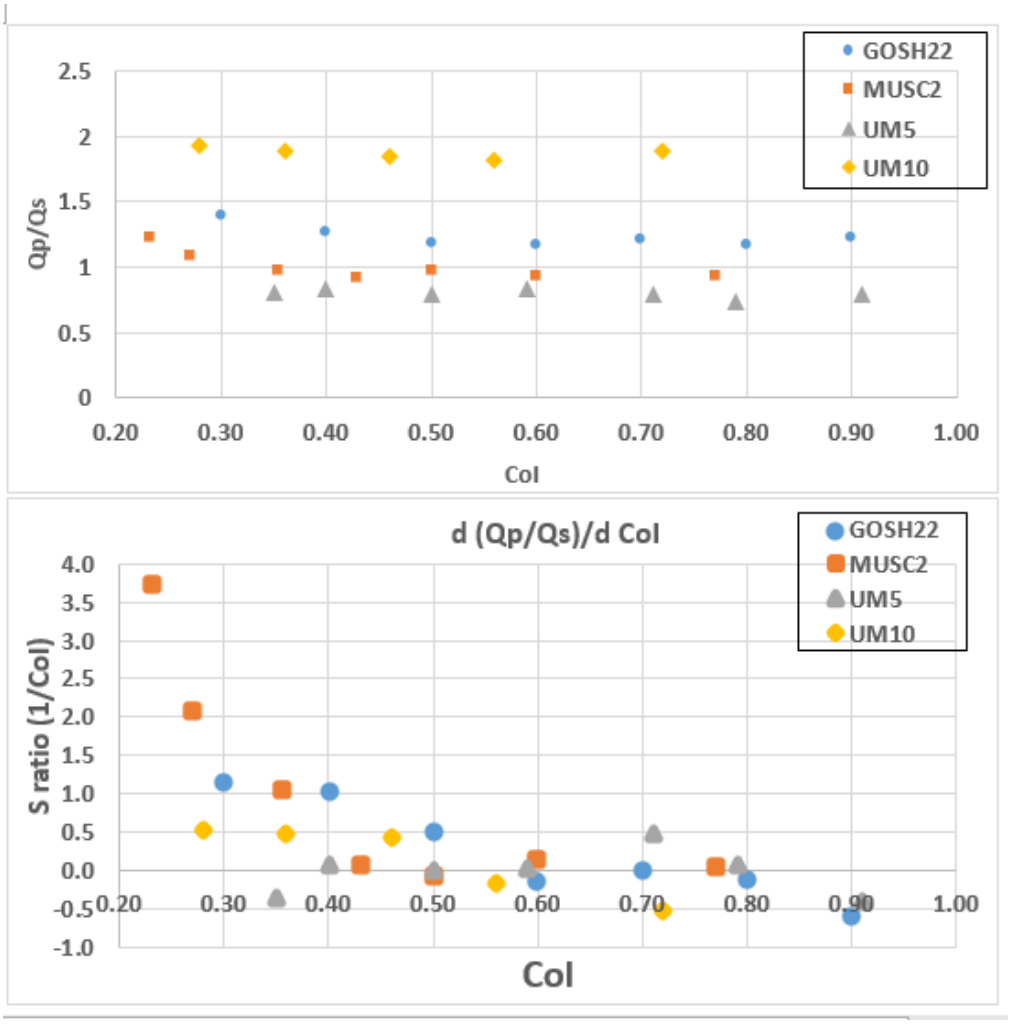

Figure 4.15. Scatter plot of (a) Q_p/Q_s vs. CoI and (b) S_{ratio} against CoI for all four cases.

There exists the potential for arch morphology to affect the phase of shunt flow. Specifically, it was investigated if the cardiac cycle phase with shunt flow rate is different among four patients. Figure 4.16 shows relative phase difference between cardiac cycle and shunt flow rate for the four cases. It can be concluded from Figure 4.16 that there is no discernable difference of cardiac-shunt flow phase difference among the four cases. In all four cases, shunt flow rates have no retrograde flow, and

peak of shunt flow rates occurred just a little before VAD valve closure. Hence aortic morphology does not have an effect on cardiac-shunt flow phase for these patients.

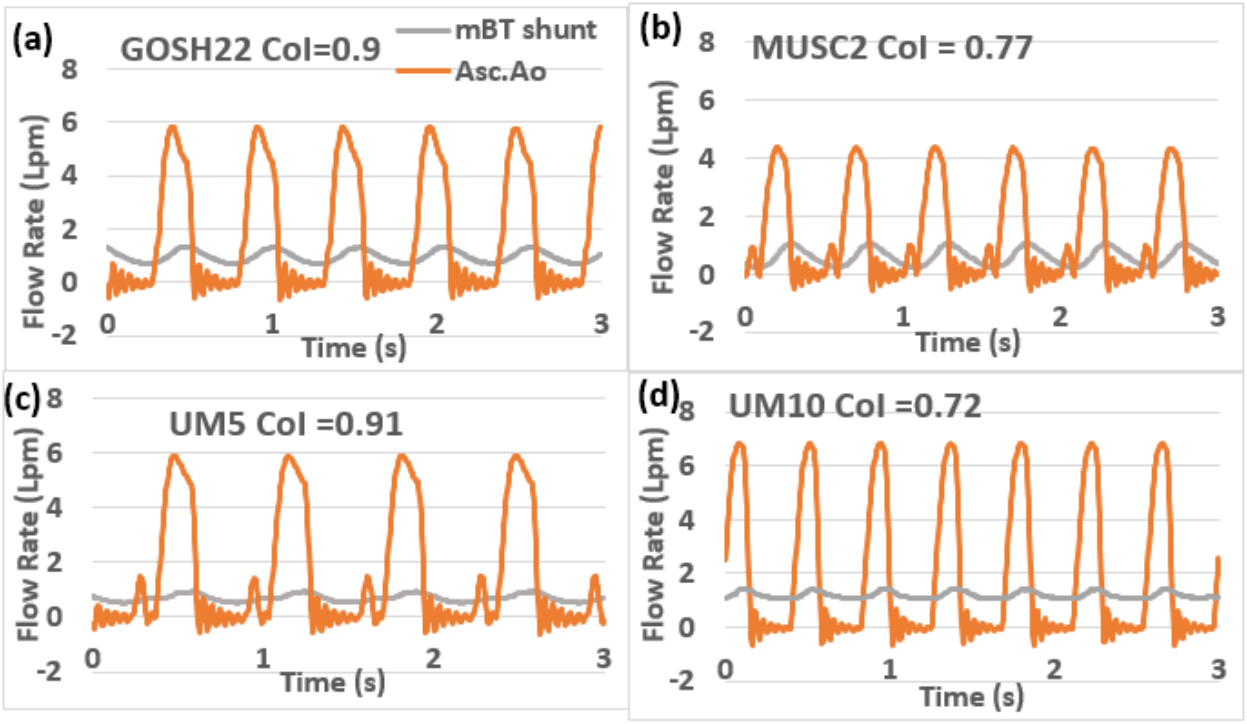

Figure 4.16. Ascending aortic flow rate and shunt flow rate in (a) GOSH22 (b) MUSC2 (c) UM5 (d) UM10.

From the foregoing analysis, aortic arch morphology affected SVP. Abnormal shapes (tubular or dilated) required increases in ventricular power from a normal shape.

Comparisons with Previous Work

These results confirmed some observations made in previous studies. Overall, the tests indicated that the pressure difference response to CoI severity was non-linear, which was also reported by Engvall et al. (Engvall, 1991). From an engineering point-of-view, the pressure difference across an obstruction, such as an orifice, is non-linear

with obstruction diameter. What this study here shows is the systems-level response to CoI severity.

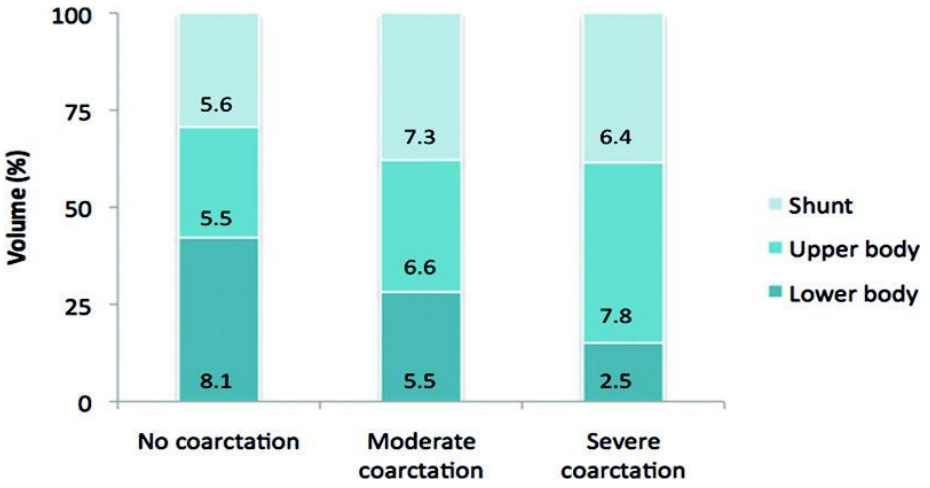

Figure 4.17. Volume distribution variations (%) for the three anatomical models, with the amount to the lower body being reduced with the presence and increased severity of coarctation. Volumes to each lumped vascular bed (upper body, lower body, and shunt) are also reported in ml on the graph bars. (Biglino, 2012)

Decrease in Q_{lb}, increase in both Q_{ub} and Q_{pul} and overall increased Q_p/Q_s were observed as COA narrows, which was also reported by Corsini et al. (Corsini, 2014). Figure 4.17 illustrates results in a study conducted by Biglino's group. Biglino et al's result confirmed results in this study that COA causes Q_{lb} decrease, Q_{ub} increase. However Q_{shunt} trend is not clear in their study, it increased in the case moderate coarctation, but decreased in the case severe coarctation. This counter-intuitive result can be attributed to the fact that author claimed their Q_p/Q_s is not physiological.

Overestimation of pressure gradient caused by COA due to pressure recovery was reported by Giardini et al. (Giardini, 2010). Defining Error = (SBE predicted

/actual gradient -1)×100, Giardini et al demonstrated the Error vs. Reynolds number (Re) relationship, using 3 different simplified Bernoulli equations in Figure 4.18. Figure 4.18 shows when Re is low, error is minimal, error increases as Re increases till Re=4000. Then Error decreases as Re continuously increases. Compare with results in this study, it was possible to measure pressure recovery in some specific patients at specific CoI. In this case, define Error = (Pre-1D gradient/ Pre-Post gradient -1) ×100, which is comparable to the scenario $DPG = 4((V_2)^2 - (V_1)^2)$ in Figure 4.18 (grey dots). The maximum error is 20%, with the maximum Re 1000. These observations echo with the Giardini results.

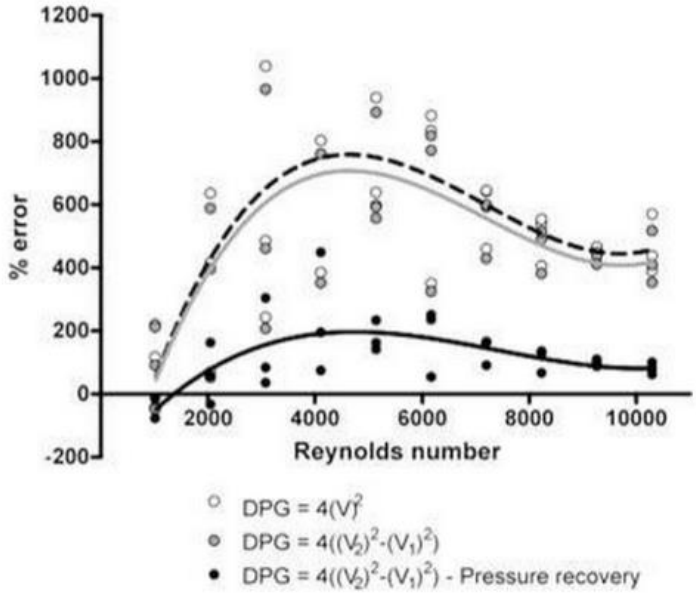

Figure 4.18: The relationship between Reynolds number and Doppler/Actual percent error using the simplified Bernoulli equation, the extended Bernoulli equation and considering pressure recovery effects. (Giardini, 2009)

Table 4.1 revealed an unexpected phenomenon regarding an ascending aortic pressure increase. How much ascending aortic pressure increase should be expected

as coarctation develops? One animal study conducted on biventricular dogs indicated that from "Normal" to CoI=0.3, mean ascending aortic pressure increased around 37 mmHg (Gupta, 1951). However, this study suggests that for a univentricular Norwood patient with mBT shunt, the situation is quite different. The data here show around a 5 mmHg increase from 1 < CoI <0.3. Even when CoI narrowed to 0.23, the highest pressure increase in ascending aorta observed was 15mmHg. Such small ascending aortic pressure increase was not expected.

The reason why there is such a different result is twofold. First, Norwood circulation is categorically different from normal biventricular circulation. The added pulmonary flow, roughly equal to the total systemic flow and competing directly with the lower body flow, greatly reduces the sensitivity of the system to throttled lower body flow. The mBT shunt is like a bypass, relieving pressure increase in the aortic arch. Second, the MCS uses a VAD, which is different from a natural ventricle in its performance. Cardiac output and heart rate were deliberately maintained constant in this study; in practice, CO and HR may behave differently as developing coarctation changes both preload and afterload and the body responds to maintain oxygen delivery. However, it remains unclear if the pattern observed would be different. The relationship between Reynolds number and Doppler/actual percent error using the simplified Bernoulli equation, the extended Bernoulli equation, and considering pressure recovery effects. The relationship between Reynolds number and Doppler/actual percent error using the simplified Bernoulli equation, the extended Bernoulli equation, and considering pressure recovery effects.

Regarding the effect of transverse aortic arch morphology on hemodynamics response, one possible conclusion is that transverse arch and isthmus hypoplasia does not affect hemodynamics response due to COA. Ntsinjana et al pointed out that it is the transverse arch and isthmus hypoplasia, rather than acute arch angulation, plays a role in the pathophysiology of BP response to peak exercise following CoA repair (Ntsinjana, 2013). In this study, it was also concluded that aortic arch dilation affects hemodynamics response.

More importantly, this study revealed many phenomena that have not been produced before. Previous COA studies are mostly in the context of biventricular circulation, but this study of COA in the context of univentricular circulation (Norwood Circulation) in particular breaks new ground.

Secondly, most of the early COA studies have used generic aortic phantoms with an idealized coarctation profile. Norwood patients have a wide spectrum of aortic morphology, which could contribute to various fluid dynamics phenomena in the aorta. Using a generic aortic phantom with idealized coarctation profile is not sufficient to study this morphological effect. The model described here used a sampling of patients with a range of realistic aortic morphologies, while also keeping the native geometrical profile at COA site while decreasing its diameter. This strategy permitted investigation of differences from patient to patient.

Thirdly, this study investigated COA's effect on global hemodynamics. In most of the previous studies, adopted cfd model of a generic aorta domain was used with boundary conditions prescribed at inlet and outlets and the effect of progressive

COA narrowing within this domain was studied. There is no coupling with the entire circulation. There are very impressive studies conducted using this approach, such as LaDisa et al 2011. However, as discussed in section 3.2, using this method does not allow investigating the effect of COA on global hemodynamics. The multiscale MCS presented in this study allows studies into how the progressive coarctation impacts the lower body flow rate, distribution of flows to the various territories, PA pressure, and other variables.

Lastly, the reason why COA is especially harmful to the Norwood patient is because it adds an extra work burden to the already overloaded single ventricle. Due to the hemostasis process, the single ventricle works even harder to maintain CO in spite of COA. This process was approximated in this study by maintaining CO constant as coarctation severity was increased. This enabled a means to quantify the hydraulic workload, which is especially important to Norwood patients. The final aim is to provide guidance to the clinical professional on when surgical intervention is necessary. These factors were never modeled in the previous *in vitro* studies.

CHAPTER FIVE

IN VITRO MULTI-SCALE PATIENT-SPECIFIC STUDY OF COARCTATION IN NORWOOD PATIENTS WITH A RIGHT VENTRICLE SHUNT (RVS) RESULTS

The modified BT shunt (mBT) and the right ventricular (Sano) shunt (RVS) are two of the most prevalent options in the Norwood procedure. There has been no study that directly compares RVS and mBT potential performance on the patient-specific level in the context of recurring neoaortic coarctation (NAO). It is still unknown which one of the two surgical options is more sensitive to NAO narrowing, and if there is any difference with regard to hemodynamic response? The MCS provides a means to assess any differences and perhaps delineate their causes. The goal of this part of the study is to improve the understanding of the differences between the RVS and mBT in a NAO context by direct comparison. An outcome would be to reveal which type of circulation is more sensitive to NAO, and identify the difference in hemodynamic response as NAO develops. To accomplish this, the MCS was modified to a RVS setup based on the alterations described in Biglino et al. (Biglino, 2013).

Methods

This is an *in vitro* study of hemodynamics in Stage 1 Norwood patients with a ventricular-to-pulmonary RVS. The previously described MCS was modified to

model the the SVS circulation (Biglino, 2013). Using rapid manufacturing techniques, patient-specific test models of the neoaorta were constructed. For each patient model, the severity of coarctation was increased using separate test sections.

Selection of patients

Patients selected in this study are GOSH22, MUSC2, UM5, and UM10. Patient parameters were given previously in Figure 2.2 and Table 2.1.

Mock Circulatory Design

Certain modifications were necessary to complete the RVS mock circulatory design, as shown in the layout of Figure 5.1. In particular, the RVS (shunt) was connected directly to the lumen of the VAD. The de-airing valve located on the liquid-side chamber of the VAD was selected as the site having the best structural support. The de-airing valve was hollowed out to create a 5 mm outflow port, and a Tygon tube was connected from there to the pulmonary circulation, at the compliance chamber, thus completing the RVS. The same test sections used previously were used here, but with the mBT shunt blocked off. Because the mBT shunt nub on these models is located downstream in the brachiocephalic artery, the stagnant zone in the nub should not affect hemodynamics in the aortic arch. .

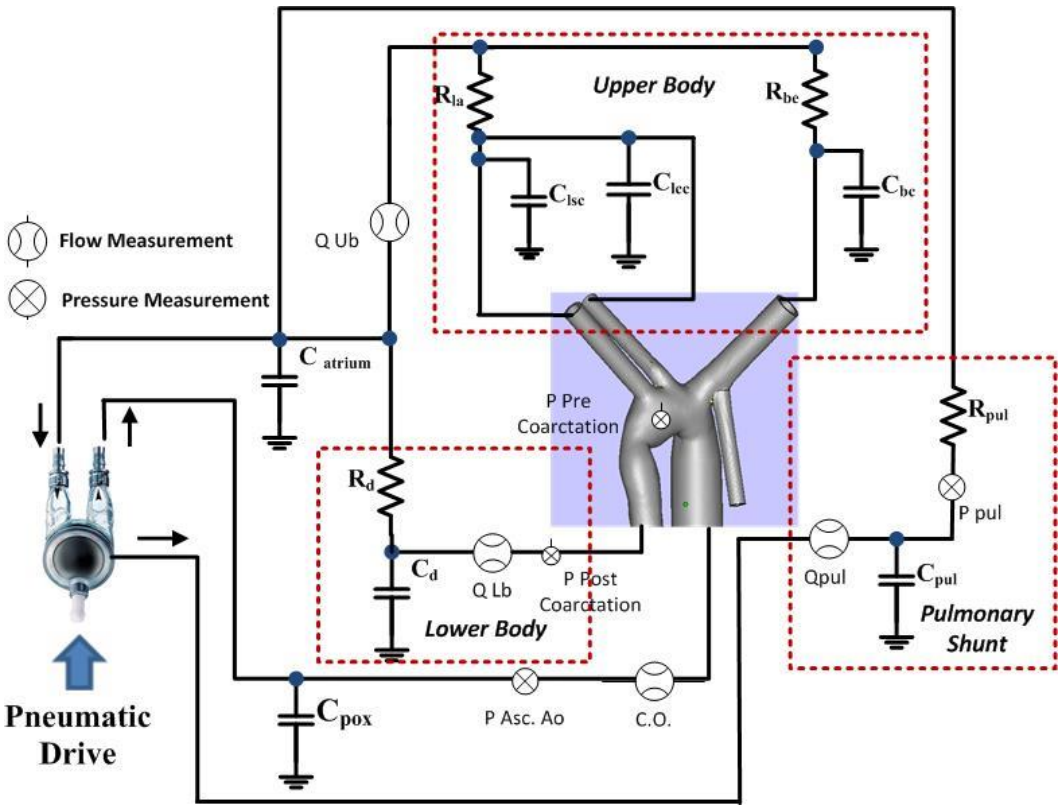

Figure 5.1 Reduced Lumped parameter network model used for mock circulatory system in RVS setup with measurements points shown. R, resistance; C, compliance; P, pressure; Q, flow rate; C.O., Cardio output; Asc.Ao, Ascending aorta; Prox, proximal; pul, pulmonary shunt; d, descending aorta; atrium, atrium; bc, brachiocephalic artery; lcc, left common carotid artery; lsc, left subclavian artery.

In vitro realization of homeostasis

As described in section 4.2, the human body reacts to changes of circulation by attempting to maintain perfusion. This physiological response was realized *in vitro* by controlling the cardiac output (CO), which was maintained constant. The mock circulatory system was first tuned using the parameters of Table 1.1 for a given patient in mBT circulation. Then, after changing the coarctation, the driving pressure of the VAD was adjusted to restore the CO to the baseline value. Mean aortic

pressure and the distribution of flows among the upper body, lower body, and lungs were allowed to change in response to COA. When the system was converted to RVS circulation all the system parameters exclusive of the mBT shunt were kept the same, so a different baseline pulmonary flow (Q_p) and CO were allowed. As the coarctation was changed, the VAD was adjusted again to maintain the value of CO for RVS.

Single ventricular power

Single ventricular power (SVP) was measured in a different manner with the RVS setup. Figure 5.2 shows the schematic of the VAD in RVS circulation. The VAD has two outflows as opposed to one outflow in the mBT setup. Q_{in} and P_{in} denote the inlet flow and pressure, with inlet pressure taken as equal to atrium pressure. For the outflows, P_{out} denotes the liquid side pressure of the VAD, which is the driving pressure for both pulmonary and systemic circulations. Q_{out1} and Q_{out2} denote systemic flow and pulmonary flow respectively. The formula to calculate VP in a RVS setup is:

$$Power = \frac{1}{T_{cycle}} \int [Q_{out1}(t)+Q_{out2}(t)] \cdot P_{out}(t)\, dt - \int Q_{in}(t) \cdot P_{in}(t) dt \qquad (5.1)$$

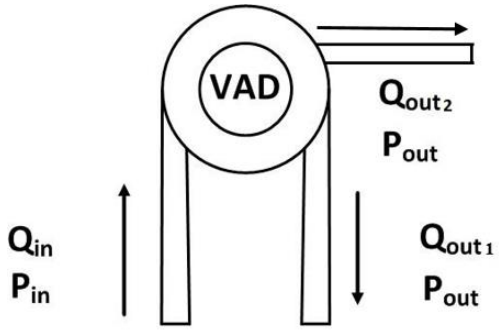

Figure 5.2. A Ventricular Assist Device (VAD) diagram, Qin Qout1 and Qout2 denote volumetric flow rate of inflow, systemic and pulmonary circulation outflow, Pin Pout denote flow pressure of inflow and outflow.

Due to the nature of RVS flow, regurgitation fraction was calculated using the time-based RVS flow rate data and the following equation:

$$RF = [\%] = \frac{Q_{reverse}}{Q_{forward}} \times 100 \qquad (5.2)$$

Results

The experiments were designed to measure systems-level hemodynamics changes in response to increasing coarctation severity in the RVS circulation. From these results, a comparison to the mBT procedure was made.

Mean pressure differences were calculated using two methods. In method 1, mean pressure differences between PRE and 1D were calculated, while in method 2, mean pressure difference between PRE and POS were calculated. Also, peak pressure gradients were calculated using the same methods.

Mean flows were also measured. Time-averaged mean flows were calculated at ascending aorta, mBT shunt, upper body, and lower body. For the ease of comparison, flows are presented as the percentage of the total flow or systemic flow. The pulmonary to systemic ratio Qp/Qs was also calculated for each of the cases.

GOSH22

GOSH22 had a slight tubular aortic arch. Figure 5.3(a) shows the mean pressure difference response vs. CoI. In the RVS scenario, the pressure difference is 5 mmHg or less from CoI=0.9 to 0.5. From CoI=0.5 to 0.3, pressure difference increased to over 20 mmHg. The overall pressure difference response to CoI change demonstrates an exponential-like curve. There is no significant difference between RVS and mBT here. Similarly in Figure 5.3(b), peak pressure gradients demonstrate a similar non-linear response, that is, pressure gradient is more sensitive to CoI change at low CoI. Small difference are observed between RVS and mBT pressure gradient. RVS pressure gradients are higher than the mBT counterparts from CoI=1 to CoI=0.5, by 8mmHg maximum. From CoI =0.3 down to CoI=0.1, mBT pressure gradients are higher than the RVS counterparts by up to 5 mmHg.

Figure 5.3(c) shows the SVP response. Overall there is no significant change in SVP from CoI = 0.9 to 0.6. From CoI =0.6 to 0.3, SVP of each increased by 22mW. There is a systemic reduction (25mW) of RVS vs. mBT SVP, mainly due to the lower Q_p of the RVS.

Figure 5.3(d) shows the flow changes in both cases. Total flow (CO) for each case was held constant as CoI was reduced. Note that RVS has less CO than mBT, due to reduced pulmonary flow. With a generic 5 mm diameter ventriculotomy and 5 mm RVS shunt size, shunt flow was 0.67 lpm which yields a Q_p/Q_s ratio of 0.8. The reason is that this is a physiologically realistic condition. Pulmonary flows (Q_p) are presented as a percentage to CO. RVS Q_p to CO ratio had negligible changes (<0.01)

as CoI=0.9~0.3, while the mBT counterpart increased by 0.03. Q_{ub}/Q_{sys} increased 0.05 from CoI =0.9 to 0.3. Q_{lb}/Q_{sys} decreased 0.04 from CoI =0.9 to 0.3. Differences in Q_{ub}/Q_{sys} and Q_{lb}/Q_{sys} between RVS and mBT were negligible.

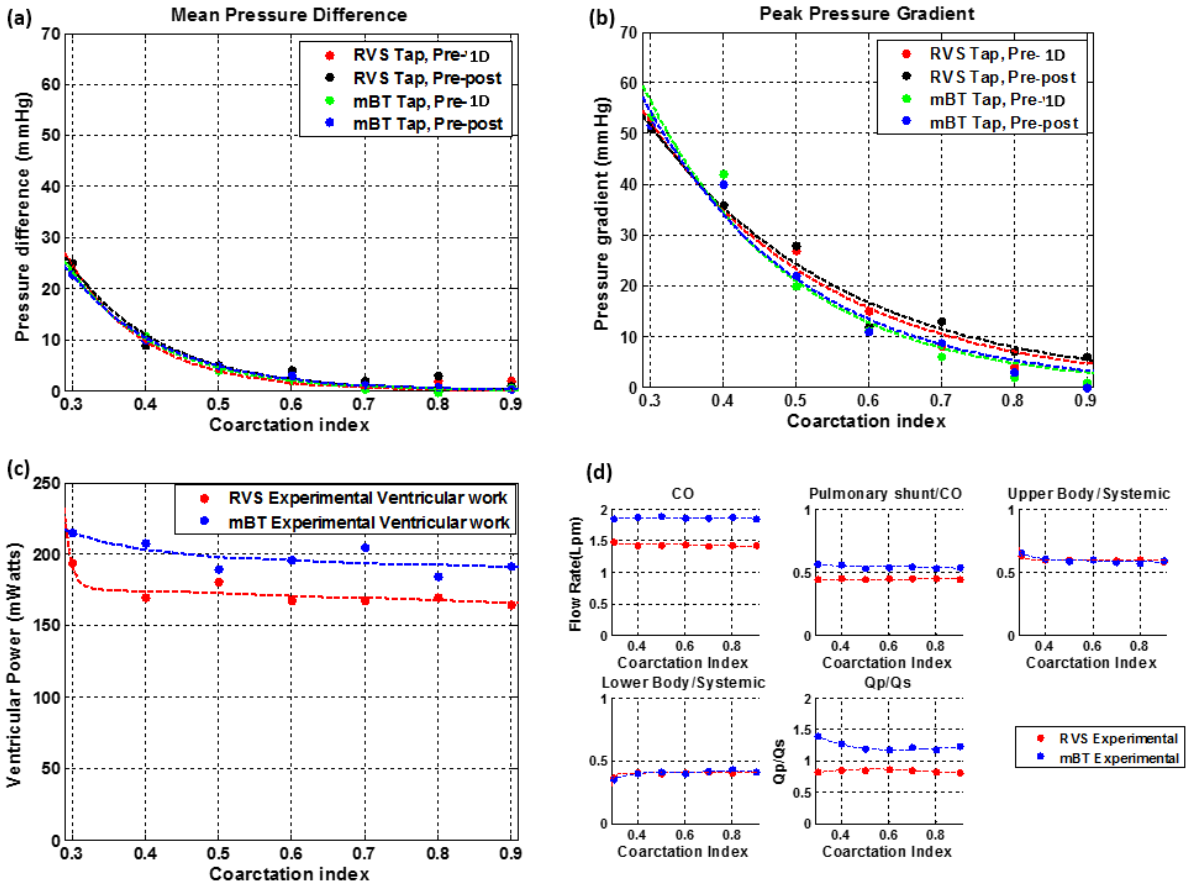

Figure 5.3. Measured hemodynamics of GOSH22 case in response to CoI variation: (a) mean pressure differential (b) peak to peak pressure gradient, (c) Single Ventricle Power, (d) flow rates.

MSUC2

MUSC2 had a normal tubular aortic arch, as shown in Figure 5.4(b). This patient's left subclavian artery was removed during the Norwood surgery.

Figure 5.4 (a) illustrates the mean pressure difference response. In the RVS scenario, the pressure difference is less than 10 mmHg for CoI=0.78 to 0.35, with a linear shape. Pressure difference increases dramatically from CoI =0.35 to 0.23, rising to around 50 mmHg with a highly non-linear response. In Figure 5.4(b) pressure gradients demonstrate a more consistently exponential-like response, that is, pressure gradient is more sensitive to CoI change at lower CoI. Difference between RVS and mBT responses is minimal, with almost no difference for CoI >0.35. Less than 10 mmHg of difference between shunt types was observed for CoI <0.35, and no more than 15 mmHg difference for intermediate CoI.

The nonlinear response was also observed in ventricular work, Figure 5.4 (c). There is a systemic difference between the two responses, but unlike GOSH22, it is not explained by a proportionate reduction of Q_p. Instead, this reveals improved efficiency of the RVS, due to some shunt flow continuing during diastole, at lower ventricular pressure. Both RVS and mBT SVP increase significantly only for CoI<0.35.

Figure 5.4 (d) shows the volumetric flow changes in both cases. CO for each case was held constant at the initial value for CoI=0.78. Overall the flows responded similarly to GOSH22. In both mBT and RVS, Q_{pul}/CO increased, Q_{ub}/Q_{sys} increased, and Q_{lb}/Q_{sys} decreased, all becoming significant only in the lower CoI values. In terms of Qp/Qs, there was a divergence between RVS and mBT in the lower CoI values, with a maximum difference of about 0.1 from CoI=0.35 ~0.27. The same phenomenon occurs in subfigure (b), RVS peak to peak pressure gradient responses demonstrates an exponential shape. From CoI=0.78 to 0.35, there is a pressure

gradient around 25 mmHg. From CoI =0.35 to 0.23, pressure gradient increases by 45 mmHg. Overall the differences between RVS and mBT pressure gradient response are very minimal (<7mmHg). With the only exception of from CoI=0.6~0.35, mBT pre-1D gradient is lower than RVS counterpart by around 10mmHg.

The exponential like response is also observed in subfigure (c). Like the previous case, there is systemic difference between the two responses because of the difference in CO. Besides that, both RVS and mBT SVP responses increases noticeably only after CoI<0.35.

Subfigure (d) illustrates the volumetric flow rate changes in both cases. Total flow for both cases were held at constant. Due to the same reason stated in the previous case, there is difference in CO. Overall the flow rates responses are very similar as in the previous case. In both mBT and RVS, Q_{pul}/CO increased slightly especially at lower CoI region, Q_{ub}/Q_{sys} increases by a more noticeable value at lower CoI region, and Q_{lb}/Q_{sys} decreases by a noticeable amount at lower CoI region. Overall Q_p/Q_s increases noticeably at lower CoI region, and difference around 0.1 is observed between the RVS and mBT from CoI=0.35 ~0.27.

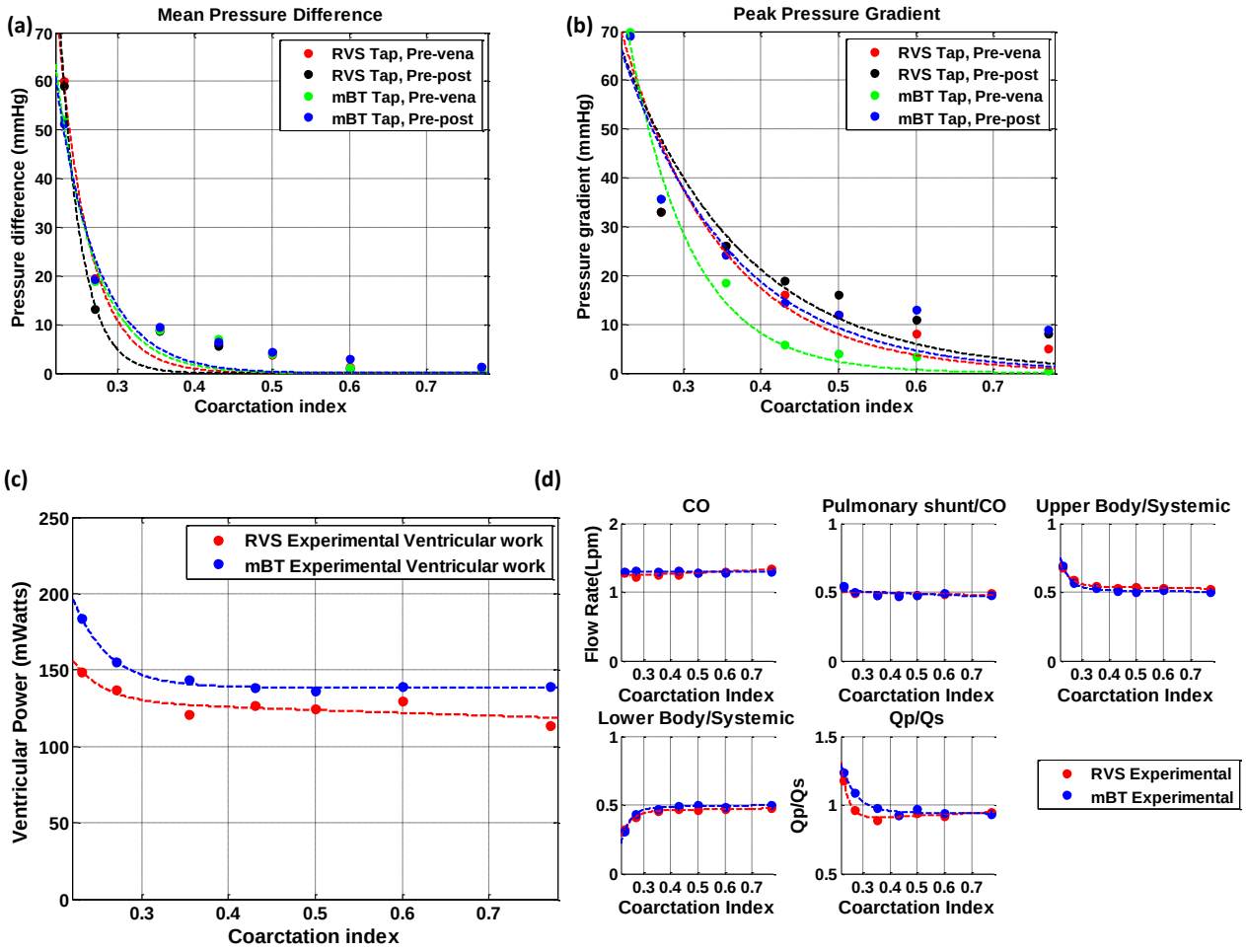

Figure 5.4. Measured hemodynamics of GOSH22 case in response to CoI variation: (a) mean pressure differential (b) peak to peak pressure gradient, (c) Single Ventricle Power, (d) flow rates.

UM5

UM5 had a dilated aortic arch. In Figures 33 (a) and 33 (b), pressure response to CoI is more linear, in contrast to the previous two cases. Although both demonstrate linear shape, mBT and RVS pressure differences show a noticeable divergence when CoI<0.6, and this difference increased as CoI decreased. The same pattern occurs in pressure gradient response, and in mBT the peak pressure gradient increased about 28mmHg overall.

SVP did behave similarly to the preceding cases, increasing significantly only at the smallest CoI=0.35. The RVS required much less power than the mBT, and the difference is only partly attributable to the lower CO in the RVS sequence.

In Figure 5.5 (d), Q_{pul}/CO increased slightly as CoI decreased. Q_{ub}/Q_{sys} increased by noticeable amount and Q_{lb}/Q_{sys} decreased by a noticeable amount, both in a linear fashion. Differences between the RVS and mBT flows were minimal.

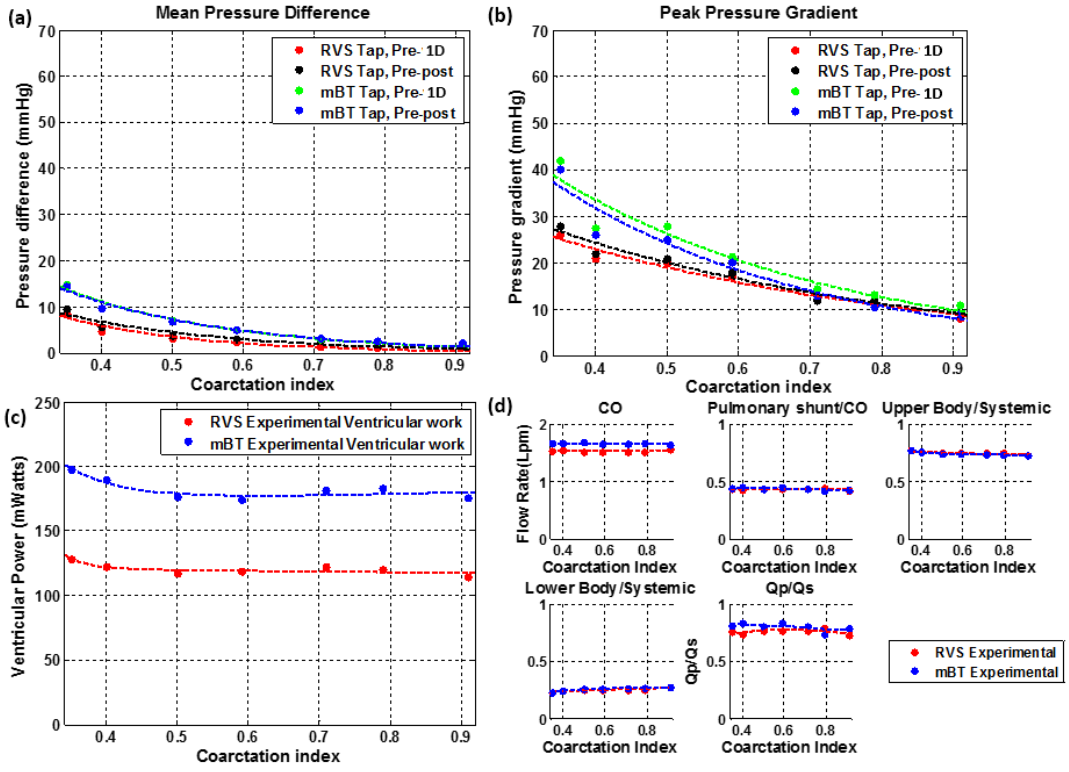

Figure 5.5. Measured hemodynamics of UM5 case in response to CoI variation: (a) mean pressure differential (b) peak to peak pressure gradient, (c) Single Ventricle Power, (d) flow rates.

UM10

UM10 had a dilated aortic arch. Due to the native NAO of the patient, CoI variation could only be realized from 0.72 to 0.28. Figure 5.6 shows the hemodynamic responses of UM10 to CoI variation.

From Figure 5.6 (a), it can be seen that both the mBT and RVS cases show a linear response of pressure difference to CoI. The differences between RVS and mBT are within 6 mmHg. The same trend was observed in pressure gradient responses in Figure 5.6(b), where the maximum difference between the two cases is 9 mmHg.

Figure 5.6(c) describes the ventricular power. Both cases remain nearly constant, except power of mBT increases only at smallest CoI=0.28. The large systemic difference between the two cases can only partly be explained by the difference in CO.

In Figure 5.6 (d) flow changes are linear, and Q_{ub} and Q_{lb} show no differences between mBT and RVS, except at CoI=0.23 where RVS has a higher Q_{lb}/Q_{sys} and a lower $Q_{ub}\backslash Q_{sys}$. In this case the original patient-specific Q_p/Q_s was excessive.

Overall responses of the four cases are summarized Table 5.1.

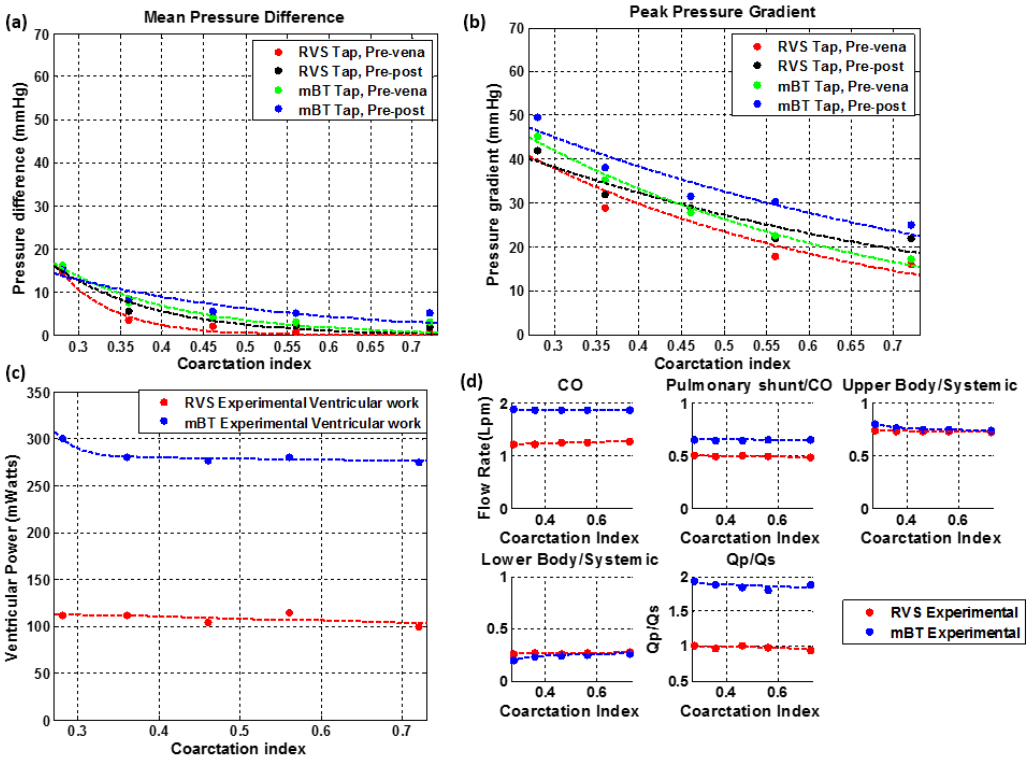

Figure 5.6. Measured hemodynamics of UM10 case in response to CoI variation: (a) mean pressure differential (b) peak to peak pressure gradient, (c) Single Ventricle Power, (d) flow rates.

	GOSH22		MUSC2		UM5		UM10	
Dilation/Tubular	Tubular		Normal		Dilated		Very dilated	
CoI	0.90~0.30		0.77~0.23		0.95~0.35		0.72~0.28	
	mBT	RVS	mBT	RVS	mBT	RVS	mBT	RVS
CO ± STD	1.86±0.01	1.43±0.02	1.29±0.01	1.28±0.03	1.67±0.02	1.53±0.02	1.87±0.02	1.25±0.02
Change in Q_{ub}/Q_{sys}	+0.07	+0.07	+0.19	+0.15	+0.05	+0.05	+0.05	+0.02
Change Q_{lb}/Q_{sys}	-0.07	-0.05	-0.19	-0.15	-0.05	-0.05	-0.05	-0.02
Change Q_{pul}/CO	+0.02	<0.01	+0.07	+0.04	+0.02	+0.02	<0.01	+0.02
Change in SVP (mW)	+23.01	+29.30	+44.81	+35.00	+21.76	+14.04	+24.63	+12.55
Change in Q_p/Q_s	+0.15	<0.01	+0.30	+0.24	+0.04	+0.03	+0.01	+0.05
Change in $P_{asc.ao}$ (mmHg)	+5	+10	+15	+12	+3	+7	+5	+4
Change in $P_{ventricle}$ (mmHg)	NA	+1	NA	+2	NA	+1	NA	+1

Table 5.1. Flow rates, SVP and pressure changes in four patients.

Discussion

The noticeable difference between the systems-level response of the RVS and mBT lies within the pulmonary flow. In Figure 5.7, the case GOSH22 CoI=0.9 is used to illustrate this difference from the flow perspective. Figure 5.7 (a) shows the ascending aortic flow and shunt flow in the RVS scenario. The ascending aortic flow and RVS shunt flow occur concurrently. There is a considerable proportion of pulmonary retrograde flow during diastole, so the RF is 39%. In Figure 5.7 (b), the mBT shunt scenario, there is a phase lag between the ascending aortic flow and the mBT shunt flow, with the peak of mBT shunt flow occurring just before aortic valve closure. Pulmonary flow is always antegrade in the mBT shunt. The reasons are known and clear: the right ventricle pressure falls below the aortic pressure during diastole in the RVS, whereas the aortic pressure remains above the pulmonary pressure in the mBT.

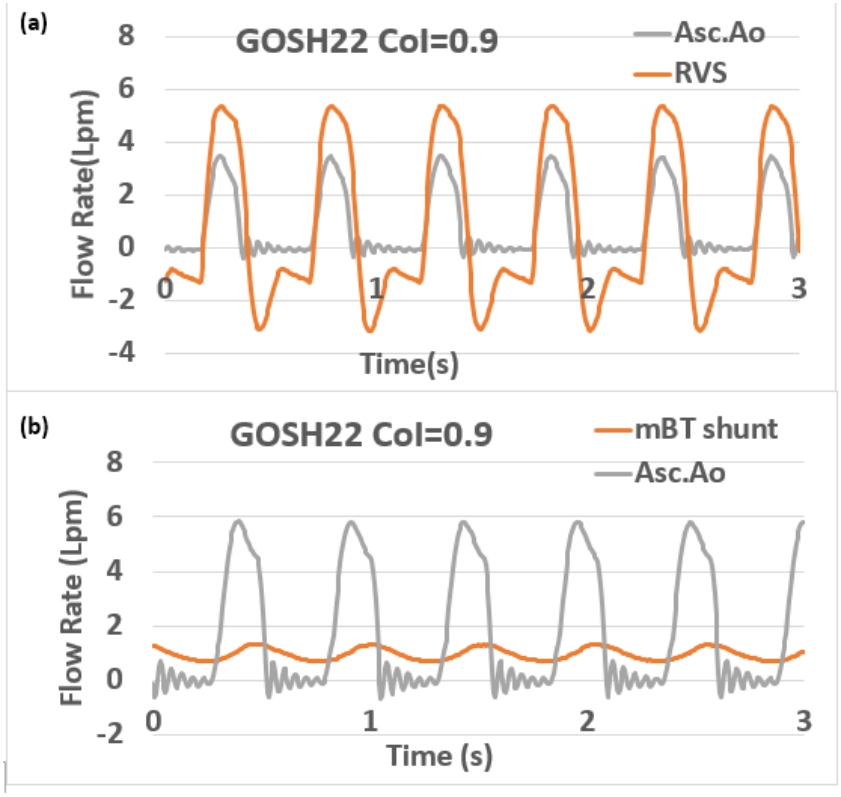

Figure 5.7. Three seconds of instantaneous flow measurements of (a) GOSH22 CoI=0.9 with a RVS. (b) GOSH22 CoI=0.9 with an mBT shunt.

Next, examining the flow responses for all four RVS cases (Figures 5.3-5.6, and Table 5.1), as coarctation narrows (CoI decreases), decreases in Q_{lb} were observed as expected, due to increasing coarctation gradient in series with the constant LBSVR. With reduced Q_{lb}, the VAD was adjusted to maintain CO, increasing aortic pressure. This increased Q_{ub}, as expected. The changes in Q_{lb}/Q_{sys} and Q_{ub}/Q_{sys} were very similar between RVS and mBT cases.

As the VAD was adjusted to higher aortic pressure, the mean ventricular pressure also increased, hence increasing the RVS shunt flow. Q_{pul}/CO changes in RVS were lower than those of mBT for GOSH22 (tubular arch) and MUSC2 (normal

arch). However in the cases of UM5 and UM10 (dilated arch), Q_{pul}/CO changes in RVS and mBT were very similar in magnitude.

Overall, the pulmonary to systemic flow ratio (Q_p/Q_s) increased for all four cases. Changes in Q_p/Q_s are smaller in RVS cases than mBT except in UM10. Also noteworthy in GOSH22 and UM10, the mBT Q_p/Q_s ratios are high, meaning there was excessive pulmonary flow. Applying an RVS brought down Q_p/Q_s ratio of these two cases closer to unity. While the RVS scenarios are less sensitive to changes in COA than the mBT scenarios, the differences are marginal and likely not clinically significant..

Why do systemic flows in the mBT and RVS behave similarly while pulmonary flows show significant differences? Referring to Table 5.1, the difference in $P_{asc.ao}$ between the two cases is not significant (<5mmHg), so the pressure differences driving flow through the systemic branches are very similar for all these cases. However in the pulmonary branch, mBT cases

$$Q_{pul} = \frac{P_{asc.ao} - P_{atr}}{R_{mBT} + PVR} \qquad (5.3)$$

while for RVS cases

$$Q_{pul} = \frac{P_{ventricle} - P_{atr}}{R_{RVS} + PVR} \qquad (5.4)$$

The R_{RVS}+PVR < R_{mBT}+PVR because the RVS diameter is larger than mBT diameter by almost 50%. Because CO was maintained constant, aortic pressure increased with coarctation severity. As CoI narrowed, it was observed that Δ ($P_{asc.ao}$-P_{atr}) >Δ ($P_{ventricle}$-P_{atr}). So, the mBT cases generally saw a greater change of driving pressure,

while RVS was more sensitive due to lower total resistance. Both effects contributed to changes in Q_{pul}, and depending on which effect was stronger, pulmonary flow rate changes in RVS could be higher, lower or equal to those in mBT.

The SVP response to CoI with the RVS indicated a similar behavior as those with mBT. The SVP required did not change significantly until CoI was severe. However, the SVP with RVS requirements for each patient were generally lower than those SVP values measured with the mBT and by 74.5 mW on average. The reason why RVS baseline was lower is twofold. First, the shunt is larger in all cases: a 5 mm diameter RVS connected the VAD to pulmonary chamber in all four cases (RVS cases are extrapolative rather than patient-specific in this respect). The resulting baseline Q_p was reduced in three cases, with the exception of MUSC2. Since SVP depends upon total flow, the effect of reduced Q_p reduces the SVP baseline. Secondly, from the perspective of pressure, with an mBT shunt, the single ventricle has to pump blood to the higher pressure of the systemic circulation. While with a RVS, ventricular flow can be pumped directly to pulmonary arteries, which have lower pressure than systemic system. These two effects work together, hence SVP baselines with RVS are generally lower than those with mBT shunt. This phenomenon was also observed in previous studies. In 2001, Shimizu et al. together with Dr. Shunji Sano conducted a 0D simulation study comparing mBT and RVS. One important observation they made is that RVS is associated with lower ventricular power. Shimizu et al claimed that this phenomenon is consistent with clinical observation, (Shimizu S, 2011). Also due to the same reason, from Table 2.2, the SVP changes in most RVS cases with CoI are smaller than those with mBT shunt except GOSH22.

Overall, the SVP change with RVS is less than that with mBT, by 5.8 mW on average for the cases studied.

From a hemodynamics-only view point, the RVS is a better option for some cases but any such difference is minimal, because the sensitivity of either circulation type to coarctation is similar. While the advantages may be statistically different, the difference is very small.

When looking at morphological differences in the Sano procedure, four parameters of clinical interests are examined similar to those studied with the mBT.

Figure 5.8 (a) plots the SVP changes with coarctation SVP does not change much in response to CoI between 0.4 < CoI < 1. For all cases, the change is less than 15 mW. Below CoI < 0.4, the increase in SVP becomes increasingly greater. The aortic arch morphological affects the SVP baselines in this study. It can be seen from Figure 5.8 (a) that GOSH22 (tubular) has the highest SVP requirements. MUSC2 (normal) has the second highest SVP. UM5 is (dilated) about same as MUSC2. UM10 SVP (strongly dilated) is lower than MUSC2 SVP. This pattern indicates that with an RVS, it is possible that tubular arch morphology is associated with higher SVP while dilated aortic arch is associated with lower SVP.

As before, define a sensitivity

$$S_{svp} = \frac{d\,\mathrm{SVP}}{d\,CoI} \qquad (5.5)$$

From Figure 5.8 (b), the increased sensitivity to CoI is noticeable for CoI < 0.5. In comparison with the results of the mBT shunt, the trend behaviors are quite similar.

This is a strong implication that regardless with which shunt configuration, the region of CoI < 0.5 is of clinical concern.

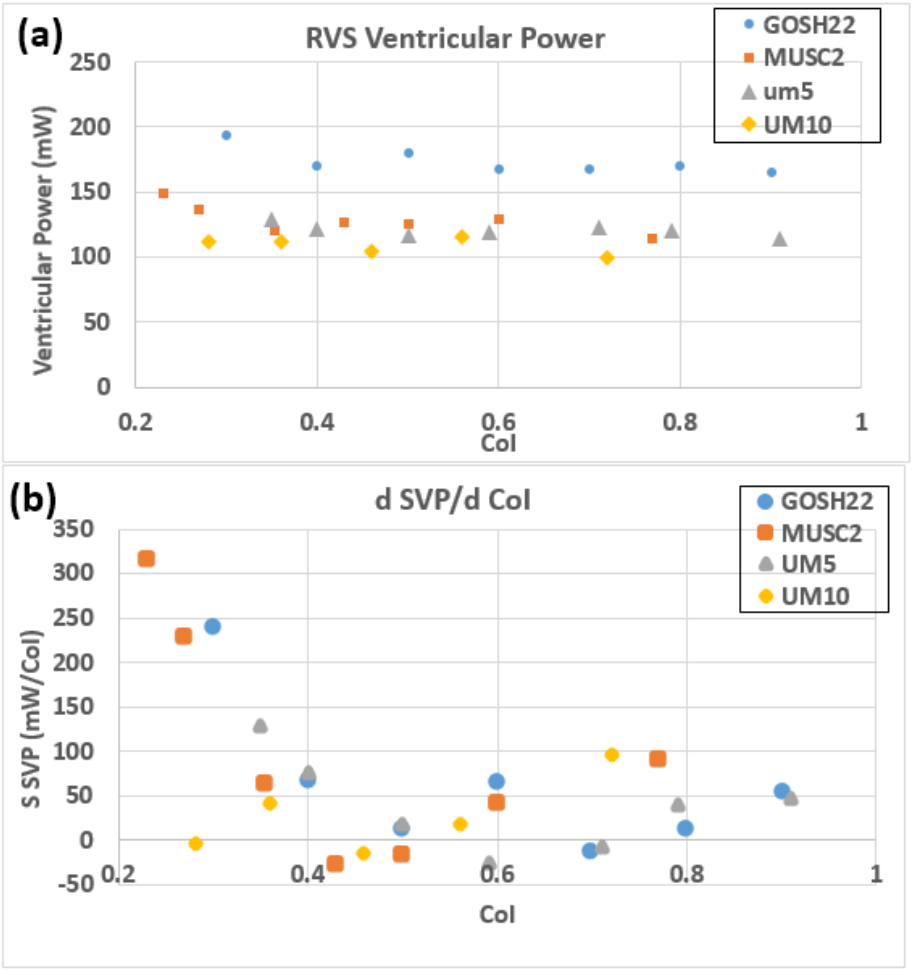

Figure 5.8. (a) SVP versus CoI scatter plot of all four cases. (b) S_{svp} of all four cases against CoI.

In order to quantify when statistically significant occurs, piecewise regression was conducted on SVP data. Piecewise regression partitions CoI into several separated intervals and fits a separate linear regression model to each interval of CoI. Piecewise analysis results in Figure 5.9 shows that breakpoint in the case GOSH22 is CoI=0.6, for MUSC2 are CoI= 0.3, for UM5 is CoI= 0.42, and piecewise regression

was not applicable for UM10. Overall, the results suggests that breakpoint for four five cases occurs when CoI<0.6. This is when statistically significant changes occur.

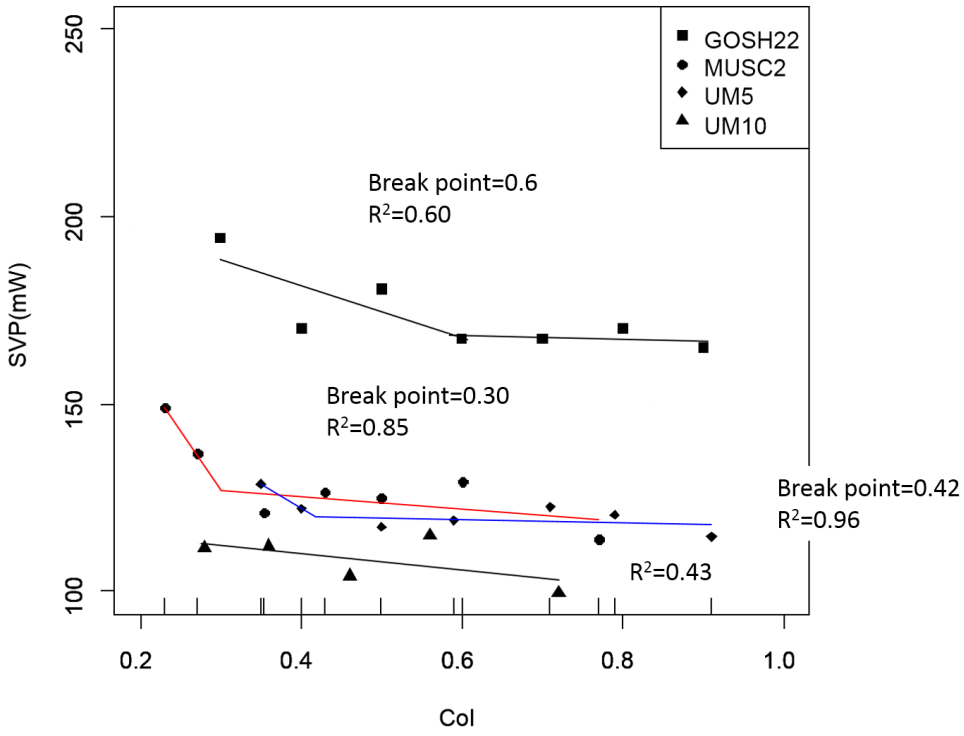

Figure 5.9. Piecewise regression results for five cases' SVP data, with estimated breakpoints and R^2 indicating the goodness of fit.

Figure 5.10 (a) illustrates the Qp/Qs response to CoI. There is little change between 0.4 < CoI < 1. For CoI < 0.4, the change becomes increasingly greater and nonlinear. This can be quantitatively confirmed by plotting the sensitivity, as shown in Figure 5.9(b). Define

$$S_{ratio} = \frac{d\ \text{ratio}}{d\ CoI} \qquad (5.6)$$

The rate of change becomes noticeably significant for CoI < 0.4. Similarly, it can be seen that all four cases demonstrated similar behavior, with no discernable difference among four cases. In the RVS, the Qp/Qs change occurs closer to 0.4 than with the mBT, which noticed the change closer to 0.5. The difference is subtle and well within experimental error.

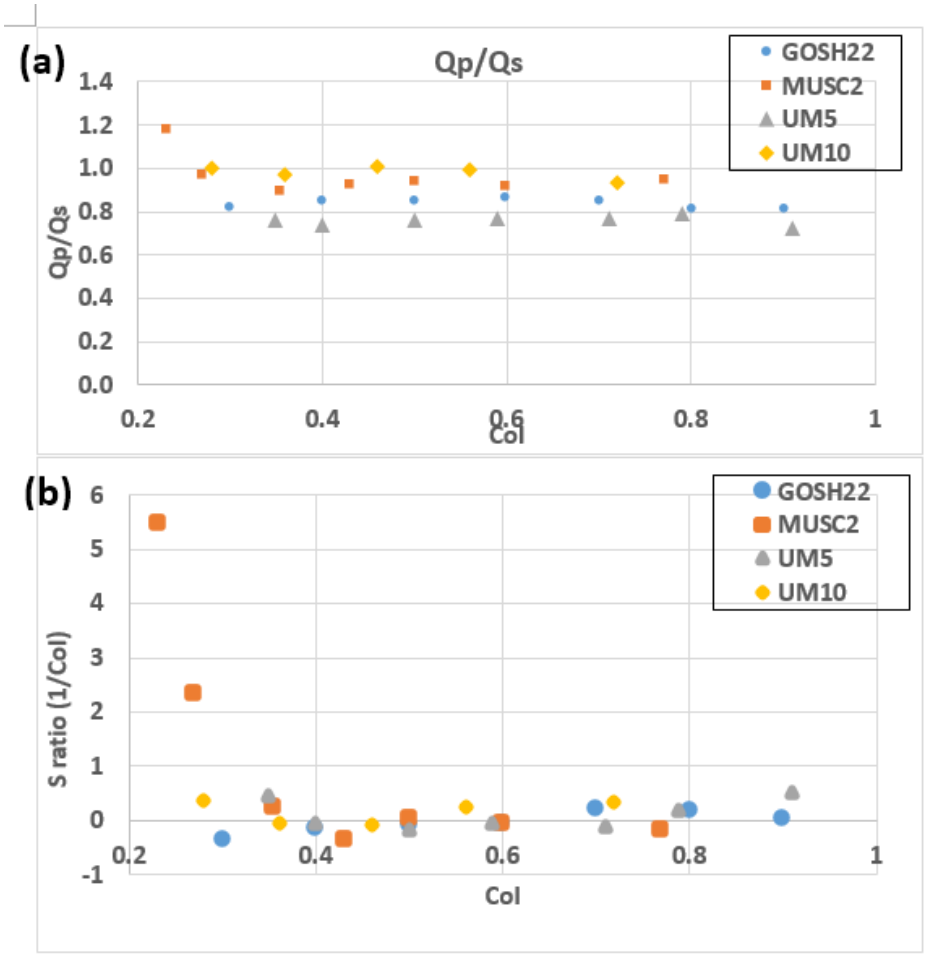

Figure 5.10: Scatter plot of (a) Q_p/Q_s vs. CoI and (b) S_{ratio} against CoI for all four cases**.**

Figure 5.11(a) illustrates Pre- to Post- mean pressure difference measured using wall taps. In Figure 5.11 (a), mean pressure difference tendencies are very

similar but there are differences between morphologies. There is little change between 0.4 < CoI < 1. When CoI dropped below 0.4, GOSH22 was 9 mmHg higher than UM10 and MUSC2.

Define the sensitivity,

$$S_{pm} = \frac{d \text{ mean difference}}{d\ CoI} \qquad (5.7)$$

As shown in Figure 5.11(b), there is little change in sensitivity above CoI > 0.4. Below CoI < 0.4, sensitivity progressively increased. The trend behavior between the RVS and mBT procedures show little difference in response to coarctation.

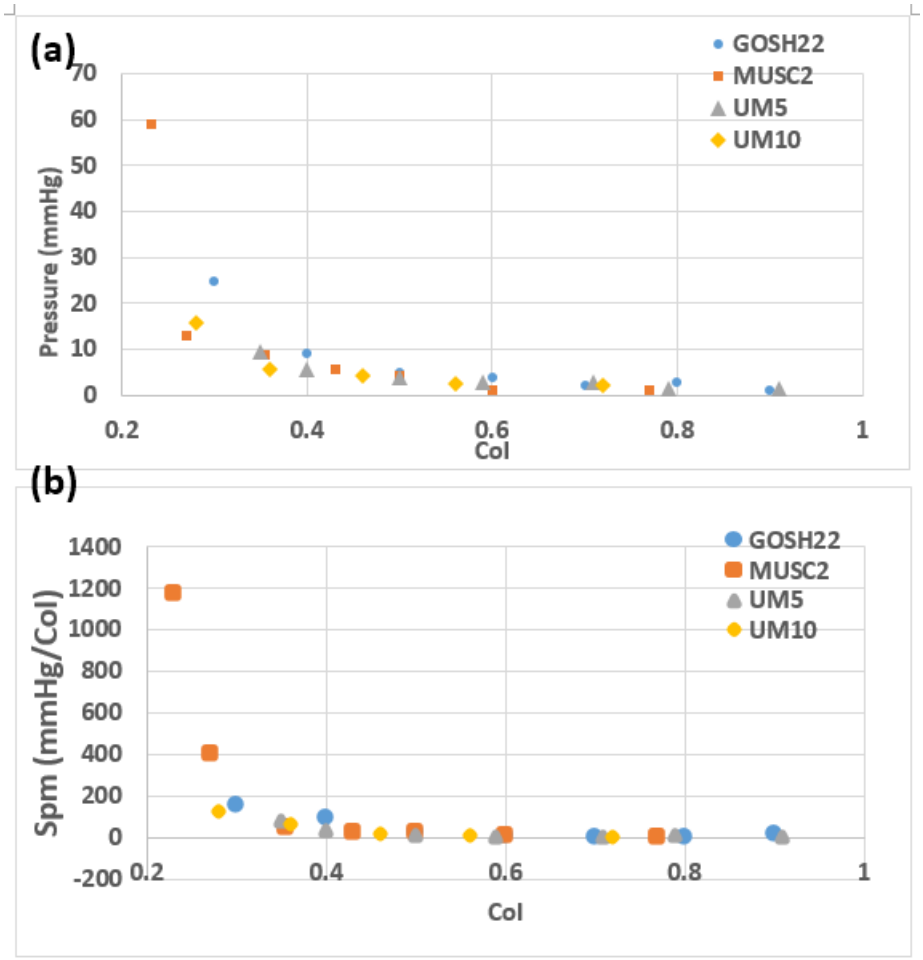

Figure 5.11. Scatter plot of (a) mean pressure difference vs. CoI and (b) Spm against CoI for all four cases.

Figure 5.12 (a) illustrates the peak to peak pressure gradients response to CoI for all four patients with RVS. Overall the pressure gradient responses demonstrate more comparatively linear behavior than the SVP and mean pressure difference, as noted in the mBT. There is a gradual increase in pressure with CoI. Define the peak to peak pressure gradient sensitivity as

$$S_{pg} = \frac{d\,\Delta peak\ to\ peak\ gradient}{d\ CoI} \tag{5.8}$$

This is plotted in Figure 5.12 (b). The sensitivity changes noticeably around CoI = 0.5 and markedly below CoI < 0.3. Comparing the RVS peak to peak pressure gradient response with its mBT counterpart, there is no difference in overall general behavior. All four cases demonstrate similar behavior, with no discernable difference among four cases that have a wide range of arch morphology.

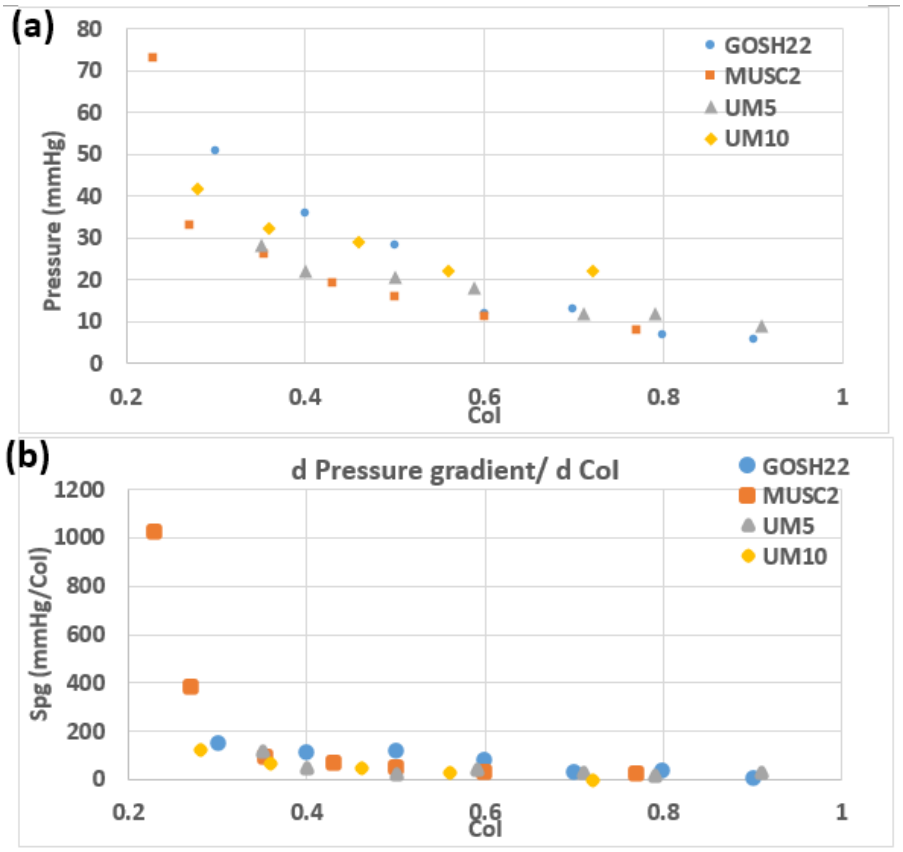

Figure 5.12. Scatter plot of (a) peak to peak pressure gradient vs. CoI and (b) S_{pg} against CoI for all four cases.

The SVP requirements vary with aortic morphology and physiology associated with each patient. However, there is not sufficient evidence that can be drawn from the results supporting the hypothesis that aortic arch morphology affects hemodynamics responses in the RVS circulation with increasing coarctation severity.

This is the first *in vitro* study to compare the hemodynamics of the RVS and mBT shunt circulations in the COA context. This study confirmed some clinical observations and hypotheses made in previous *in silico* and *in vivo* studies. Shimizu et al. together with Dr. Shunji Sano conducted a 0D simulation study comparing mBT

and RVS in 2011. One important observation they made, which is consistent with clinical observation, is that RVS is associated with lower ventricular power. Table 5.2 illustrates part of their results. This can be attributed to fact that with mBT shunt, single ventricle has to pump blood to higher pressure system, that is, the systemic circulation (Shimizu, 2011). While with a RVS, pulmonary circulation can be pumped directly to PA, which has lower pressure than systemic circulation. This observation is also observed in this study.

	SW(mmHg ml)	Mechanical efficiency (%)
3.5-mm SPS	905	78.2
6.0-mm non-valved RV-PA	827	84.7
5.0-mm valved RV-PA	702	80.3

Table 5.2. Influence of different shunt configuration on stroke works. SW: Stroke work (Shimizu, 2011).

In addition, it has been reported repeatedly that due to diastolic run off in the RVS shunt, RVS can prevent pulmonary overcirculation and is usually associated with lower Q_p/Q_s (Shimizu S, 2011; Fischbach, 2013; Ohye, 2007). This phenomenon was also observed in this study, and differences in Qp/Qs are significant especially in study GOSH22 and UM10. Figure 5.13 illustrates Shimizu's results. Figure 5.13 illustrates Shimizu's results, it can be seem that in 3.5 mm SPS case, due to the diastolic run-off from systemic to pulmonary circulation, yields Q_p/Q_s of 1.27. In the case of 5.0mm valved RV-PA shunt, there is no interaction between pulmonary and systemic circulation, yields Q_p/Q_s of 1.18. In 6.0mm non-valved RV-PA case, due to

pulmonary diastolic run off to RV, Q_p is lowest thus yields the lowest Q_p/Q_s of 1.08. This is consistent with the observations that were made in this study.

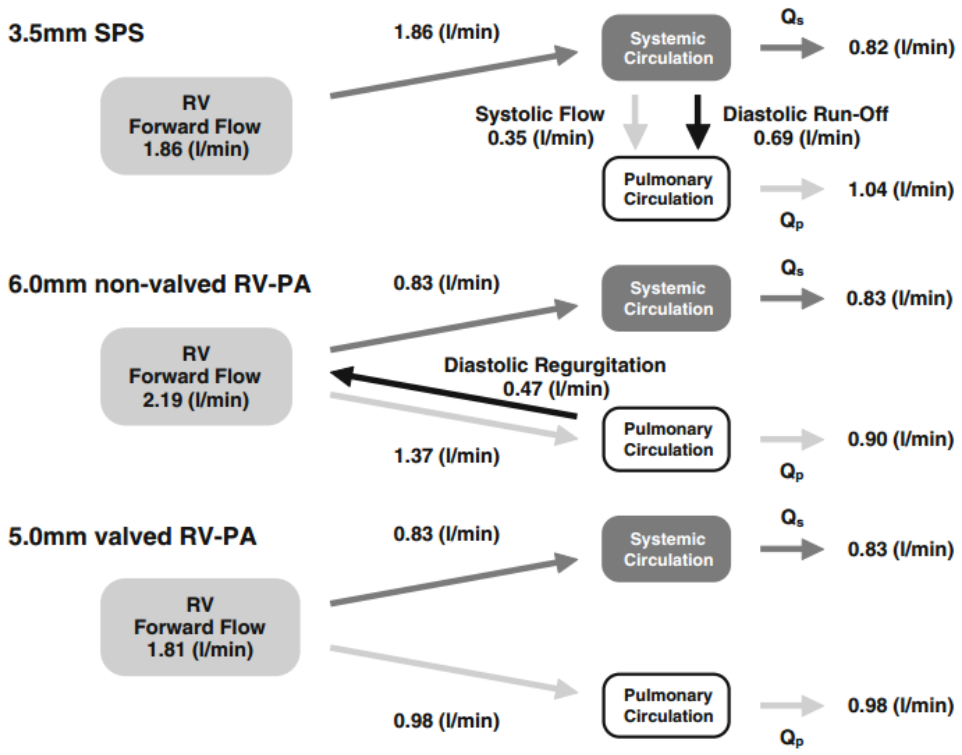

Figure 5.13. Hemodynamics obtained from the 3.5-mm systemic-to-pulmonary shunt (SPS) model, and 6.0-mm nonvalved and 5.0-mm valved right ventricle to pulmonary artery (RV-PA) shunt models.

CHAPTER SIX

SUMMARY AND CONCLUSIONS

An *in vitro* multi-scale, patient-specific Norwood circulation model was described and validated against clinical data. Using separate anatomically accurate phantoms of five patients having differing aortic morphologies following a Norwood procedure with BT shunt (mBT), the system was tuned to clinical patient-specific physiological parameters. Patient-specific conditions were achieved and pressure and flow rate were measured throughout the system and compared against clinical measurements. Results demonstrated that the time-based experimental measurements are physiological in form and statistical analysis shows that experimental time-based measurements are very similar to clinical measurements ($0.72 < R^2 < 0.95$). These results showed good fidelity in replicating the mean values of the Norwood circulation at the patient-specific level ($p > 0.10$). In validation, the system was able to recapitulate the hemodynamics of different Norwood patients at the patient-specific level, and judged suitable to study the physiological and morphological differences at the local and systems-levels between patients and to study changes occurring over time within a patient.

The validated MCS was applied to studies of coarctation effects in the Norwood with mBT circulation. Four patient-specific hemodynamic responses to neoaortic coarctation (NAO) variation were studied. A coarctation index was used as a measure of coarctation severity. CoI was changed between mild to severe to demonstrate the effect of NAO on hemodynamics. System level pressure and flow

rates responses were measured throughout the system. Overall, this study revealed that NAO caused increases in upper body flow (0.04 Lpm on average) and mBT shunt flow (0.05 Lpm on average), decreases in descending aorta flow (0.08 Lpm on average). NAO also caused hypertension in the aortic arch (7 mmHg increase on average) while hypotension in lower body (18.5 mmHg increase on average). NAO also increased SVP by 28.55 mW on average. It was also concluded from sensitivity analysis that for all four cases, the single ventricle power (SVP), mean pressure difference and Q_p/Q_s increased noticeably only when CoI < 0.5. The results also indicated that CoI < 0.5 presents noticeable hemodynamic changes suggesting that surgical intervention should be considered. Differences in the single ventricle power (SVP) between patients of differing aortic morphology were observed with abnormal aortic arch morphology (dilated or tubular) associated with increased SVP. In summary, it was demonstrated that aortic morphology does affect hemodynamics, and NAO may not need immediate surgical intervention until reaching severe for patients.

The mock circulatory system was modified to simulate the Norwood procedure with RVS. Four patient-specific hemodynamic responses to NAO variation were studied using this arrangement as direct comparison to the mBT shunt study. The RVS shunt flow occurred concurrently with ascending aortic flow while the mBT shunt flow showed a phase lag, between ascending aortic and shunt flow rate. The results showed that substituting the mBT with RVS can relieve pulmonary overcirculation in two of the cases (GOSH22, UM10), with average reverse to forward flow ratio of 39%, further causing Q_p/Q_s in those two cases to be closer to unity than the mBT scenario (by 0.7 on average). This behavior also contributed to

the reduction of total CO by 0.3 Lpm (four cases average compared with mBT scenarios) and brought down SVP requirements by 74.5 mW (four case average compared with mBT scenarios). In terms of sensitivity to CoI, the RVS cases mirrored the responses of the mBT cases in that no noticeable difference in SVP was noted until CoI < 0.6, whereby it increased significantly. Overall, the total changes of SVP in RVS with CoI in 3 out of 4 patients were slightly lower than those in mBT by 5.8 mW (4 cases average). Differences in SVP required in the RVS cases were noted for the four different aortic arch morphologies studied. A tubular arch morphology was associated with a higher SVP than those with a dilated arch. Overall, the results showed that RVS eliminates the pulmonary overcirculation observed by mBT, and is associated with a lower SVP compared with mBT counterparts. RVS is slightly insensitive to NAO change compared with mBT counterparts (5.8 mW difference in SVP).

Limitations and Recommendations:

Overall the results are satisfactory and some of the results presented in this dissertation confirmed the observations that were made in previous studies. This dissertation furthers our understanding of the Sage 1 Norwood circulation due to its advantageous modelling method and patient-specific nature. However, there are a few limitations of the present study and future directions for continued studies.

The study used rigid models of the aorta. A proximal compliance was used to allow realistic aortic pressure waveforms and excellent correlation with clinical waveforms was demonstrated. This also allows direct comparisons with numerical

models that use rigid test sections. However, a flexible model would enable accurate wall shear measurements and may offer other subtle benefits.

The RVS study was conducted using a VAD rather than a real heart model. The difference between the VAD and a realistic heart model might affect the results. The VAD used in this study is not a realistic ventricle model, in a sense that it cannot simulate the contractility of a real ventricle physiologically. This discrepancy contributes to the fact that the reverse to forward flow ratio is higher in this study than clinical empirical data (39% vs. 25%). A realistic heart model would be beneficial in the future to further our understanding of RVS.

This study did not attempt to measure velocity or wall shear within the 3D phantoms. To better understand why aortic arch morphology has an impact on hemodynamics, particle image velocimetry (PIV) should be used to measure the flow field in aortic arch. For example, while reverse flow in lower body flow rate was measured, the amounts going to the upper body versus to the mBT shunt were not measured. Future work can be conduct in this direction.

APPENDICES

Appendix A

Uncertainty Analysis

In this appendix A, the uncertainty estimates for the results presented in this dissertation are discussed.

The error sources considered affecting the pressure and flow estimates included: zero-point systemic error, instrumental error, data acquisition error, and the random error found both within and between cardiac cycles. Propagation of elemental uncertainties to the uncertainty estimate is calculated by the Taylor expansion method (Figliola, 2014). In general elemental errors are propagated as:

$$u_r = (\sum_k (\theta \cdot u_k))^{\frac{1}{2}} \qquad \text{(A.6)}$$

where θ is the sensitivity, u_k is the elemental uncertainty and u_r is the resultant uncertainty.

Uncertainty in Pressure and Flow Rate Measurements:

There are two types of contributing errors: systematic (mean offset from zero) and random (fluctuations due to noise about the mean set point) errors. Systemic error includes zero-point systemic error, instrumental error, and data acquisition error. The random error was found both within and between cardiac cycles.

In the category of systemic error, zero-point errors indicate how well the instruments can be tuned to zero. Instrument errors were assigned as systematic uncertainty according to manufacturer's manual statement of error. Data acquisition

errors were assigned based on the voltage range of the sensors and number of bits of the DAQ board, the equation utilized is:

$$u_{DAQ} = \frac{(\frac{V_R}{2^n})}{S} \qquad \text{(A.7)}$$

where VR is the voltage range of the sensors and n is the number of bits of the DAQ board.

Lastly, statistical random uncertainties were calculated as:

$$S_{\bar{x}} = \frac{S_x}{\sqrt{N}} \qquad \text{(A.8)}$$

where s_x is the standard deviation, N is the number of samples, and $S_{\bar{x}}$ is the random standard error. In the case of estimating the uncertainty in a mean value extracted from many cycles, a data set of N mean values were used to compute a standard deviation from which a standard error was computed as per (2.8) Random error dominated, a random uncertainty was calculated 0.1 mmHg for pressure measurement and 0.01 Lpm for flow rate measurement .

The elemental errors in pressure and flow rate measurements were considered to be independent (i.e., sensitivities set to equal 1) and uncorrelated and then propagated using the root-sum-square method $u_C = \sqrt{\sum_i (u_i)^2}$. Random uncertainty was propagated separately from systemic uncertainties. The final total uncertainty was propagated from the random uncertainty and the systemic uncertainty using the

root-sum-square method. The total uncertainty in the reported pressure and flow rate measurements are both under 3% at the 95% confidence level (critical t=2).

For example, in the case of UM5 CO measurement, random uncertainty was found to be ±0.01 Lpm, zero-point uncertainty was assigned to be ±0.01 Lpm, instrument error was assigned to be ±0.008 Lpm (0.5% of the reading), data acquisition error was calculated to be ±0.003 Lpm. The propagated total uncertainty is ±0.02 Lpm.

Similarly, for the case of UM 10 $P_{Asc.Ao}$, random uncertainty was found to be ±0.41mmHg, zero-point uncertainty was assigned to be ±0.1mmHg, instrument error was assigned to be ±0.365 mmHg (0.5% of the reading), data acquisition error was calculated to be ±0.004 mmHg. The propagated total uncertainty is ±0.56 mmHg.

Table A1 below shows the sample uncertainty calculation details for two measurements assuming confidence level 95%.

	Systemic uncertainties (b)				Random uncertainty (s)	Total Uncertainty (u)	Relative Value
Name	Reading	Instrument Uncertainty	Zero-point uncertainty	Data acquisition uncertainty	Random standard uncertainty		
UM5 CO (Lpm)	1.60	0.008	0.01	0.003	0.01	0.04	2.5%
UM10 $P_{Asc.Ao}$ (mmHg)	73	0.365	0.1	0.004	0.41	1.12	1.5%

Tabel A.1. Standard systematic uncertainties (b), and random uncertainty (s) and 95% confidence level uncertainties (u) for 2 examples.

The uncertainty in the reported pressure and flow rate measurements are both under 5% at the 95% confidence level in this dissertation.

Uncertainty in Resistances and Compliances:

Uncertainty in resistance and in compliance are functions of pressure, flow rate, and dimensional measurements. With$R = \frac{\Delta P}{Q}$, uncertainty in resistances can be estimated as:

$$u_R = \sqrt[2]{(\frac{\partial R}{\partial P} \cdot u_P)^2 + (\frac{\partial R}{\partial Q} \cdot u_Q)^2} \qquad \text{(A.9)}$$

With $C = \frac{V}{P\ abs}$, contributing factors to compliance were identified as air volume measurement error and working pressure measurements error.

$$u_C = \sqrt[2]{(\frac{\partial C}{\partial P} \cdot u_P)^2 + (\frac{\partial C}{\partial V} \cdot u_V)^2} \qquad \text{(A.10)}$$

The uncertainty associated with resistances and compliances are reported in Table 2.2.

For the example of MUSC2 LBSVR, total uncertainty in lower body flow rate (u_Q) was calculated to be ±0.02 Lpm, total uncertainty in ascending aortic pressure (u_P) was calculated to be ±1.28 mmHg. Sensitivity term $\frac{\partial R}{\partial P}$ was calculated to be 3.0 (1/Lpm), $\frac{\partial R}{\partial Q}$ was calculated to be 459.1 (mmHg/Lpm^2). Total uncertainty in LBSVR was calculate to be 9.4 WU.

Table A2 show the details in MUSC2 LBSVR uncertainty estimation.

Name	R Value	$\frac{\partial R}{\partial Q}$	u_Q	$\frac{\partial R}{\partial P}$	u_P	Total Uncertainty	Relative Uncertainty
MUSC2 LBSVR (WU)	157.2	459.1	0.02	3.0	1.28	9.4	5.9%

Tabel A2. Uncertainty propagation for MUSC2 LBSVR.

As for compliance values, take the example of GOSH22 C_{prox}, total uncertainty in air volume (u_V) was calculated to be ±0.0004 ml, total uncertainty in working pressure (u_P) was calculated to be ±1.03 mmHg. Sensitivity term $\frac{\partial C}{\partial V}$ was calculated to be 0.001235 (1/mmHg), $\frac{\partial C}{\partial P}$ was calculated to be 0.0003 (ml/mmHg^2). Total uncertainty in C_{prox} was calculate to be 0.02 ml/mmHg. Table A3 shows the detail of this example.

Name	C Value	$\frac{\partial C}{\partial V}$	u_V	$\frac{\partial R}{\partial P}$	u_Q	Total Uncertainty	Relative Uncertainty
GOSH22 C_{Prox} (ml/mmHg)	0.23	0.001	0.0004	0.0003	1.03	0.02	8.6%

Tabel A3. Uncertainty propagation for MUSC2 proximal compliance.

REFERENCE

Agarwal KC, Ali Khan MA, Amato JJ, Marbey ML. (1984). Pulmonary and subclavian steal phenomenon following modified Blalock-Taussig shunt. *Am Heart J, 108*(6), 1567-1570.

Atallah J, Dinu IA, Joffe AR, Robertson CM, Sauve RS, Dyck JD, Ross DB, Rebeyka IM; tWestern Canadian Complex Pediatric Therapies Follow-Up Group. (2008). Two-year survival and mental and psychomotor outcomes after the Norwood procedure: an analysis of the modified Blalock-Taussig shunt and right ventricle-to-pulmonary artery shunt surgical eras. Circulation, 118(14), 1410-8.

Baim SD, Grossman W. (1991). *Cardiac Catheterization Angiography, and Intervention* (Fourth ed.). Baltimore, Maryland: Williams & Wilkins.

Bakir I, Van Tricht I, Verdonck P, Meyns B. (2006). In vitro set-up of modified Blalock Taussig shunt: vascular resistance-flow relationship. *Int J Artif Organs, 29*(3), 208-317.

Baretta A, Corsini C, Yang W, Vignon-Clementel IE, Marsden AL, Feinstein JA, Hsia TY, Dubini G, Migliavacca F, Pennati G; Modeling of Congenital Hearts Alliance (MOCHA) Investigators.. (2011). Virtual surgeries in patients with congenital heart disease: a multi-scale modelling test case. *Philos Trans A Math Phys Eng Sci., 369*(1954), 4316-30.

Barnea O, Austin EH, Richman B, Santamore WP. (1994). Balancing the circulation:theoretic optimization of pulmonary /systemic flow ratio in hypoplastic left heart syndrome. *J Am Coll Cardiol, 24*, 1376-1381.

Barnea O, Santamore WP, Rossi A, Salloum E, Chien S, Austin EH. (1998). Estimation of oxygen delivery in newborns with a univentricular circulation. *Circulation, 98*, 1407-1413.

Barth H, Hassberg D, Schmaltz AA, Steil E, Apitz J. (1987). Continuous-wave Doppler velocimeters and blood pressure difference in aortic coarctation. A simultaneous comparative study of 52 children. *Herz, 12*(3), 217-25.

BaumgartnerH, Schima H, Tulzer G, Kühn P. (1993). Effect of stenosis geometry on the Doppler-catheter gradient relation in vitro: a manifestation of pressure recovery. *J Am Coll Cardiol., 21*(4), 1018-25.

Biglino G, Giardini A, Baker C, Figliola RS, Hsia TY, Taylor AM, Schievano S; MOCHA Collaborative Group.. (2012). In vitro study of the Norwood palliation: a patient-specific mock circulatory system. *ASAIO J., 58*(1), 25-31.

Biglino G, Corsini C, Schievano S, Dubini G, Giardini A, Hsia TY, Pennati G, Taylor AM; Mocha Collaborative Group. (2014). Computational models of aortic coarctation in hypoplastic left heart syndrome: considerations on validation of a detailed 3D model. *Int J Artif Organs, 37*(5), 371-381.

BiglinoG, Giardini A, Baker C, Figliola RS, Hsia TY, Taylor AM, Schievano S; MOCHA Collaborative Group.. (2013). Implementing the Sano modification in an experimental model of first-stage palliation of hypoplastics left heart syndrome. *ASAIO J, 59*(1), 86-89.

Biglino G, Giardini A, Hsia TY, Figliola R, Taylor AM, Schievano S; MOCHA Collaborative Group. (2013). Modeling single ventricle physiology: review of engineering tools to study first stage palliation of hypoplastic left heart syndrome. *Frontier in Pediatrics, 1*(31), 1-9.

Blalock A, Taussig HB. (1945). The surgical treatment of malformations of the heart in which there is pulmonary stenosis or pulmonary atresia. *Journal of the American Medical Association, 128*(3), 189-202.

Bonnet, L. (1903). Sur la lesion dite stenose congenitale de l'aorte dans la region de l'isthme. *Rev. Med., 23*, 108.

Bove E, Migliavacca F, de Leval MR, Balossino R, Pennati G, Lloyd TR, Khambadkone S, Hsia TY, Dubini G. (2007). Use of mathematic modeling to compare and predict hemodynamic effects of the modified Blalock–Taussig and right ventricle–pulmonary artery shunts for hypoplastic left heart syndrome. *J Thorac Cardiovasc Surg, 136*(2), 312-320.

Camp TA. (2009). Evaluation of fluid diodes for use a pulmonary heart valve replacememts.

Campbell M, Polani PE. (1961). The aetiology of coarctation of the aorta. *Lancet, 1(7175),* 463-8.

Corsini C. (2012). Computational models of the hemodynamics in stage 1 palliations for the treatment of single ventricle heart disease.

Corsini C, Cosentino D, Pennati G, Dubini G, Hsia TY, Migliavacca F. (2011). Multiscale models of the hybrid palliation for hypoplastic left heart syndrome. *J Biomech, 44*(4), 767-70.

Crafoord C, Nylin G. (1945). Congenital coarctation of the aorta and its surgical treatment. *Journal of Thoracic Srugery, 14*, 347-361.

Corsini C, Biglino G, Schievano S, Hsia TY, Migliavacca F, Pennati G, Taylor AM; MOCHA Collaborative Group. (2014). The effect of modified Blalock-Taussig shunt size and coarctation severity on coronary perfusion after the Norwood operation. *Ann Thorac Surg.* 98(2):648-54

De Mey S, Segers P, Coomans I, Verhaaren H, Verdonck P.. (2001). Limitations of Doppler echocardiography for the post-operative evaluation of aortic coarctation. *J Biomech, 34*(7), 951-60.

DeGroff CG, Shandas R, Kwon J, Valdes-Cruz L. (2000). Accuracy of the Bernoulli Equation for Estimation of Pressure Gradient Across Stenotic Blalock–Taussig Shunts: An In Vitro and Numerical Study. *Pediatric Cardiology, 21*(5), 439-447.

Edwards JC. (1965). In *Congenital Heart Disease* (Vol. 2, p. 677). Philadelphia, W. B. Saunders Co.

Edwards JE. (1948). Pathologic considerations in coarction of aorta. *Proc Staff Meet Mayo Clin, 23*, 324.

Engvall J, Ask P, Loyd D, Wranne B. (1991). Coarctation of the aorta – a theortical and experimental analysis of the effects of a centrallylocated arterial stenosis. *Med. & Biol. Eng. & Comput*. 29,291-296.

Figliola RS, Beasley D. (2014). *Theory and Design for Mechanical Measurements.* New Jersery: John Wiley & Sons, Inc.

Figliola R, Giardini A, Conover T, Camp TA, Biglino G, Chiulli J, Hsia TY. (2010). In Vitro Simulation and Validation of the Circulation with Congenital Heart Defects. *Prog Pediatr Cardiol., 30*((1-2)), 71-80.

Fischbach J, Sinzobahamvya N, Haun C, Schindler E, Zartner P, Schneider M, Hraška V, Asfour B, Photiadis J. (2013). Interventions After Norwood Procedure: Comparison of Sano and Modified Blalock-Tausig Shunt. *Pediatric Cardiology, 34*(1), 112-118.

Fontan F, Baudet E. (1971). Surgical repair of tricuspid atresia. *Thorax, 26*(3), 240–248.

Giardini, A. (n.d.).

Giardini A, Tacy TA. (2010). Pressure recovery explains doppler overestimation of invasive pressure gradient across segmental vascular stenosis. *Echocardiography, 21*(1), 21-31.

Glenn WW. Ordway NK, Talner NS, Call EP Jr. (1965). Circulatory Bypass of the Right Side of the Heart: VI. Shunt between Superior Vena Cava and Distal Right Pulmonary Artery; Report of Clinical Application in Thirty-eight Cases. *Circulation, 31,* 172-189.

Mozaffarian D, Benjamin EJ, Go AS, Arnett DK, Blaha MJ, Cushman M, de Ferranti S, Després JP, Fullerton HJ, Howard VJ, Huffman MD, Judd SE, Kissela BM, Lackland DT, Lichtman JH, Lisabeth LD, Liu S, Mackey RH, Matchar DB, McGuire DK, Mohler ER 3rd, Moy CS, Muntner P, Mussolino ME, Nasir K, Neumar RW,Nichol G, Palaniappan L, Pandey DK, Reeves MJ, Rodriguez CJ, Sorlie PD, Stein J, Towfighi A, Turan TN,Virani SS, Willey JZ, Woo D, Yeh RW, Turner MB; American Heart Association Statistics Committee and Stroke Statistics Subcommittee. (2014). AHA Statistical Update: Heart Disease and Stroke Statistics—2014 Update. *Circulation*, e28-e292.

Gupta TC, Wiggers CJ. (1951). Basic hemodynamic changes produced by aortic coarctation of different degrees.*Circulation, 3*(1):17-31 .

Hoffman JI, Kaplan S. (2002). The incidence of congenital heart disease. *Journal of American College of Cardiology, 39,* 1890-1900.

Hornik CP, He X, Jacobs JP, Li JS, Jaquiss RD, Jacobs ML, O'Brien SM, Peterson ED, Pasquali SK. (2011). Complications after the Norwood operation: an analysis of The Society of Thoracic Surgeons Congenital Heart Surgery Database. *The Annals of Thoracic Surgery, 92*(5), 1734-1740.

Hsia TY, Cosentino D, Corsini C, Pennati G, Dubini G, Migliavacca F; Modeling of Congenital Hearts Alliance (MOCHA) Investigators. (2011). Use of mathematical modeling to compare and predict hemodynamic effects between hybrid and surgical Norwood palliations for hypoplastic left heart syndrome. *Circulation, 124*(11 Suppl), S204-10.

Hsia TY, Migliavacca F, Pennati G, Balossino R, Dubini G, de Leval MR, Bradley SM, Bove EL. (2009). Management of a stenotic right ventricle-pulmonary artery shunt early after the Norwood procedure. *Ann Thorac Surg, 88*(3), 830-7.

Itu L, Sharma P, Ralovich K, Mihalef V, Ionasec R, Everett A, Ringel R, Kamen A, Comaniciu D. (2013). Non-invasive hemodynamic assessment of aortic coarctation: validation with in vivo measurements. *Ann Biomed Eng, 41*(4), 669-81.

Keshavarz-Motamed Z, Garcia J, Pibarot P, Larose E, Kadem L. (2011). Modeling the impact of concomitant aortic stenosis and coarctation of the aorta on left ventricular workload. *J Biomech, 44*(16), 2817-25.

Keshavarz-Motamed Z, Garcia J, Maftoon N, Bedard E, Chetaille P, Kadem L. (2012). A new approach for the evaluation of the severity of coarctation of the aorta using Doppler velocity index and effective orifice area: in vitro validation and clinical implications. *J Biomech., 45*(7), 1239-45.

Kim HJ, Vignon-Clementel IE, Figueroa CA, LaDisa JF, Jansen KE, Feinstein JA, Taylor CA. (2009). On coupling a lumped parameter heart model and a three-dimensional finite element aorta model. *Ann Biomed Eng, 37*(11), 2153-69.

Ladisa JF Jr, Taylor CA. Feinstein JA. (2010). Aortic Coarctation: Recent Developments in Experimental and Compuationtal Methods to Access Treatments for This Simple Condition. *Prog Pediatr Cardiol., 30*(1), 45-49.

LaDisa JF Jr, Dholakia RJ, Figueroa CA, Vignon-Clementel IE, Chan FP, Samyn MM, Cava JR, Taylor CA, Feinstein JA.. (2011). Computational simulations demonstrate altered wall shear stress in aortic coarctation patients treated by resection with end-to-end anastomosis. *Congenit Heart Dis., 6*(5), 432-43.

LaDisa JF Jr, Alberto Figueroa C, Vignon-Clementel IE, Kim HJ, Xiao N, Ellwein LM, Chan FP, Feinstein JA,Taylor CA.. (2011). Computational simulations for aortic coarctation: representative results from a sampling of patients. *J Biomech Eng, 133*(9), 091008.

Laganà K, Balossino R, Migliavacca F, Pennati G, Bove EL, de Leval MR, Dubini G.. (2005). Multiscale modeling of the cardiovascular system: application to the study of pulmonary and coronary perfusions in the univentricular circulation. *J Biomech, 38*(5), 1129-41.

Lanfranchi PA, Somers VK. (2002). Arterial baroreflex function and cardiovascular variability: interactions and implications. *Am J Physiol Regul Integr Comp Physiol., 283*(4), R815-26.

Lee MY. (2013). Coatctation of the Aorta. In D. I. Eduardo M. Da Cruz, *Pediatric and Congenital Cardiology, Cardiac Surgery and Intensive Care* (pp. 1631-1646). New York: Springer Reference.

Mahle WT, Cuadrado AR, Tam VK (2003). Early experience with a modified Norwood procedure using right ventricle to pulmonary artery conduit. *Ann Thorac Surg., 76*(4), 1084-1088.

Mair R, Tulzer G, Sames E, Gitter R, Lechner E, Steiner J, Hofer A, Geiselseder G, Gross C.. (2003). Right ventricular to pulmonary artery conduit instead of modified Blalock-Taussig shunt improves postoperative hemodynamics in newborns after the Norwood operation. *J Thorac Cardiovasc Surg., 128*(5), 1378-1384.

Małota Z, Nawrat Z, Kostka P.. (2007). Computer and physical modeling of blood circulation pump support for a new field of application in palliative surgery. *Int J Artif Organs., 30*(12), 1068-74.

Marx GR, Allen HD. (1986). Accuracy and pitfalls of Doppler evaluation of the pressure gradient in aortic coarctation. *J Am Coll Cardiol., 7*(6), 1397-85.

Migliavacca F, Balossino R, Pennati G, Dubini G, Hsia TY, de Leval MR, Bove EL. (2005). Multiscale modelling in biofluidynamics: application to reconstructive paediatric cardiac surgery. *J Biomech, 39*(6), 1010-20.

Migliavacca F[1], Yates R, Pennati G, Dubini G, Fumero R, de Leval MR.. (2000). Calculating blood flow from Doppler measurements in the systemic to pulmonary artery shunt after the Norwood operation: a mthod based on computational fluid dynamics. *Ultrasound Med Biol, 26*, 209-219.

Migliavacca, Dubini G, de Leval MR. (2000). Pressure flow relationship in systemic to pulmonary shunt evaluated by means of 3D Steady and pulsatile computational models. *J Biomech, 33*, 549-557.

Migliavacca F, Pennati G, Dubini G, Fumero R, Pietrabissa R, Urcelay G, Bove EL, Hsia TY, de Leval MR. (2001). Modeling of the Norwood circulation: effects of shunt size, vascular resistances, and heart rate. *Am J Physiol Heart Circ Physiol, 280*(5), H2076-86.

Morgagni, J. (1760). De sedibus et causis morborum. *Epist, 18,* Article 6.

Moulaert AJ, Bruins CC, Oppenheimer-Dekker A. (1976). Anomalies of the aortic arch and ventricular septal defects. *Circulation, 53*(6), 1011-15.

Moulton AL, Brenner JI, Ringel R, Nordenberg A, Berman MA, Ali S, Burns J. (1985). Classic versus modified Blalock-Taussig shunts in neonates and infants. *Circulation, 72*(3), II35 - 44.

Muller WH Jr, Danimann JF Jr. (1952). The treatment of certain congenital malformations of the heart by the creation of pulmonic stenosis to reduce pulmonary hypertension and excessive pulmonary blood flow; a preliminary report. *Surg Gynecol Obstet., 95*(2), 213-9.

Norwood WI, Lang P, Casteneda AR, Campbell DN. (1981). Experience with operations for hypoplastic left heart syndrome. *J Thorac Cardiovasc Surg*, 511-519.

Ohye RG, Devaney EJ, Hirsch JC, Bove EL. (2007). The modified Blalock-Taussig shunt versus the right ventricle-to-pulmonary artery conduit for the Norwood procedure. *Pediatr Cardiol., 28*(2), 122-125.

Ohye RG, Sleeper LA, Mahony L, Newburger JW, Pearson GD, Lu M, Goldberg CS, Tabbutt S, Frommelt PC,Ghanayem NS, Laussen PC, Rhodes JF, Lewis AB, Mital S, Ravishankar C, Williams IA, Dunbar-Masterson C,Atz AM, Colan S, Minich LL, Pizarro C, Kanter KR, Jaggers J, Jacobs JP, Krawczeski CD, Pike N, McCrindle BW, Virzi L, Gaynor JW; Pediatric Heart Network Investigators.. (2010). Comparison of Shunt Types in the Norwood Procedure for Single-Ventricle Lesions. *The New England Journal of Medicine, 362*, 1980-1992.

Paris M. (1791). Rétrècissement considerable de l'aorte pectorale observé à l'Hotel Dieu de Paris. *Jour de Chirurgie de Desault, ii*, 107.

Pekkan K, Dasi LP, Nourparvar P, Yerneni S, Tobita K, Fogel MA, Keller B, Yoganathan A.. (2008). In vitro hemodynamic investigation of the embryonic aortic arch at late gestation. *J Biomech, 41*(8), 1697-706.

Pennati G, Corsini C, Hsia T-Y, Migliavacca F. (2001). Hemodynamics in patients with systemic-to-pulmonary shunt: mathmatical modelling and clinical data. *J Surg Invest, 3*(2), 141-150.

Pennati G[1], Fiore GB, Migliavacca F, Laganà K, Fumero R, Dubini G. (2001). In vitro steady-flow analysis of systemic-to-pulmonary shunt haemodynamics. *J Biomech, 34*(1), 23-30.

Pennati G, Migliavacca F, Dubini G, Bove EL. (2010). Modeling of systemic-to-pulmonary shunts in newborns with a univentricular circulation: State of the art and future directions. *Progress in Pediatric Cardiology, 30*(1-2), 23–29.

Reivich M, Holling HE, Roberts B, Toole JF. (1961). Reversal of blood flow through the vertebral artery and its effect on cerebral circulation. *N Eng J Med., 2*(265), 878-885.

Samanek M, Voríšková M. (1999). Congenital heart disease among 815,569 children born between 1980 and 1990 and their 15-year survival: a prospective Bohemia survival study. *Pediatric Cardiology, 20*, 411-417.

Sano S, Ishino K, Kawada M, Arai S, Kasahara S, Asai T, Masuda Z, Takeuchi M, Ohtsuki S. (2003). Right ventricle–pulmonary artery shunt in first-stage

palliation of hypoplastic left heart syndrome. *The Journal of Thoracic and Cardiovascular Surgery, 126*(2), 504-510.

Schievano S, Migliavacca F, Coats L, Khambadkone S, Carminati M, Wilson N, Deanfield JE, Bonhoeffer P,Taylor AM.. (2007). Percutaneous pulmonary valve implantation based on rapid prototyping of right ventricular outflow tract and pulmonary trunk from MR data. *Radiology, 242*(2), 490-7.

Seifert BL, DesRochers K, Ta M, Giraud G, Zarandi M, Gharib M, Sahn DJ.. (1999). Accuracy of Doppler methods for estimating peak-to-peak and peak instantaneous gradients across coarctation of the aorta: An In vitro study. *J Am Soc Echocardiogr, 12*(9), 744-53.

Sharma S, Anand R, Kanter RK, Williams HW, Dolley KJ, Jones DW, Vincent RN. (1992). The usefulness of echocardiography in the surgical management of infants with congenital heart disease. *Clin Cardiol, 15*(12), 891-7.

Shimizu S, Une D, Shishido T, Kamiya A, Kawada T, Sano S, Sugimachi M.. (2011). Norwood procedure with non-valved right ventricle to pulmonary artery shunt improves ventricular energetics despite the presence of diastolic regurgitation: a theoretical analysis. *J Physiol Sci*, 457-65.

Sinha SN, Kardatzke ML, Cole RB, Muster AJ, Wessel HU, Paul MH.. (1969). Coarctation of the Aorta in Infancy. *Circulation, 40*, 385-398.

Song MH, Sato M, Ueda Y.. (2001). Three-dimension simulation of the Blalock-Taussig shunt using computational fluid dynamics. *Surg Today, 31*, 688-94.

Tacy TA, Whitehead KK, Cape EG. (1998). In Vitro Doppler Assessment of Pressure Gradients Across Modified Blalock-Taussig Shunts. *Am J Cardiol, 81*(10), 1219-1213.

The Children's Hospital of Philadelphia. (n.d.). Retrieved from http://www.chop.edu/img/cardiac-center/hlhs-surgery-three-stages.html

Tomoyasu T, Miyaji K, Miyamoto T, Inoue N.. (2009). The bilateral pulmonary artery banding for hypoplastic left heart syndrome with a diminutive ascending aorta. *Interactive Cardiovascular and Thoracic Surgery, 8*, 479-81.

Vukicevic M, Chiulli JA, Conover T, Pennati G, Hsia TY, Figliola RS; MOCHA Network.. (2013). Mock circulatory system of the Fontan circulation to study respiration effects on venous flow behavior. *ASAIO J., 59*(3), 253-60.

Vukicevic M, Conover T, Jaeggli M, Zhou J, Pennati G, Hsia TY, Figliola RS.. (2014). Control of respiration-driven retrograde flow in the subdiaphragmatic venous return of the Fontan circulation. *ASAIO*, Epub ahead of print.

Waniewski J, Kurowska W, Mizerski JK, Trykozko A, Nowiński K, Brzezińska-Rajszys G, Kościesza A. (2005). The effects of graft geometry on the patency of a systemic-to-pulmonary shunt: a computational fluid dynamics study. *Artif Organs, 29*(8), 642-50.

Westerhof N. (2005). *Snapshots of Hemodynamics.* New York: Springer.